12

NSWCDD/TR-93/551

AD-A273 680

STATE-OF-THE-ART ENGINEERING AEROPREDICTION METHODS WITH EMPHASIS ON NEW SEMIEMPIRICAL TECHNIQUES FOR PREDICTING NONLINEAR AERODYNAMICS ON COMPLETE MISSILE CONFIGURATIONS

BY FRANK G. MOORE
WEAPONS SYSTEMS DEPARTMENT

NOVEMBER 1993

Approved for public release; distribution is unlimited.

NSWC
Naval Surface Warfare Center
DAHLGREN DIVISION

NAVAL SURFACE WARFARE CENTER
DAHLGREN DIVISION
Dahlgren, Virginia 22448-5000

NSWCDD/TR-93/551

STATE-OF-THE-ART ENGINEERING AEROPREDICTION METHODS WITH EMPHASIS ON NEW SEMIEMPIRICAL TECHNIQUES FOR PREDICTING NONLINEAR AERODYNAMICS ON COMPLETE MISSILE CONFIGURATIONS

BY FRANK G. MOORE

WEAPONS SYSTEMS DEPARTMENT

Accesion For		
NTIS CRA&I		X
DTIC TAB		☐
Unannounced		☐
Justification		
By		
Distribution /		
Availability Codes		
Dist	Avail and / or Special	
A-1		

NOVEMBER 1993

Approved for public release; distribution is unlimited.

NAVAL SURFACE WARFARE CENTER

DAHLGREN DIVISION

Dahlgren, Virginia 22448-5000

FOREWORD

The work described in this report is based on an invited lecture series by the Advisory Group for Aerospace Research and Development (AGARD) to be given in June 1994 at the Von Karman Institute (VKI) in Belgium and the Middle East Technical University in Ankara, Turkey. While the lecture series is generic in nature, it focuses on a Class of Aeroprediction codes that are semiempirical in nature (a mixture of analytical and empirical methods). By design of the invitation, the report also emphasizes many of the new methods the author has developed over his thirty year career at NSWCDD. These lectures are being documented in the form of a technical report in order that those who are not able to attend the presentations will have easier access to the material

While the new methods are the authors principally, implementation of these methods was done primarily by coworkers. As a result, a lengthy acknowledgement is given at the end of the report which includes not only the technical personnel but sponsors as well. This particular report was supported by the Office of Naval Research (Dave Siegel) and more specifically, the Surface Launched Weapons Technology Program managed at NSWCDD by Robin Staton and the Air Launched Weapons Technology Program managed at NAWC/China Lake by Tom Loftus. Appreciation is expressed to these individuals for their support.

Approved by:

David Malyevac

DAVID S. MALYEVAC, Deputy Department Head
Weapons System Department

ABSTRACT

This report discusses the pros and cons of numerical, semiempirical and empirical aeroprediction codes and lists many state-of-the-art codes in use today. It then summarizes many of the more popular approximate analytical methods used in State-of-the-Art (SOTA) semiempirical aeroprediction codes. It also summarizes some recent new nonlinear semiempirical methods that allow more accurate calculation of static aerodynamics on complete missile configurations to higher angles of attack. Results of static aerodynamic calculations on complete missile configurations compared to wind tunnel data are shown for several configurations at various flight conditions. Calculations show the new nonlinear methods being far superior to some of the former linear technology when used at angles of attack greater than about 15 degrees.

CONTENTS

CONTENTS (CONTINUED)

ILLUSTRATIONS

ILLUSTRATIONS (CONTINUED)

ILLUSTRATIONS (CONTINUED)

ILLUSTRATIONS (CONTINUED)

TABLES

1.0 INTRODUCTION AND BACKGROUND

1.1 USES FOR AERODYNAMICS

Aerodynamics are required throughout the design process of any flight vehicle. These aerodynamics are used for flight performance estimates including range, maneuverability, miss distance, and stability analysis. In addition, they are used for structural analysis including material requirements and selection, structural member thicknesses required to withstand the loads, and as inputs for heat transfer or ablation analysis (Table 1-1). Generally, an interactive design process occurs between the aerodynamicist, the structural designer, and the flight dynamicist to arrive at a configuration that meets some set of desired launcher constraints and performance requirements given a warhead and possibly a guidance system as well.

TABLE 1-1. WHAT AERODYNAMICS ARE USED FOR

Flight Dynamics	Structures
o Range Computation	o Loads (Pressure)
o Engagement of Target and Miss Distance	o Aeroheating (Inputs to Heat Transfer Codes)
o Maneuverability Estimates	
o Any Trajectory Analysis (3 DOF, 5 DOF, 6 DOF)*	o Ablation Analysis Inputs

* DOF = Degree of Freedom

Prior to 1971, the tactical weapons aerodynamicist could do one of three things to obtain aerodynamics. The individual could perform flight tests of a full-scale configuration; or design, build, and test a wind tunnel model over the flight range of interest; or finally, utilize existing handbooks, wind tunnel data reports, and theoretical analysis to estimate empirically the aerodynamics of a given configuration.

The first two approaches were often more costly. time consuming, and accurate than needed in the preliminary design stages, whereas the latter approach was more time consuming than desired but also had no general accuracy assessment.

A fourth alternative (which did not exist prior to 1971), to compute aerodynamics on a complete configuration over the Mach number and angle of attack range of interest, is to have a general computer program to perform such a task. There are three alternative theoretical approaches to develop such a code (see Table 1-2). The first of these is solution of the full Navier Stokes equations. The only assumptions associated with this set of equations is continuum flow (that is the flowfield region is not sparsely populated with air molecules such as at altitudes greater than about 200 to 250 thousand ft) and the turbulence model selected. A second theoretical alternative is to assume the viscous flow region lies in a thin layer near the body and thus solution of the Navier Stokes equations can be reduced to that of an inviscid flowfield plus a thin boundary layer near the surface. This, combined with empirical estimates of base drag and other protuberance aerodynamics, gives a complete set of aerodynamics for the configuration of interest. A third theoretical alternative is to assume the body perturbs the flowfield only slightly and then to make appropriate approximations to the Euler and Boundary Layer Equations. These approximate theories are then combined with other theoretical approaches and empirical data for the complete aerodynamics code.

TABLE 1-2. HOW WE GET AERODYNAMICS

1. Wind Tunnel, Free Flight Data, Ballistic Range
2. Empirical Estimates: Wind Tunnel Reports, Handbooks, Experience, etc.
3. Aeroprediction Codes
   - A. Navier Stokes -- Continuum Flow
   - B. Euler Equations + Boundary Layer -- inviscid outer layer + thin viscous layer near surface + some empirical techniques
   - C. Approximations to Euler and Boundary Layer Equations + Empirical Techniques

There are several uses that can drive the type of theory chosen for the aeroprediction code. These are listed in Table 1-3. For example, if missile synthesis is being performed where a very large number of configurations are investigated to conduct top level trade studies involving engine types, warhead types, material requirements, etc. as a function of range, maneuverability, or response time, then it is desirable to have an easy to use, robust, and computationally fast code. At the same time, accuracy may be sacrificed to achieve these goals.

After a missile synthesis of a large number of concepts has been conducted, generally several of these concepts are taken a step further in the design process. Here, structural layouts, packaging of all components, and better definition of weights are typical requirements that allow improved estimates of range, maneuverability, and preliminary miss distance. This means that the aerodynamic code requirements need a blend of robustness, ease of use, and accuracy while still being computationally cost effective. Accuracies in aerodynamics of 10 percent or so are generally expected.

Finally, one or two configurations are selected for more detailed performance estimates. This means accuracy in the aerodynamics estimates of better than 5 percent in most cases. Each of the three design levels discussed require different levels of accuracy, computational speed, and robustness and, therefore, aid in the choice of the level of theoretical complexity needed to meet the requirements.

TABLE 1-3. AERODYNAMIC CODE REQUIREMENTS AND USES IN VARIOUS MISSILE DESIGN STAGES

Design Stage	Aero Code Design Requirements	Trade Studies (Typical)	Aerodynamics Uses
Missile Synthesis	Robustness Ease to Use Minimal Input Parameters Extremely Fast Computationally 25 percent Accuracy	Engine Types Warhead Types Material Requirements Typical Weights Guidance Types Airframe Control Type	Range Maneuverability Response Time
Missile Preliminary Design	Blend of Robustness, Ease of Use, and Accuracy Fast Computationally 10 percent Accuracy	Structural Layout (Material, Thickness, etc.) Aero Shape vs. Engineering and Guidance Size Hot vs. Cold Structure	Range Maneuverability Miss Distance (3 DOF) Structural Design
Detailed Design and Problem Solving (or Analysis Codes)	Accuracy (<5 percent) Computationally Affordable User Friendliness and Robustness Still Important	Detailed Structural Design Including Material Selection Investigating Critical Problem Areas	Range Maneuverability Miss Distance (6 DOF) Structural Design

To meet the theoretical aerodynamics computer code needs, the Navy began developing such a code in 1971 based on the 3C approach of Table 1-2. This code falls into the second category of Table 1-3. Since the first version of the NSWCDD Aeroprediction code was released, there have been four versions produced since that time.

Each of these versions attempted to meet the requirements as seen by the tactical weapons community. The first version was for general-shaped bodies alone.[1] It was the first such weapons code known that combined a good mix of accuracy in aerodynamic computations, ease of use and computational time. It is believed that this mix led to the code's initial popularity and requests for additional capability. In 1974,[2,3] the code was extended to allow up to two sets of lifting surfaces in the computational process. In 1977,[4,5] dynamic aerodynamic derivatives were added to the code's capability. In 1981, the code extended the Mach number range up to eight and added high angle-of-attack capability for a narrow range of configurations[6,7]. Finally, the last version of the code extended the Mach number range higher to include real gas effects, added new nonlinear lift methodology for wings and interference effects, and developed an improved base drag methodology.[8,9]

This report will serve several purposes. First, a review of the state-of-the-art (SOTA) semiempirical aerodynamic prediction codes will be given. Second, a review of some of the more useful approximate theoretical methods will be made. These methods are conventional and have been in use for many years. Third, a more detailed review of the new nonlinear aerodynamic methods introduced over the past 3 years into the fifth version of the Aeroprediction Code (AP93) will be given. Finally, a comparison of the static aerodynamics using experiment, the AP93 and the older version of the Aeroprediction Code (AP81) will be made on several complete missile configurations.

1.2 TYPES OF AEROPREDICTION CODES

Aeroprediction Codes will be defined and broken down into three classes. These classes are empirical, semiempirical, and numerical codes. The empirical codes are analogous to the codes used in Missile Synthesis in Table 1-3. The semiempirical and some numerical codes are used primarily in the missile preliminary design stage of Table 1-3. Finally, the numerical codes are the only ones with the accuracy and capability to do the detailed design application as shown in Table 1-3.

In terms of a definition, empirical codes typically calculate aerodynamics by a series of simple formulas that have been approximated based on data fits. Typically, these codes can be implemented on a hand calculator in many cases and are the most simplistic and least accurate of the code classes.

The semiempirical codes typically attempt to calculate a force or moment using approximations to the exact equations of motion. When this approach fails (such as at higher angles of attack), empirical estimates or methods are used. This blend of approximate theories and empirical estimates is why this class of codes is termed semiempirical. The semiempirical codes, in contrast to the empirical codes, generally will calculate pressure distribution on the body and lifting surfaces. It is this blend of theory with the empirical estimates that allows the semiempirical codes to improve accuracy over the empirical codes.

The third class of codes is called numerical. These codes will define a grid around the configuration that is composed of points in two or three dimensions. Numerical techniques are then employed to solve the equations of motion at all grid points in the flow field that is bounded by the body and shock or body and outer boundary of the flow if the Mach number is subsonic. Numerical Codes are generally based on the linearized or full potential equations of motion, the full Euler equations or the full or reduced level of Navier Stokes equations. If the potential or Euler equations are used, other methods (such as boundary layer equations) must be used for skin friction. Also, empirical estimates are used for base drag. Hence, even though these codes are numerical, in most cases to get complete forces and moments on a configuration, the use of some empirical data will be necessary. Also, if the potential equations are solved in a numerical form, the accuracy is similar to the semiempirical codes. The only difference between the two is that the semiempirical codes seek pressure distributions on the body and wings without solving the entire flowfield. This saves a tremendous amount of computational time.

A final point worthy of discussion are the assumptions inherent in each level of theory. These assumptions are given as a function of the theoretical approach in Table 1-4. Upon examination of Table 1-4, the level of code sophistication, computational time, overall cost and accuracy goes down in going from the top to the bottom of the table.

One way to try to compare the level of sophistication versus accuracy, and the cost of the various codes, is through the examination of the total cost to obtain a set of aerodynamics. To do this, Table 1-5, which compares the educational, computer, and computational time requirements of the various Aeroprediction Codes in use at NSWCDD has been prepared. Referring to Table 1-5, the level of sophistication increases in going from top to bottom of the Table. For example, the MAIR Code is close to an empirical code but it does have some theory included so that it would be in the class of semiempirical codes. The Missile III, Aeroprediction versions 81 and 93, HABP, and missile DATCOM, are all semiempirical codes. NANC and BODHEAT are primarily numerical codes based on approximations to the Euler and Boundary Layer equations. SWINT/ZEUS, CFL3DE and GASP, of course, are all numerical codes. The Aeroprediction 81/93, SWINT/ZEUS, MAIR, NANC, and BODHEAT were all developed at NSWCDD. The Missile III was developed by Nielsen Engineering and Research (NEAR), HABP and Missile DATCOM by McDonnel Douglas of St. Louis, and the Navier Stokes Codes were developed jointly by NASA/LRC and VPI.

Included in Table 1-5 is the time required to learn how to use the code, the set-up time for a typical geometry, and the computer time for the one case referenced to the same computer (CDC 865). Also shown are other criteria including typical educational level of the user as well as the size of the computer required. To get the total cost of using a code, it is necessary to add the manpower set-up time to the computer cost and prorate the training time over some nominal expected usage. Experience has shown that most project and program managers are willing to pay the costs of SWINT/ZEUS type codes and any above that in Table 1-5. However, the cost and requirements of the full Navier Stokes codes must come down substantially before they will be used on a routine basis for design. This means much additional research as well as advancements in computer speed are still needed in this area.

To illustrate this point, a particular example was chosen for cost comparisons. The example is to develop a set of trim aerodynamics on a typical missile configuration to be used as an input to a three-degree-of-freedom (3 DOF) flight simulation model. This example is quite typical of what an empirical or semiempirical code would be used for. By definition, trim is that combination of angles of attack (α's) and control deflections (δ's) that give zero pitching moment about the vehicle center of gravity. To determine the (α, δ) map as a function of Mach number, one must compute the static aerodynamics over enough α, δ, M conditions so the flight envelope will be covered. Also, it will be assumed that the missile is a surface launched, tail control, cruciform fin configuration which has a Mach range of 0 to 4, angle of attack range of 0 to 30°, control deflection of 0 to 20°, and attitude 0 to 80,000 feet. These conditions are reasonable for many of the worlds missiles. To cover the flight envelope, 7 Mach numbers, 5 α's and 5 δ's are assumed. This gives a total of $7 \times 5 \times 5 = 175$ cases. Furthermore, skin friction varies with attitude so 5 altitudes will be chosen, giving a total of 180 cases for which aerodynamics are to be computed on a single configuration.

TABLE 1-4. ASSUMPTIONS OF FLOW FIELD EQUATIONS

1. Full Navier Stokes (high angle of attack)
   - A. Continuum Flow
   - B. Turbulence Model
2. Thin Layer Navier Stokes (moderate separation)
   - A. Neglect Streamwise and Circumferential Gradients of Stress Terms
   - B. Turbulence Model
   - C. Continuum Flow
3. Parabolized Navier Stokes (small separation)
   - A. Steady State
   - B. Neglects Streamwise Viscous Gradient
   - C. Approximate Streamwise Pressure Gradient in Subsonic Portion of Flow Near Surface
   - D. Turbulence Model
   - E. Continuum Flow
4. Euler Equations + Boundary Layer (small separation)
   - A. Viscous Region Confined to Thin Region Near Body Surface
   - B. Large Reynold's Number
   - C. Neglect Streamwise Gradients of Stress Terms
   - D. Neglect Normal Pressure Gradient
   - E. Turbulence Model
   - F. Continuum Flow
5. Euler Equations
   - A. Neglect all Viscous Terms
   - B. Continuum Flow
6. Full Potential Equations
   - A. Neglect all Viscous Terms
   - B. Flow is Isentropic (no shock waves)
   - C. Continuum Flow
7. Linearized Potential Equations
   - A. Neglect all Viscous Terms
   - B. Flow is Isentropic (no shock waves)
   - C. Body Creates Small Disturbances in Flowfield
   - D. Continuum Flow
8. Theoretical Approximations
   - A. Certain Other Simplifications to Euler, Potential Equations, or Boundary Layer Equations
   - B. Continuum Flow
9. Empirical Data Base
   - A. Data Base Covers Vehicles and Flight Regime of Interest
   - B. Enough Data is Available to do Good Interpolations

TABLE 1-5. EDUCATIONAL AND TIME REQUIREMENTS FOR AEROPREDICTION CODES IN USE AT NSWCDD

Code		Typical User Educational Level	Typical Time Required to Learn to Use Code	Set-Up Time	Computational Time for 1 Case (Same Computer)	Computer Required
1.	MAIR	Coop, B.S., M. S., Ph. D	< 1 wk	< 1 day	< 1 second	P. C.
2.	Missile III	Coop, B.S., M. S., Ph. D	≈ 1 wk	< 1 day	<1 second	P. C.
3.	Aeroprediction 81 and 93	Coop, B.S., M. S., Ph. D	≈ 1 wk	< 1 day	< 1 second	P. C.
4.	HABP	B. S., M. S., Ph. D.	≈ 2 wk	< 1 wk	< 1 second	Micro Vax
5.	Missile DATCOM	B. S., M. S., Ph. D.	≈ 2 wk	< 1 wk	< 1 second	Micro Vax
6.	NANC	M. S., Ph. D.	≈ 3 wk	< 2 wks	10 seconds	Vax CDC Super Mini
7.	BODHEAT	M. S., Ph. D.	≈ 3 wk	< 1 wk	10 seconds	Vax CDC Super Mini
8.	SWINT/ZEUS	M. S., Ph. D.	≈ 1 month	< 1 month	1-3 minutes	Vax CDC Super Mini
9.	N.S. (CFL3DE, GASP)	Ph. D., some M. S.	≈ months-yrs	≈ months	≈ hrs-days	Cray or Super Mini

Before costs of each computer code can be made for this particular example, some assumptions must be made. These assumptions are given in Table 1-6. These assumptions are based on NSWCDD experience in using the various aeroprediction codes. The cost to perform the set of trim aerodynamics calculations using these codes is shown in Figure 1-1. It should be noted that the cost assumes that Parabolized Navier Stokes and Euler plus boundary layer are used at subsonic axial Mach number conditions although the codes in use at NSWCDD are steady hyperbolic marching solutions and will not function where the axial Mach number decreases to one. To go to unsteady computation would require costs to be multiplied by a factor of at least 10. Hence, the PNS and Euler plus B.L. costs are based on steady flow of supersonic Mach numbers. For a combination of steady and unsteady computations, the cost of these codes would probably be about five times greater than those shown in Figure 1-1.

TABLE 1-6. ASSUMPTIONS IN COST ESTIMATES TO COMPUTE SET OF TRIM AERODYNAMICS WITH VARIOUS AEROPREDICTION CODES

Estimated Cost
- o Cray II Computer at $500/HR
- o Engineer Time = 110K/work year
- o Engineer is assumed to know how to use codes so no training time is involved.
- o Need enough resolution in grid size to predict skin friction drag
- o Wind Tunnel (W/T) includes model and test cost

CODE	SET UP TIME	COMPUTER TIME
FNS	5 Weeks	20 Hours
TLNS	5 Weeks	17 Hours
PNS	2-5 Weeks	12 Minutes
EULER + BL + B.D.	2 Weeks	1.5 Minutes
AEROPREDICTION	0.5 Day	1.0 Seconds

There are several points worthy of note in analyzing Figure 1-1. First, for practical routine computations, Full Navier Stokes and Thin Layer Navier Stokes are beyond the cost most program managers are willing to pay. Secondly, they are even beyond the wind tunnel cost to obtain comparable aerodynamics. Thirdly, steady PNS, steady Euler plus boundary layer, and semiempirical (Aeroprediction) are all within most allowable aerodynamics budgets. Going to unsteady computations for subsonic axial Mach numbers makes the cost requirements much higher and may not be affordable and robust to cover the entire flight regime.

A second way of comparing aerodynamic computations is the total time it takes to get the complete set of computations performed. These results are estimated, again based on NSWCDD experience, and shown in Figure 1-2. Again, the same caveat, with respect to the PNS and Euler Codes, applies here as to Figure 1-1. For most development programs, the semiempirical codes obviously have the most desirable turn-around-time (TAT). The Euler and PNS are marginal and experimental and Navier-Stokes (N-S) and Thin Layer Navier-Stokes (TLNS) generally unacceptable except as long lead items. The combination of cost, accuracy, and complexity of the various means of computing aerodynamics has led most agencies to a mix of the various approaches. The most used codes still remain the semiempirical codes with Euler plus Boundary Layer becoming more and more prevalent as the robustness and ease of use improves. Navier Stokes and Thin Layer Navier Stokes are used for specialized problems or a few validation cases of other codes; much work is still needed to improve user friendliness for this class of codes. Wind tunnel data still remains the most reliable but time consuming method to obtain Aerodynamics.

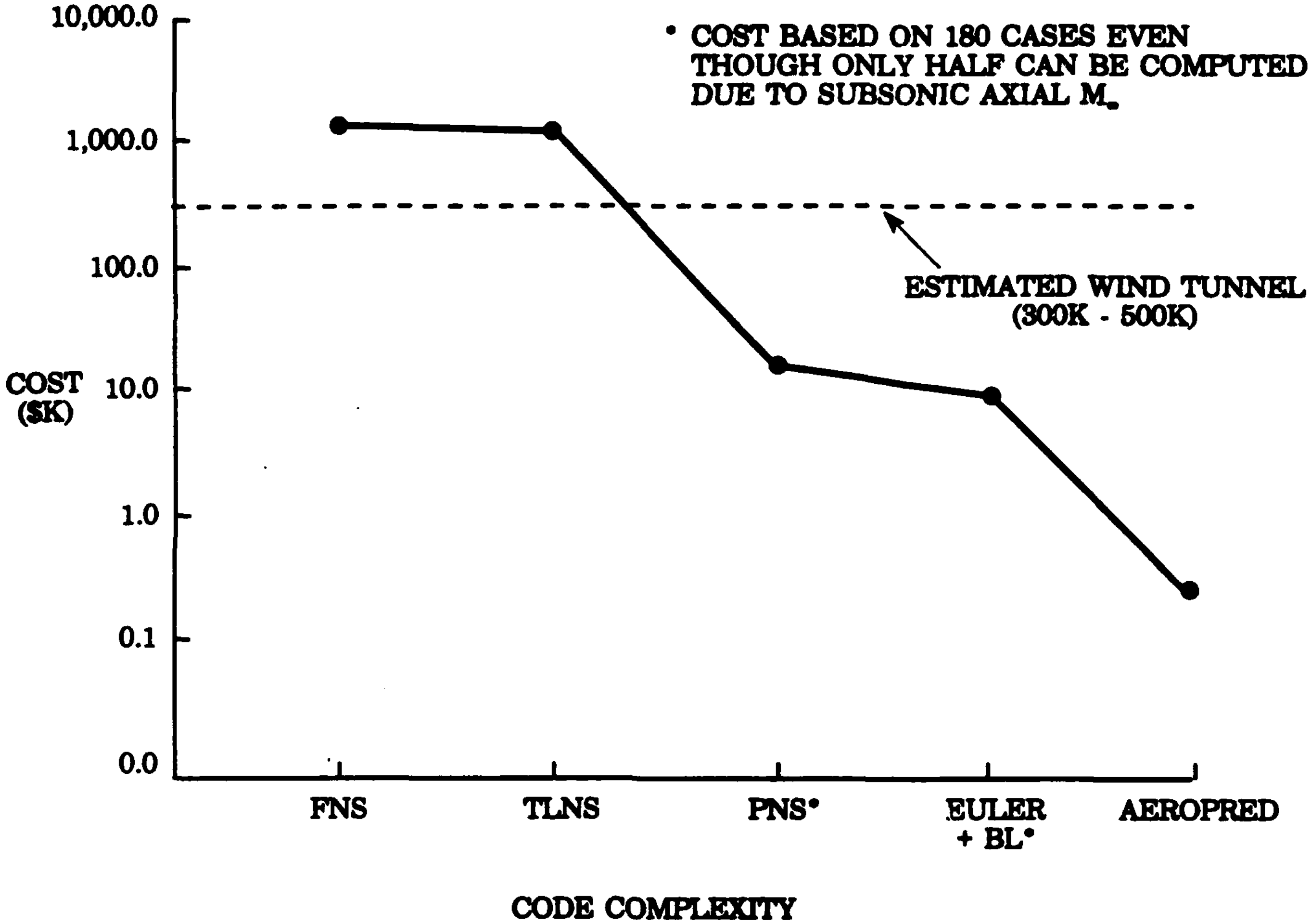

FIGURE 1-1. ESTIMATED COST TO OBTAIN SET OF TRIM AERODYNAMICS

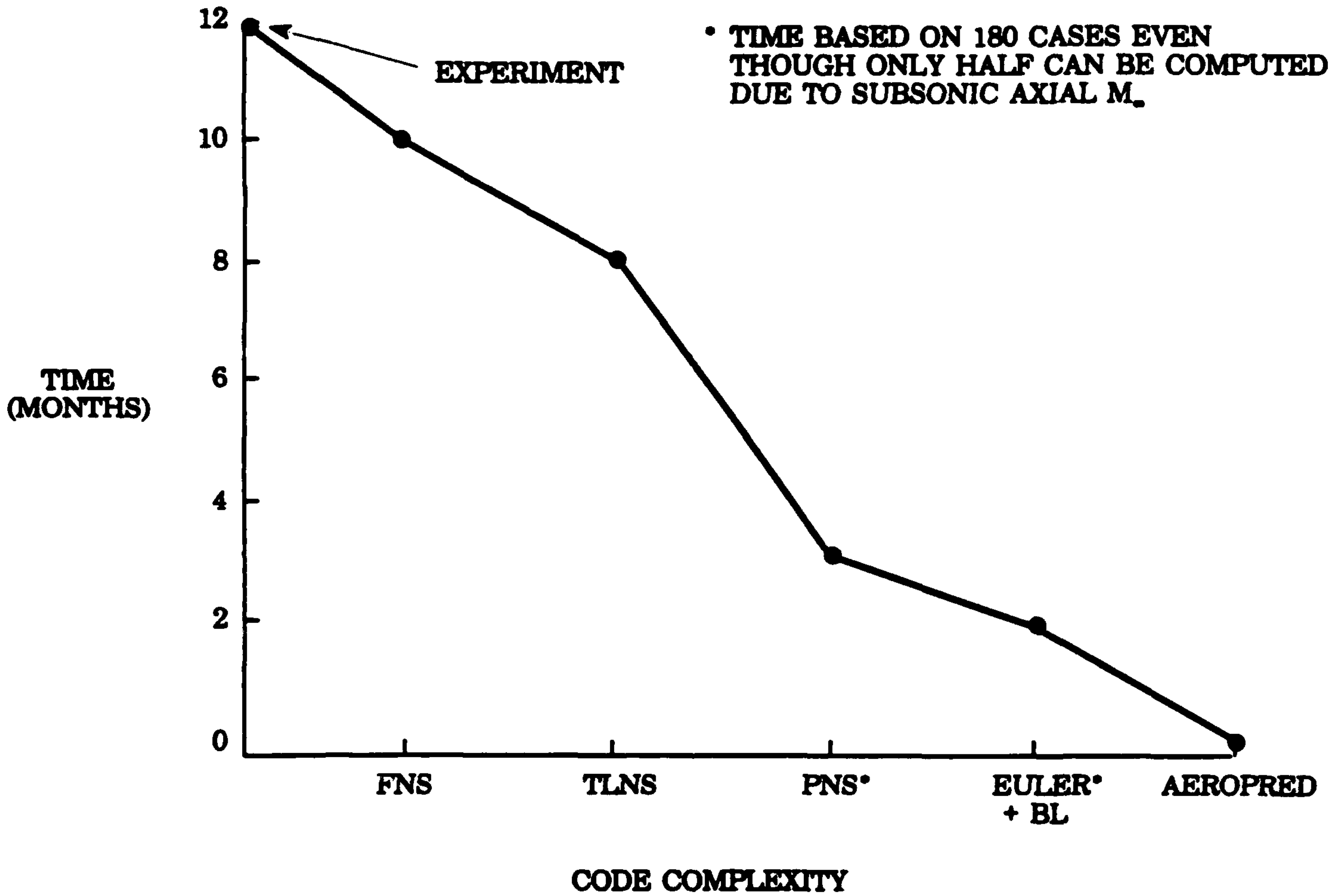

FIGURE 1-2. ESTIMATED TIME TO GENERATE SET OF TRIM AERODYNAMICS

Codes in Use

Tables 1-7 through 1-12 list many of the aerodynamic codes in use today. These tables were taken primarily from Lacau,[10] with some of the more important codes developed since 1988 added to the tables. References 11 - 57 are the references one could use for each of the codes listed in Tables 1-7 through 1-12.[10] (Note that some of the references are incomplete but were taken directly from Reference 11.) The tables are given in a similar fashion to the theoretical assumptions given in Table 1-4. All the previous comments, with respect to the general types of codes, should also be kept in mind when considering a particular type of code to accomplish a given task. No attempt will be made here to expose the good and bad points of each of the codes. This would require a personal knowledge in terms of usage on a set of configurations for a given problem(s). This obviously would be prohibitively expensive and time consuming. The best that one can generally hope for, is a comparison of a few codes for a limited class of conditions.

This completes the discussion on the state-of-the-art in aerodynamic codes and the various means to obtain aerodynamics. The bulk of the remainder of this paper will be directed at the semiempirical code known as NSWC Aeroprediction or NSWC-AP as given in Table 1-7. To that extent, the next section will briefly cover many of the more popular approximate theoretical techniques used by many of the semiempirical codes in Table 1-7. This will be followed by the new technology developed for the latest version of the Aeroprediction Code (AP93). Finally, a comparison with experiment of the AP93 and AP81 will be given for several missile configurations.

TABLE 1-7. CAPABILITIES OF EMPIRICAL AND SEMIEMPIRICAL CODES FOR MISSILES (from ref. 10)

1CF: ONE CRUCIFORM-FINNED SECTION
2CF: TWO " " "
3CF: THREE " " "
DD: DOUBLE DIAMETER

CODE NAME	ORIGIN	REF N°	DATE	CONVENTIONAL (circular cross section shapes)			UNCONVENTIONAL (arbitrary cross section shapes)		
				CLASSICAL		BOOSTED	LIFTING	AIRBREATHING	
								INTAKES	
				1CF	2CF	DD + 3CF	ELLIPTIC	OPEN	CLOSED
ABACUS	BAe (UK)	11	1977	▒	▒	▒	/	/	/
AERAM	FFA (SW)	12, 13	1980	▒	▒	/	/	▒	/
AMI300	aerospatiale (FR)		1980	▒	▒	/	/	/	/
BAKER	A.E.D.C (USA)	14	1980	▒	/	/	/	/	/
BOV/NCV	MBB (FRG)		1967	▒	/	/	/	/	/
CARENG	L.R.B.A (FR)		1974	▒	▒	/	/	WITHOUT WINGS	
CASAERO	MATRA (FR)		1982	▒	▒	▒	/	/	▒
DOPRAM	DORNIER (FRG)		1985	▒	▒	▒	C	/	/
DRAG	BAe (UK)		1974	▒	▒	▒	/	/	/
DTMB	DTMB (USA)	15	1966	▒	▒	/	/	/	/
MAP	HUGUES (USA)	16	1984	▒	▒	/	/	/	/
MASP	MBT (Israel)		1985	▒	▒	C	/	/	/
MISSILE DATCOM	McDonnell Douglas (USA)	17	1985	▒	▒	▒	C	C	C
MISSILE aerospatiale	aerospatiale/ ONERA (FR)		1988	▒	▒	/	/	WITHOUT WINGS	
MISSILE ONERA	ONERA (FR)	18	1985	▒	▒	/	/	/	/
MISSILE 1	NEAR (USA)	19	1980	▒	▒	C	/	/	/
MISSILE 2A	NEAR (USA)	20, 21	1982 1986	▒	▒	/	/	/	/
MISSILE 3	NEAR (USA)	22, 23	1986	▒	▒	/	/	/	/
MRRT	CITEFA (ARG.)		1984	▒	/	/	/	/	/
NFR	BAe (UK)		1980	▒	▒	▒	/	/	/
NSWC - AP	NSWC (USA)	1, 2, 4, 6	1972, 1974, 1979, 1981	▒	▒	C	/	/	/
PORTANCE	aerospatial (FR)		1980	▒	▒	/	/	/	/
SEA Datcom	CITEFA (ARG)	24	1986	▒	C	C	▒	C	C
S/HARP	AFWAL (USA)	25	1973	▒	▒	▒	▒	▒	▒
TAD	NASA (USA)	26	1979	▒	▒	▒	/	/	/
TASK2	MBB (FRG)		1974	▒	▒	▒	SQUARE	/	/
TRAIFRO	MATRA (Ffe)		1983	▒	▒	▒	/	/	▒
AP93	NSWC	8	1993	▒	▒	C	/	/	/

▒ Configuration type has been computed /For no C Configuration type could be computed

TABLE 1-7. CAPABILITIES OF EMPIRICAL AND SEMIEMPIRICAL CODES FOR MISSILES[10] (CONTINUED)

CODE NAME	MACH RANGE	INCIDENCE RANGE	ROLL RANGE ($\phi=0°$ for + configuration)	FINS		CONTROL DEFLECTIONS	AERODYNAMIC COEFFICIENTS		
				IN-LINE	INTERDI-GITATED	($\delta 1, \delta 2, \delta 3, \delta 4$)	AXIAL-FORCE CA TOTAL CAw WAVE CAf FRICTION Cab BASE	STATIC STABILITY CN, Cm CY, Cn Cℓ	DYNAMIC DERIVATIVES Cmq, Cmα̇, CnR, Clp,...
ABACUS	$M_\infty \le 5.0$	$-90° \le \alpha \le 90°$	$0° \le \phi \le 360°$			PITCH/YAW	/		
AERAM	$1.2 \le M_\infty \le 5$	$\alpha \le 30°$	$\phi \le 0°, 45°$		/	$\delta \le 40°$		CN, Cm	Cmq, Cmα̇
AMI300	$M_\infty \ge 3.0$	$0 \le \alpha \le 180°$	$\phi = 0°$		/	$\delta \le 15°$	/	CN, Cm	/
BAKER	$0.6 \le M_\infty \le 3.0$	$0 \le \alpha \le 180°$	$\phi = 0°$	/	/	/	/	CN, Cm	/
BDV/NCV	$4 \le M_\infty \le 12$	$\alpha \le 2°$	$\phi = 0°$	/	/	/			/
CARENG	$M_\infty \le 4$	$\alpha \le 20°$	$\phi = 0°$		/	/	/	CN, Cm	/
CASAERO	$M_\infty \le 4.0$	$\alpha \le 30°$	$\phi = 0°$			$\delta \le 25°$	/	CN, Cm	
DOPRAM	$M_\infty \le 4.0$	$\alpha \le 90°$	$0° \le \phi \le 360°$			PITCH/YAW		CN, Cm Cy, Cn	
DRAG	$M_\infty \le 7.0$	$\alpha = 0°$	/			/		/	/
DTMB	$0.6 \le M_\infty \le 3.0$	$\alpha \le 20°$	$\phi = 0°$		/	$\delta \le 10°$			/
MAP	$M_\infty \le 8.0$	$\alpha \le 15°$	$0° \le \phi \le 90°$			$\delta \le 15°$			/
MASP	$M_\infty \le 3.0$	$\alpha \le 15°$	$\phi \le 0°, 45°$		/	δ pitch $\le 15°$			
MISSILE DATCOM	$M_\infty \le 8.0$	$\alpha \le 30°$	$0° \le \phi \le 360°$			$\delta \le 20°$			
MISSILE aerospatiale	$M_\infty \le 4$	$\alpha \le 25°$	$0° \le \phi \le 360°$			$\delta \le 15°$			
MISSILE ONERA	$M_\infty \le 4$	$\alpha \le 25°$	$0° \le \phi \le 360°$			$\delta \le 15°$	/		/
MISSILE 1 NEAR	$M_\infty \le 4$	$\alpha \le 45°$	$0° \le \phi \le 360°$		/		CAw, CAf		/
MISSILE 2A NEAR	$M_\infty \le 5$	$\alpha \le 45°$	$0° \le \phi \le 90°$			$\delta \le 15°$	/		/
MISSILE 3 NEAR	$M_\infty \le 4.5$	$\alpha \le 45°$	$0° \le \phi \le 90°$			$\delta \le 40°$	/		/
MRRT	$M_\infty \le 5$	$\alpha = 0°$	$\phi = 0°$	/	/	/		/	/
NFR	$M_\infty \le 5$	$-90° \le \alpha \le 90°$	$-180° \le \phi \le 180°$		/		/	CN, Cm Cy, Cn	/
NSWC-AP	$M_\infty \le 8.0$	$\alpha \le 15°$	$\phi = 0°$		/	δ pitch $\le 20°$		CN, Cm	
PORTANCE	$M_\infty \le 4.0$	$\alpha \le 2°$	/		/	/	/	CN, Cm	/
SEA DATCOM	$M_\infty \le 8.0$	$\alpha \le 30°$	$\phi = 0°$		/				
S/HABP	$M_\infty \le 2.0$	$-90° \le \alpha \le 90°$	$0° \le \phi \le 360°$			$\delta \le 20°$	CAw, CAf		/
TAD	$M_\infty \le 8.0$	$\alpha \le 2°$	$\phi = 0°$		/	/	/	CN, Cm	Cmq, Clp
TASK2	$M_\infty \le 4.2$	$\alpha \le 20°$	$\phi = 0°, 45°$			$\delta \le 15°$			Cmq, Clp
TRAIFRO	$M_\infty \le 4.0$	$\alpha = 0°$	/			/		/	/
AP93	$0 \le M_\infty \le \infty$	$\alpha \le 30°$	$\phi = 0°$		/	δ pitch $\le 30°$		CN, Cm	

(shaded) Computed / For no

TABLE 1-8. CAPABILITIES OF FULL POTENTIAL CODES FOR MISSILES[10]

1CF: ONE CRUCIFORM-FINNED SECTION 2CF: TWO " " " 3CF: THREE " " " DD: DOUBLE DIAMETER					CONVENTIONAL (circular cruciform cross section shapes)			UNCONVENTIONAL (arbitrary cross section shapes)		
					CLASSICAL		BOOSTED	LIFTING	AIRBREATHING	
							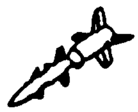		 INTAKES	
CODE NAME	ORIGIN	REF N°	DATE	MACH	1CF	2CF	DD + 3CF	ELLIPTIC	OPEN	CLOSED
SANDRAG	SANDIA (USA)	27 28	1985	< 1	Drag only		/	/	/	/
				> 1	/	/	/	/	/	/
SIMP	ROCKWELL (USA)	29	1986	< 1	/	/	/	/	/	/
				> 1	C	C	C	C	C	C

(shaded) Configuration type has been computed   /For no   C Configuration type could be computed

TABLE 1-9. CAPABILITIES OF LINEARIZED POTENTIAL CODES FOR MISSILES[10]

1CF: ONE CRUCIFORM-FINNED SECTION
2CF: TWO " " "
3CF: THREE " " "
DD: DOUBLE DIAMETER

						CONVENTIONAL			UNCONVENTIONAL		
						CLASSICAL		BOOSTED	LIFTING	AIRBREATHING	
										 INTAKES	
CODE NAME	ORIGIN	REF N°	DATE	VORTEX	MACH	1CF	2CF	DD + 3CF	ELLIPTIC	OPEN	CLOSED
DEMON/ LRCDM	NEAR (USA)	30		FS + BFS + TRW	< 1	/	/	/	/	/	/
					> 1			C			
DMOINL	NEAR (USA)	31	1986	FS + TRW	< 1	/	/	/	/	/	/
					> 1			/	C		
HISSS	MBB (FRG)	32	1985		< 1						
					> 1						
HOP	FFA (SW)	33	1983		< 1	C	/	/	C	/	/
					>	C	/	/	C	/	/
METSING	CITEFA (ARG)		1986		< 1	C	/	/	/	/	/
					> 1	/	/	/	/	/	/
NANC	NSWC (USA)	34	1987		< 1	/	/	/	/	/	/
					> 1						/
NFKRSUB/ SUP	MBB (FRG)	35	1980 1982	BFS	< 1		/	/	/	/	/
					> 1		/	/	/	/	/
NLRAERO	NLR (NL)	36		1980	< 1						
					> 1						
NLVLM	TECHNION (Israel)		1983	FS + TRW	< 1				C	/	C
					> 1	/	/	/	/	/	/
NWCDM/ NSTRN	NEAR (USA)	37	1986	BFS + TRW	< 1	/	/	/	/	/	/
					> 1			/	/	/	/
PANAIR	BOEING (USA)	38	1984		< 1	C	C	C	C	C	C
					> 1			C	C	C	C
PANEL	DORNIER (FRG)		1985		< 1			C		C	C
					> 1	/	/	/	/	/	/
PHOBOS	SAAB (SW)	39	1984		< 1	C	C	C	C	C	C
					> 1	/	/	/	/	/	/
ORFL/ DEMONI	MBB/ NIELSEN (FRG)/(USA)	40 41	1985	BFS	< 1			/	/	/	/
					> 1			/	/	/	/
SPARV	BAe (UK)		1980		< 1			C	C	C	C
					> 1	/	/	/	/	/	/
USSAERO	NASA (USA)		1973		< 1		C	C		/	/
					> 1		C	C		/	/
VORLAX	LOCKHEED (USA)		1977		< 1					/	/
					> 1			C		/	/
WBC	MBB (FRG)	42	1985	BFS	< 1					/	
					> 1	/	/	/	/	/	/
WING BODY	NASA/FFA (USA)/(SW)	43	1982		< 1			/	/	/	/
					> 1			/	/	/	/

Configuration type has been computed — TRW: Trailing edge Wake Relaxation
C — Configuration type could be computed — FS: Fins with vortex separation (panel method - vortex model)
/ — For no — BFS: Body & Fins with vortex separation

TABLE 1-10. CAPABILITIES OF EULER CODES FOR MISSILES[10]

1CF: ONE CRUCIFORM-FINNED SECTION
2CF: TWO " " "
3CF: THREE " " "
DD: DOUBLE DIAMETER

					CONVENTIONAL (circular cruciform cross section shapes)			UNCONVENTIONAL (arbitrary cross section shapes)		
					CLASSICAL		BOOSTED	LIFTING	AIRBREATHING	
							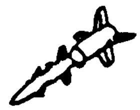		 INTAKES	
CODE NAME	ORIGIN	REF N°	DATE	MACH	1CF	2CF	DD + 3CF	ELLIPTIC	OPEN	CLOSED
EAGLE	USAF ARMAMENT LAB. (USA)	43	1987	< 1		C	C	C	/	C
				> 1		C	C	C	/	C
EUFLEX	MBB (FRG)	44	1984	< 1		C	C		C	C
				> 1		C	C		C	C
EULBMG	DORNIER (FRG)		1983	< 1		C	C			C
				> 1		C	C	C		C
EULER3D	MATRA (FR)	45	1985	< 1	C	C	C	C	C	C
				> 1			C	C	C	C
EULSSM	DORNIER (FR)		1985	< 1	/	/	/	/	/	/
				> 1		C	C		C	C
FLU3C	ONERA aerospatial (FR)	46 47	1986	< 1	C	C	C	C	C	C
				> 1						
KODIAK	USAF ARMAMENT Lab./Miss. State	48	1986	< 1			C	C	/	/
				> 1		C	C	C	/	/
MISSILE	NASA ARC (USA)		1972	< 1	/	/	/	/	/	/
				> 1					C	C
MUSE	NSWC (USA)	49	1985	< 1	/	/	/	/	/	/
				> 1					C	C
SANDIAC	SANDIA General Electric (USA)	50	1986	< 1	/	/	/	/	/	/
				> 1						
SWINT	NSWC (USA)	51	1982	< 1	/	/	/	/	/	/
				> 1						
WINGA2	FFA (SW)	43	1983	< 1	C	C	C	C	C	C
				> 1	C	C	C	C	C	C
ZEUS	NSWC (USA)	52	1986	< 1	/	/	/	/	/	/
				> 1					C	C

(shaded) Configuration type has been computed /For no C Configuration type could be computed

TABLE 1-10. CAPABILITIES OF EULER CODES FOR MISSILES[10] (CONTINUED)

CODE NAME	EQUATIONS: STEADY OR UNSTEADY (1)	EQUATIONS: CONSERVATIVE OR NON CONS. FORM (1)	METHOD: FINITE-VOLUMES FINITE-DIFFERENCE FINITE-ELEMENTS (1)	NUMERICAL SCHEME: IMPLICIT OR EXPLICIT (1)	NUMERICAL SCHEME: CENTERED OR NON-CENT. (1)	NUMERICAL SCHEME: ORDER OF ACCURACY: TIME	NUMERICAL SCHEME: ORDER OF ACCURACY: SPACE	MESH: STRUCTURED OR NON-STRUCT. (1)	MACH: < 1 (2)	MACH: > 1 (2)	NOTES ABOUT SEPARATION (KUTTA CONDITION)
EAGLE	U	C	FV	I	NC	1	2	S	*	*	
EUFLEX	U	C	FV	E + I	NC	1-2	1-4	NS	*	*	
EULBMG	U	C	FV	E	C	2	2	S	*	*	SSS
EULER3D	U	C	FV	E	C	2	2	S	*	*	SSS
EULSSM	S	C	FV	I	C	/	2	NS	/	*	
FLU3C	U	C	FV	E	NC	2	2	S	*	*	SSS
KODIAK	S	C	FV	E	NC	/	2	S	/	*	
MISSILE	S	C	FD	E	C	/	2	S	/	*	
MUSE	S	C	FD	E	C	/	2	S	/	*	SSS
SANDIAC	S	C + NC	FD	E	NC	/	2	S	/	*	
SWINT	S	C	FD	E	C	/	2	S	/	*	SSS
WINGA2	U	C	FV	E	C	2	2	S	*	*	
ZEUS	S	C	FV	E	NC	/	2	S	/	*	SSS

(1) Only the first letter(s)
(2) * for YES
/ for NO
SSS Separation on Smooth Surface with Kutta Condition

TABLE 1-11. CAPABILITIES OF FULL NAVIER-STOKES CODES FOR MISSILES[10]

1CF: ONE CRUCIFORM-FINNED SECTION
2CF: TWO " " "
3CF: THREE " " "
DD: DOUBLE DIAMETER

						CONVENTIONAL ([illegible])			UNCONVENTIONAL ([illegible])		
						CLASSICAL		BOOSTED	LIFTING	AIRBREATHING	
										 INTAKES	
CODE NAME	ORIGIN	REF N°	DATE	LAMINAR TURBULENT	MACH	1CF	2CF	DD + 3CF	ELLIPTIC	OPEN	CLOSED
ARC3D	NASA ARC (USA)			L&T	< 1	C	C	C	C	C	
					> 1		C	C	C	C	
F3D	NASA ARC (USA)		1985	L&T	< 1	C	C	C	C	C	C
					> 1		C	C	C	C	C
NASBMG	DORNIER (FRG)		1987		< 1	C	C	C	C	C	C
					> 1	C	C	C	C	C	C
UWIN	NASA ARC (USA)		1987	L&T	< 1	C	C	C	C	C	C
					> 1		C	C	C	C	C
CFL3DE	NASA	53	1987	L&T	≥ 0		C	C	C	C	C
GASP	VPI	54, 55	1990, 1992	L&T	≥ 0		C	C	C	C	C

Configuration type has been computed   C Configuration type could be computed

TABLE 1-12. CAPABILITIES OF PARABOLIZED NAVIER-STOKES CODES FOR MISSILES[10]

1CF: ONE CRUCIFORM-FINNED SECTION
2CF: TWO " "
3CF: THREE " "
DD: DOUBLE DIAMETER

						CONVENTIONAL ([illegible])			UNCONVENTIONAL ([illegible])		
						CLASSICAL		BOOSTED	LIFTING	AIRBREATHING	
										 INTAKES	
CODE NAME	ORIGIN	REF N°	DATE	LAMINAR TURBULENT	MACH	1CF	2CF	DD + 3CF	ELLIPTIC	OPEN	CLOSED
PNS (basic version)	NASA ARC (USA)	56 57	1979 1984	L&T	> 1		C	C		C	C
PNSFVM	DORNIER (FRG)		1986	L	> 1		C	C		C	C

(shaded) Configuration type has been computed C Configuration type could be computed

2.0 CONVENTIONAL APPROXIMATE AERODYNAMIC METHODS

This section of the report will review some of the more important approximate aerodynamic methods that have proved quite useful in the development of semiempirical codes. Time and space will not permit derivation of the methods from first principles. However, appropriate references will be given for the interested reader. The approach taken here, in the presentation of the material, will be to mention the assumptions inherent in each method, relevant equations, and possibly show an example or two as may be warranted.

2.1 HYBRID THEORY OF VAN DYKE (HTVD)[58]

The Hybrid Theory of Van Dyke[58] combines a second-order solution to the potential equation with a first-order crossflow solution first espoused by Tsien[59]. The advantage of this method is that it gives second-order accuracy in the axial direction where first-order accuracy is generally unacceptable for drag computations. On the other hand, first-order accuracy in the crossflow plane is typically acceptable for normal force and center of pressure computations. The fundamental reason for this is that perturbations in the flow, due to the presence of a body, have more impact in the axial as opposed to the normal force direction. Hence, to get axial force accuracy compatible with a goal of ± 10 percent require second-order methods, whereas ± 10 percent accuracy on C_N can be obtained with first-order methods in many cases.

As already mentioned, the Hybrid theory comes from the potential equation of fluid mechanics. It is limited to supersonic flow (we have used this method down to $M_\infty = 1.2$) where the assumption of isentropic flow (shock waves are weak) can be made. This typically limits the upper Mach number range to about $M_\infty = 2.0$ to 3.0, depending on the body shape. Also, the slope of the body surface must be less than the Mach Angle. The Tsien solution, or crossflow part of the solution, comes from the linearized perturbation equation. On the other hand, the second-order solution to the axial flow is found by obtaining a particular solution to a reduced version of the full potential equation. This is the key to the accuracy improvement afforded by Van Dykes solution in that some of the nonlinearity inherent in the axial flow problem is brought into the solution by this process. The beauty of the Van Dyke method is that this particular second-order solution is given entirely in terms of the first-order solution. That is, one simply solves the first-order perturbation solution for the axial flow and then solves an algebraic equation for the second-order solution where the boundary condition at the body is satisfied.

In equation form, the general first-order perturbation problem is [58]:

$$\Phi_{rr} + \Phi_r/r + \Phi_{\phi\phi}/r^2 - (M_\infty^2 - 1)\Phi_{xx} = 0 \tag{1}$$

with boundary conditions that do not allow any upstream disturbances:

$$\Phi\ (0, r, \phi) = \Phi_x\ (0, r, \phi) = 0 \tag{1a}$$

and that require the flow to be tangent to the body surface:

$$\Phi_r\ (x, r_b, \phi) + \sin\alpha\ \cos\phi = \frac{dr}{dx}\,[\cos\alpha + \Phi_x\ (x, r_b, \phi)] \tag{1b}$$

The subscripts in Equation (1) indicate partial derivatives. The solution to Equation (1) is satisfied identically by:

$$\Phi\ (x, r, \phi) = \Psi_1(x, r)\ \cos\alpha + \zeta_1\ (x, r)\ \sin\alpha\ \cos\phi \tag{2}$$

The first term of Equation (2) is the first-order axial solution, and the second term is the first-order crossflow solution. Since the equation is linear, these two solutions can be found independently, and then added together. The axial solution, Ψ_1 (x, r), for a general body is found by placing a series of sources and sinks along the x axis and satisfying the boundary conditions at each point. The crossflow solution, ζ_1(x, y), is found by placing a series of doublets along the axis, again satisfying the boundary conditions.

The particular second-order solution that Van Dyke found for the reduced full potential equation is

$$\Psi_2 = M_\infty^2\ [\Psi_{1x}\ (\Psi_1 + Nr\Psi_{1r}) - (\frac{r}{4})\ \Psi_{1r}^3]\ \text{where}\ N = (\frac{\gamma + 1}{2})\ \frac{M_\infty^2}{\beta^2} \tag{3}$$

Second-order axial velocity components Ψ_{2x} and Ψ_{2r} are also defined in terms solely of the first-order solution Ψ_1(x,r).

Once the second-order axial perturbation velocity components Ψ_{2x}, Ψ_{2r} are computed, along with the first-order crossflow components ζ_{1x} and ζ_{1r}, the total perturbation velocities are then:

$$\frac{u}{V_\infty} = (\cos\alpha)\ (1+\Psi_{2x}) + (\sin\alpha\ \cos\phi)\ \zeta_{1x} \tag{4a}$$

$$\frac{v}{V_\infty} = \cos\alpha\ (\Psi_{2r}) + (\sin\alpha\ \cos\phi)\ (1 + \zeta_{1r}) \tag{4b}$$

$$\frac{w}{V_\infty} = -(\sin\alpha\ \sin\phi)\ (1 + \frac{\zeta_1}{r}) \tag{4c}$$

The pressure coefficient at each body station is then:

$$C_p\ (x,\phi) = \frac{2}{\gamma M_\infty^2}\left\{\left[1 + \frac{\gamma - 1}{2} M_\infty^2 \left(1 - \frac{u^2 + v^2 + w^2}{V_\infty^2}\right)\right]^{\frac{\gamma}{\gamma - 1}} - 1\right\} \tag{5}$$

Finally the force coefficients are:

$$C_A = \frac{2}{\pi r_r^2}\int_0^\ell \int_0^\pi C_p\ (x,\ \phi)\ \frac{rdr}{dx}\ d\phi\ dx \tag{6}$$

$$C_N = -\frac{2}{\pi r_r^2}\int_0^\ell \int_0^\pi C_p\ (x,\ \phi)\ \cos\ (\phi)\, r\ d\phi\ dx \tag{7}$$

$$C_M = \frac{1}{\pi r_r^3}\int_0^\ell \int_0^\pi C_p\ (x,\ \phi)\ \cos\ (\phi)\, x\ r\ d\phi\ dx \tag{8}$$

and the center of pressure in calibers from the nose is

$$X_{C_p} = -C_M/C_N \tag{9}$$

It should be pointed out that in the actual numerical integration of Equations (6), (7), and (8) the integration must be carried out in segments of the body between each discontinuity due to the discontinuous pressure distribution.

Also, the hybrid theory of Van Dyke is limited to pointed bodies of revolution. Bluntness will be considered later.

2.2 SECOND-ORDER-SHOCK-EXPANSION THEORY (SOSET)

First-order Expansion Theory was first proposed by Eggers et al. for bodies of revolution flying at high supersonic speeds.[61-63] Basically, the Shock-expansion Theory computes the flow parameters at the leading edge of a two-dimensional (2-D) surface with the oblique shock wave relations and with the solution for a cone at the tip of a three-dimensional (3-D) body. Standard Prandtl-Meyer Expansion (PME) is then applied along the surface behind the leading edge or tip solution to get the complete pressure distribution over the body surface. Referring to Figure 2-1, this theory inherently assumes that the expansion waves created by the change in curvature around the body are entirely absorbed by the shock and do not reflect back to the body surface. Since the theory assumes constant pressure along one of the conical tangent elements of the surface, fairly slender surfaces must be assumed or many points along the surface assumed to obtain a fairly accurate pressure distribution. Another way of stating this is to minimize the strength of the disturbance created by Mach waves emanating from the expansion corner and intersecting the shock, the degree of turn should be small.

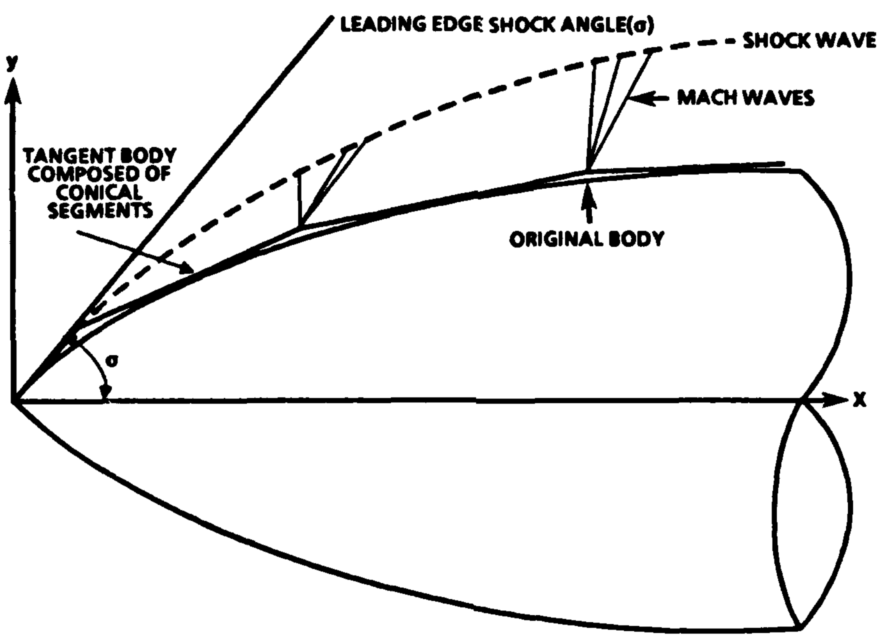

FIGURE 2-1. APPROXIMATION OF TRUE BODY BY ONE COMPOSED OF STRAIGHT LINE SEGMENTS TANGENT TO SURFACE

Syvertson (et al.) extended the generalized Shock-expansion Theory on pointed bodies and sharp airfoils to what he called a second-order theory.[60] He defined the pressure along a conical frustum by

$$p = p_C - (p_C - p_2)\, e^{-\eta} \tag{10}$$

instead of a constant on each segment as was the case in the generalized theory. Here P_c is the pressure on a cone with the given cone half angle equal to the slope of the conical segment with respect to the axis of symmetry. p_2 is the pressure just aft of a conical segment (see Figure 1) which is calculated from a Prandt Meyer Expansion (PME) of the flow around a corner (as shown in Figure 2-2, going from points 1 and 3 to points 2 or 4, for example).

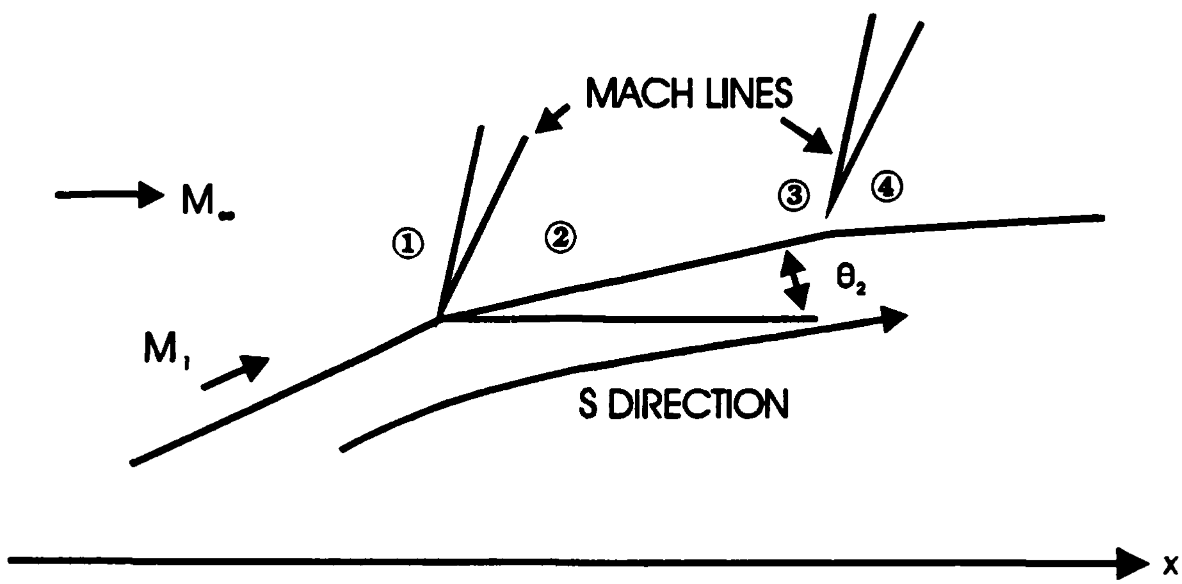

FIGURE 2-2. FLOW ABOUT A FRUSTUM ELEMENT

Also

$$\eta = \frac{\left(\frac{\partial p}{\partial s}\right)_2 (s - s_2)}{p_C - p_2} \tag{10a}$$

Thus, examining p from Equation (10), it can be seen, for example, on the frustrum element in Figure 2-2 that the pressure varies from the pressure of the generalized theory at point 2 to that of a cone of angle θ_2 and Mach number M_2 as s gets large. Syvertson and Dennis approximated the pressure gradient as[60]

$$\left(\frac{\partial p}{\partial s}\right)_2 = \frac{B_2}{r}\left(\frac{\Omega_1}{\Omega_2}\sin\theta_2 - \sin\theta_2\right) + \frac{B_2}{B_1}\,\frac{\Omega_1}{\Omega_2}\left(\frac{\partial p}{\partial s}\right)_1 \tag{11}$$

where

$$B_{1,2} = \frac{\gamma p_{1,2} M_{1,2}^2}{2\,(M_{1,2}^2 - 1)}$$

$$\Omega_{1,2} = \frac{1}{M_{1,2}} \left[\frac{1 + \frac{\gamma - 1}{2} M_{1,2}^2}{\frac{\gamma + 1}{2}} \right]^{\frac{\gamma+1}{2(\gamma-1)}}$$

Finally, for negative angles such as would occur on a boattailed configuration, p_c was replaced by p_∞. No discussion was given for blunt bodies. It should be noted that if η of Equation (10) becomes negative, the SOSET reverts to the generalized or first-order Shock-expansion Theory. This is because Equation (10) will not give the correct asymptotic cone solution for negative values of η.

Experience has shown that SOSET gives very good pressure distributions for low to moderate angles of attack and at $M_\infty \geq 2$. As Mach numbers decrease below about 2.5, the SOSET becomes increasingly inaccurate until about $M_\infty = 1.5$, where the accuracy is generally unacceptable. This applicable Mach number range is very complimentary to the Hybrid Theory of Van Dyke where the accuracy is best between $1.2 \leq M_\infty \leq 2.5$.

2.3 MODIFIED NEWTONIAN THEORY (MNT)

Newtonian Impact Theory assumes that, in the limit of high Mach number, the shock lies on the body. This means that the disturbed flow field lies in an infinitely-thin layer between the shock and body. Applying the laws of conservation of mass and momentum across the shock yields the result that density behind the shock approaches infinite values and the ratio of specific heats approaches unity. The pressure coefficient on the surface becomes[64]

$$C_p = 2\sin^2\delta_{eq} \qquad (12)$$

where δ_{eq} is the angle between the velocity vector and a tangent to the body at the point in question (see Figure 2-3). δ_{eq} is defined by:

$$\sin(\delta_{eq}) = \sin\phi\,\sin\alpha - \sin\alpha\,\cos\phi\,\cos\theta \qquad (13)$$

Lees[12] noted that a much more accurate prediction of pressure on the blunt-nose body could be obtained by replacing the constant "2" in Equation (12) with the stagnation pressure coefficient C_{p_o}. C_{p_o} can be calculated from:

$$C_{p_0} = \frac{2}{\gamma M_\infty^2}\left\{\left[\frac{(\gamma + 1) M_\infty^2}{2}\right]^{\frac{\gamma}{\gamma - 1}}\left[\frac{\gamma + 1}{2\gamma M_\infty^2 - (\gamma - 1)}\right]^{\frac{1}{\gamma - 1}} - 1\right\} \tag{14}$$

MNT is thus defined by:

$$C_p = C_{p_o} \sin^2\delta_{eq} \tag{15}$$

Equation (15) allows the calculation of the pressure coefficient all along the blunt surface of a missile nose or wing leading edge for a perfect gas where C_{p_o} is given by Equation (14) and sin δ_{eq} from Equation (13).

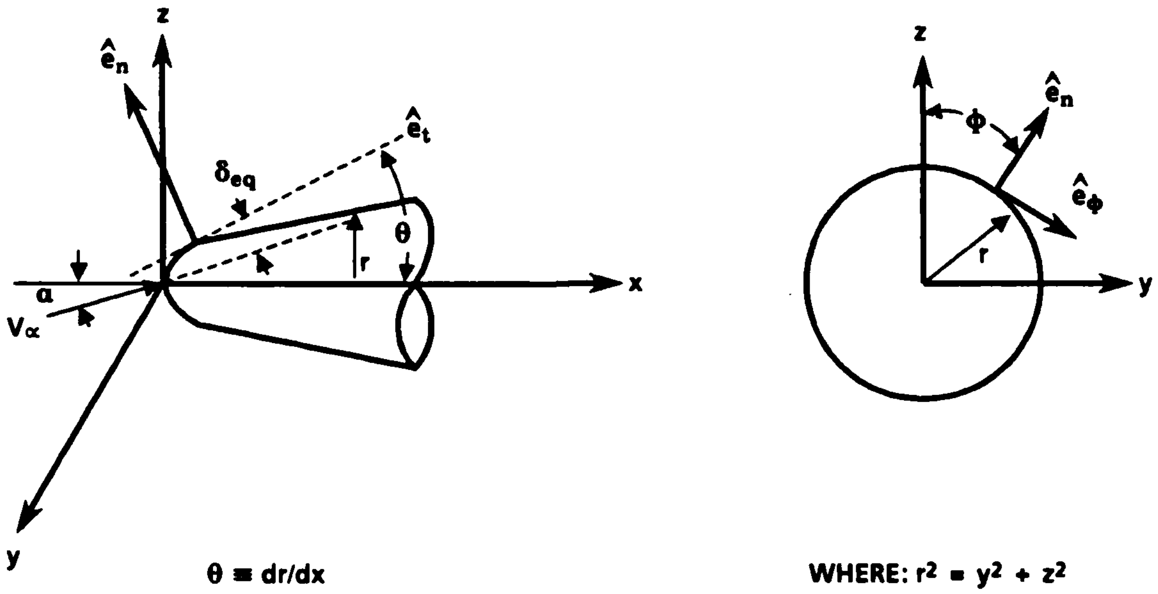

FIGURE 2-3. NOMENCLATURE USED FOR DETERMINATION OF ANGLE δ_{eq}

Experience has shown that the MNT gives very acceptable estimates of pressure coefficient on the blunt portion of a nose or leading edge, even at Mach numbers where the assumptions of Newtonian Impact Theory are violated.

2.4 HYBRID THEORY OF VAN DYKE COMBINED WITH MODIFIED NEWTONIAN THEORY (HTVD/MNT)[1]

As noted in the discussion on the Hybrid Theory, it is limited to conditions where the body slope is less than the local Mach angle. This means it is not applicable in the nose region of a blunt missile. On the other hand, MNT gives very acceptable estimates of pressure coefficients in the nose region, even for low supersonic Mach numbers where the assumptions, inherent in the Newtonian Impact Theory, are violated. Moore[1] was the first to recognize the possibility of combining these two theories. The key to the successful combination was in the starting solution. At low supersonic Mach numbers, the pressure overexpands on a blunt nose tip as it proceeds around the blunt portion from the stagnation point to the given portion of the nose. In order to capture this overexpansion, Moore found that it was necessary to start the HTVD near its maximum acceptable slope and allow the pressure to expand around the surface.[1] Simultaneously, the MNT was started at the stagnation point and allowed to expand until the pressure coefficients of the MNT and the HTVD were equal. This was defined as the Match point. Upstream of the Match point, MNT was used in the force and moment calculations, whereas downstream, HTVD was used. Figure 2-4 is an illustration of the boundaries of perturbation and Newtonian theories. Figures 2-5 and 2-6 illustrate the capability of this theory to accurately predict pressure coefficients on a 35 percent blunt cone of 11.5° half angle at $\alpha = 8°$ and at $M_\infty = 1.5$ and 2.96. Note the excellent agreement of the combined theory all along the surface at $M_\infty = 1.5$. Particularly impressive is its ability to capture the overexpansion region around $x = 0.1$ to $x = 0.4$. Also, note that SOSET gives fairly poor estimates at $M_\infty = 1.5$. On the other hand, at $M_\infty = 2.96$, the HTVD/MNT is no better (and maybe slightly worse) than the SOSET/MNT, which will be discussed next.

To the authors knowledge, the HTVD/MNT remains the only accurate engineering method to estimate low supersonic Mach number aerodynamics for blunt and sharp tip bodies of revolution. Attempts were made to extend the SOSET/MNT down to the low supersonic Mach number range, but without success.

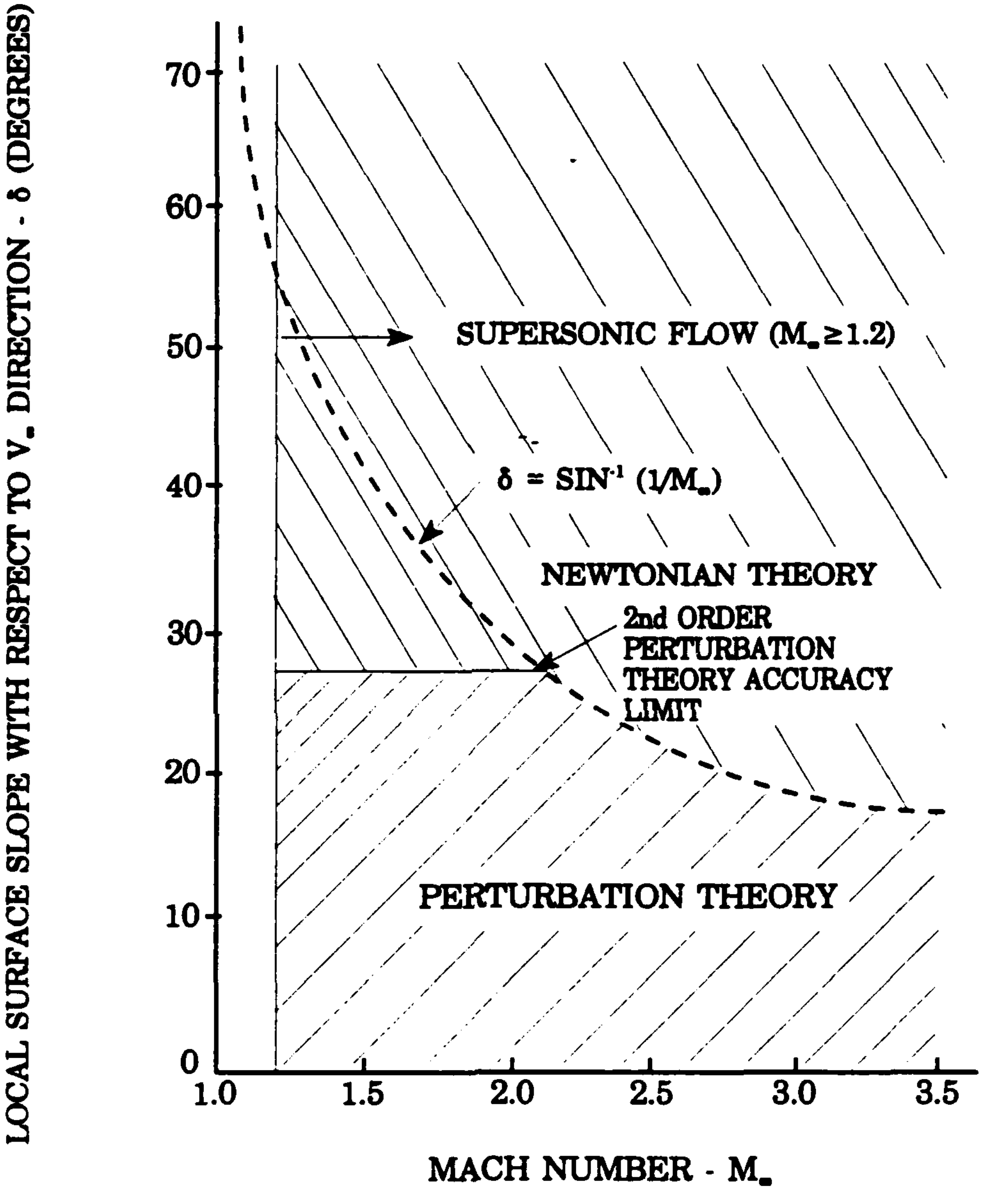

FIGURE 2-4. BOUNDARIES OF PERTURBATION AND NEWTONIAN THEORY

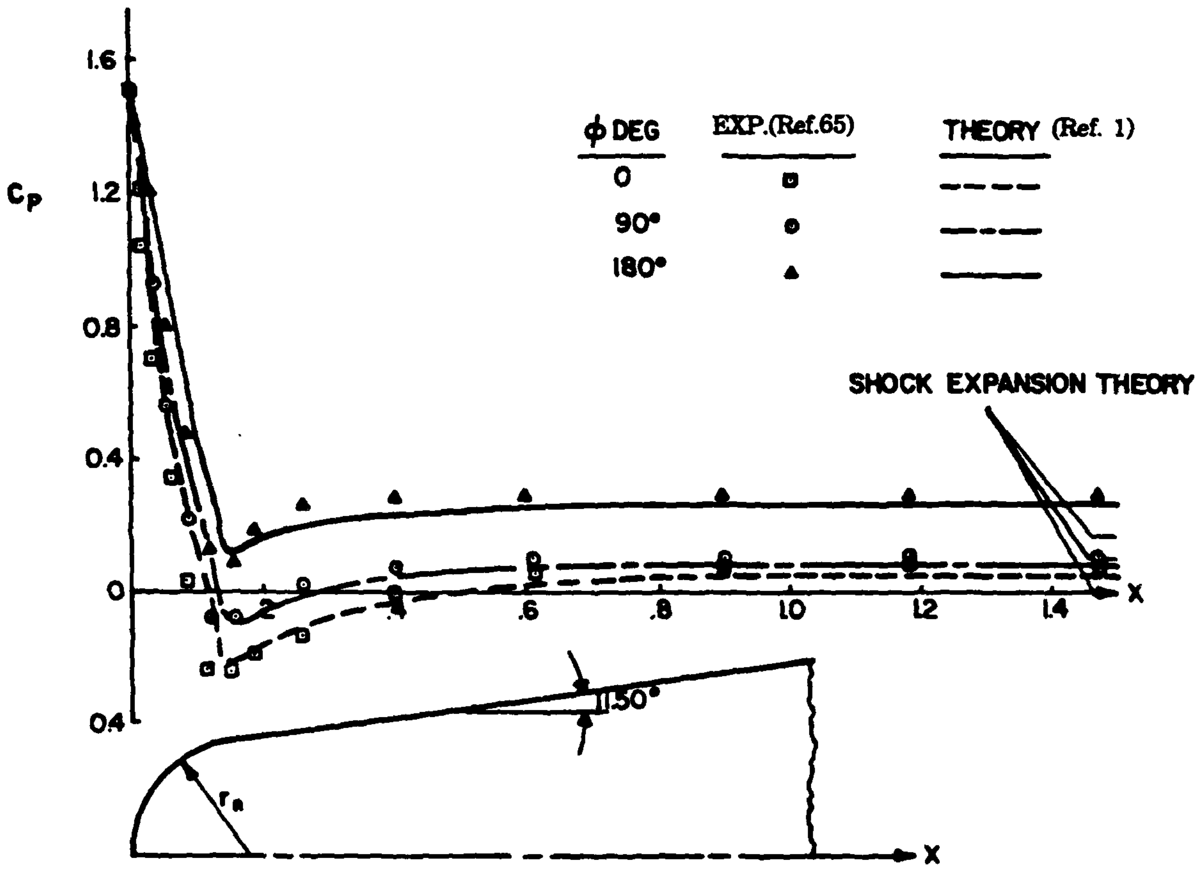

FIGURE 2-5. COMPARISON OF THEORY AND EXPERIMENT FOR BLUNTED CONE

$$\frac{r_n}{r_B} = 0.35,\ M_\infty = 1.5,\ \alpha = 8^\circ,\ \theta_c = 11.5^\circ$$

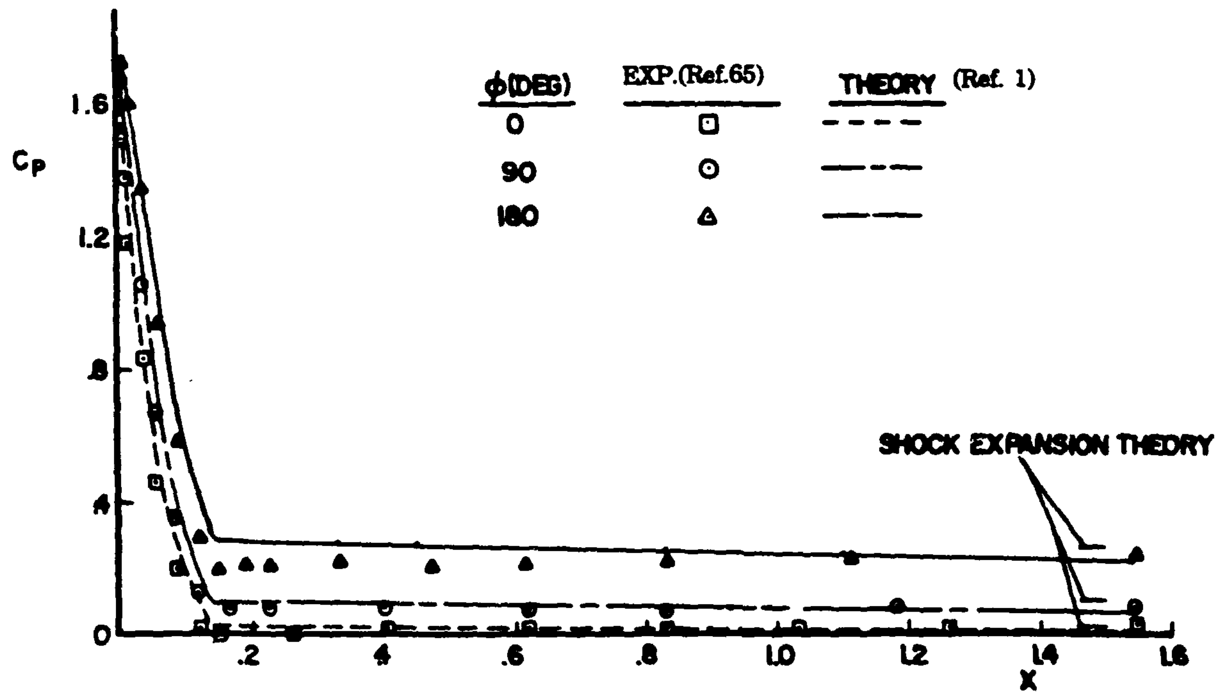

FIGURE 2-6. COMPARISON OF THEORY AND EXPERIMENT FOR BLUNTED CONE

$$\frac{r_n}{r_B} = 0.35,\ M_\infty = 2.96,\ \alpha = 8°, \theta_c = 11.5°$$

2.5 SECOND-ORDER-SHOCK-EXPANSION THEORY COMBINED WITH MODIFIED NEWTONIAN THEORY (SOSET/MNT)[65-68]

Jackson et al.[65] combined SOSET with MNT to treat blunt-nosed configurations with or without flares. Jackson et al.[65], like Syvertson and Dennis[60], assumed that the lifting properties could be predicted by assuming that the original body is made up of several equivalent bodies of revolution represented by the various meridians (see Figure 2-7). They assumed the match point between the MNT and second-order shock pressure prediction to be the angle that corresponds to shock detachment on a wedge with the given freestream Mach number.

De Jarnette et al.[66-68] made significant improvements to the work of Jackson et al.[65] and Syvertson.[60] These new improvements included the following:

1. An exact (as opposed to an approximate) expression for the pressure gradient downstream of a corner.

2. A new expression for pointed-cone pressures at angle of attack which improves the initial pressure prediction over that of tangent cone theory.

3. A new technique for calculating pressures on bodies at incidence.

The pressure computations at angle of attack, showed improvement over the method of Jackson[65], De Jarnette, el al.[23] derived a new expression for pointed-cone pressure at $\alpha > 0$ by combining Slender Body Theory, Newtonian Theory, and an approximate expression for $C_{p_{\alpha=0}}$ to give:

$$C_p(\alpha,\theta,\phi,M) = C_{p_{\alpha=o}} + \Delta C_p \tag{16a}$$

where

$$\Delta C_p = -\sin 2\alpha \sin 2\theta \cos\Phi + \sin^2\alpha \cos^2\theta \left[\left(2-\frac{1}{\beta}\right)(1-\tan^2\theta) - \left(2+\frac{2}{\beta}\right)\sin^2\Phi\right] \tag{16b}$$

$$C_{p_{\alpha=0}} = \sin^2\theta_c\left[1+\frac{(\gamma+1)K^2+2}{(\gamma-1)K^2+2}\,\ln\left(\frac{\gamma+1}{2}+\frac{1}{K^2}\right)\right] \tag{16c}$$

and

$$K^2 = (M_\infty^2 - 1)\sin^2\theta_c$$

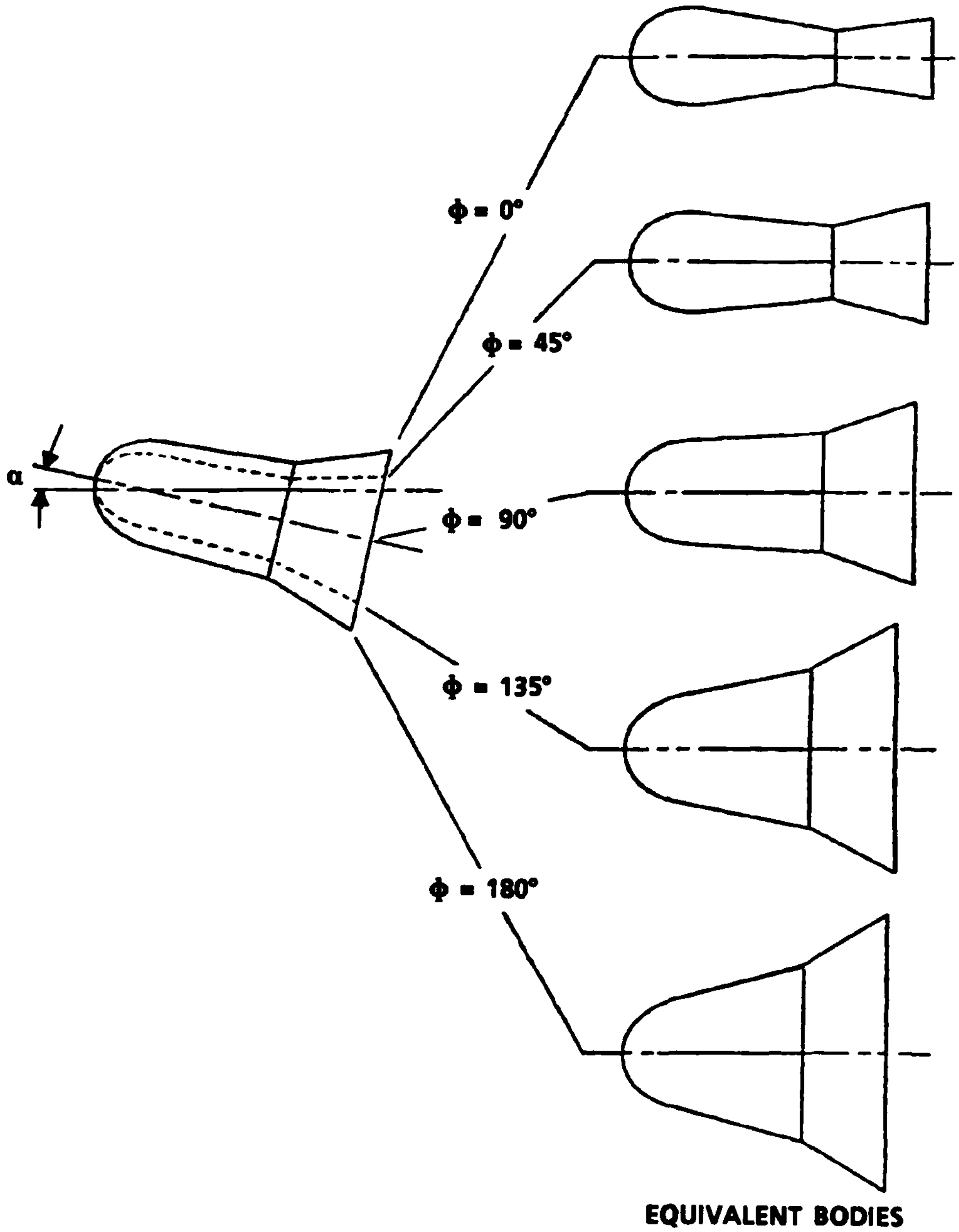

FIGURE 2-7. TYPICAL EQUIVALENT BODY SHAPES USED FOR COMPUTING LIFTING PROPERTIES WITH SECOND-ORDER SHOCK EXPANSION THEORY

Note also, that while Equation 16 was strictly defined for pointed cone pressures at angle of attack, it could also be used in a Tangent cone sense to obtain pressures at any point on a body surface. De Jarnette actually used loading functions to obtain body alone lift properties, however[68].

Figure 2-8 presents results of De Jarnette et al [68] compared to experiment. The case chosen is the same case shown in Figure 2-6, except here, the method of De Jarnette et al [68] is used versus Jackson et al[65] in Figure 2-6. While the two theories are close, in comparing Figure 2-8 with Figure 2-6, it is seen that the theory of De Jarnette et al[65] does show improvement in pressure prediction and therefore forces and moments as well.

2.6 ALLEN-PERKINS VISCOUS CROSSFLOW THEORY[69]

A fairly simple, yet quite powerful, method for computing body-alone nonlinear aerodynamics was introduced by Allen-Perkins[69]. Allen reasoned that the total force on an inclined body of revolution is equal to the potential term discussed previously plus a cross flow term. This term is based on the drag force experienced by an element of a circular cylinder of the same diameter in a stream moving at the cross component of the stream velocity, $V_\infty \sin \alpha$. This crossflow term is primarily created by the viscous effects of the fluid as it flows around the body, often separating and creating a nonlinear normal force coefficient. In equation form, the so called viscous crossflow theory is:

$$C_{N_{NL}} = \eta C_{d_c} \left(\frac{A_p}{A_{ref}} \right) \sin^2\alpha \tag{17}$$

Here η is the drag proportionality factor or crossflow drag of a cylinder of finite length to one of infinite length. C_{d_c} is the crossflow drag coefficient. Also, the crossflow theory assumes the center of pressure of the nonlinear term is at the centroid of the planform area. Generally, the total center of pressure is a weighted average of the linear and non linear components of normal force. That is

$$X_{cp} = \frac{(X_{cp})_{NL}\, C_{N_{NL}} + (X_{cp})_L\, C_{N_L}}{C_{N_{NL}} + C_{N_L}} \tag{18}$$

The pitching moment about a given point X_0 is then

$$C_M = -C_N (X_{cp} - X_0) \tag{19}$$

The original work of Allen did not include compressibility effects in η but Reynolds number effects were shown in C_{d_c} at low crossflow Mach numbers.

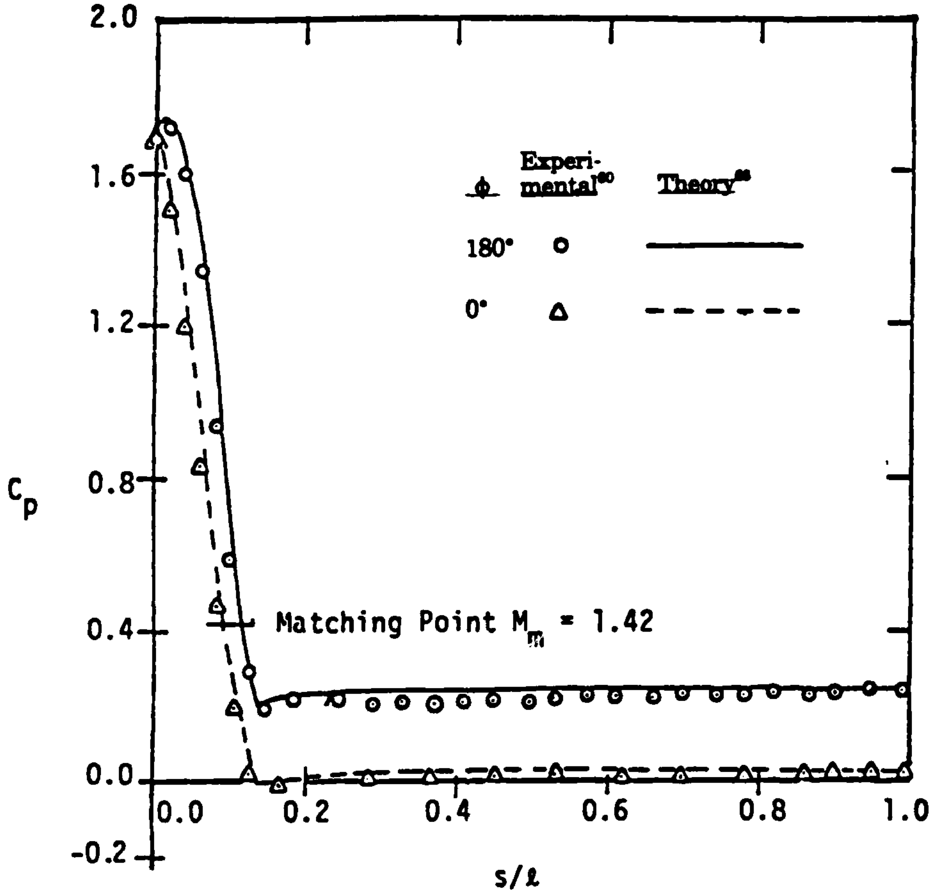

FIGURE 2-8. PRESSURE DISTRIBUTION ON A BLUNTED CONE

$\Theta_c = 11.5°$, $M_\infty = 2.96$, $\alpha = 8°$

2.7 VAN DRIEST II METHOD FOR SKIN FRICTION DRAG[70]

Another powerful, yet simple, method for performing computation, is the Van Driest II method for computing skin-friction drag. This method, as derived, is based on two dimensional turbulent boundary layer flow. Strictly speaking, it is only applicable to regions of flow on the lifting surfaces where the flow is turbulent, two dimensional, and the viscous region is primarily confined to a thin layer near the surface (boundary layer). In practice, however, it has been applied to two and three dimensional surfaces with success.

The turbulent mean skin-friction coefficient according to Van Driest[70] is:

$$\frac{0.242}{A\,(C_{f_\infty})^{1/2}} = (T_W/T_\infty)^{1/2}\,(\sin^{-1}C_1 + \sin^{-1}C_2) = \log_{10}(R_{e_\infty} C_{f_\infty}) - \left(\frac{1+2n}{2}\right)\log_{10}(T_W/T_\infty) \tag{20}$$

where

$$C_1 = \frac{2A^2 - B}{(B^2 + 4A^2)^{1/2}} \quad ; \quad C_2 = \frac{B}{(B^2 + 4A^2)^{1/2}}$$

and

$$A = \left[\frac{(\gamma-1)M_\infty^2}{2\dfrac{T_W}{T_\infty}}\right]^{1/2} \quad ; \quad B = \frac{1 + (\gamma-1)/2M_\infty^2}{T_W/T_\infty} - 1$$

The variable n of Equation (20) is the power in the power viscosity law:

$$\frac{\mu}{\mu_\infty} = \left(\frac{T_W}{T_\infty}\right)^n \tag{21}$$

The freestream Reynolds number and adiabatic wall temperature are given by:

$$R_{e_\infty} = \frac{\rho_\infty V_\infty \ell}{\mu_\infty} \tag{22}$$

$$\frac{T_w}{T_\infty} = 1 + 0.9 \frac{\gamma - 1}{2} M_\infty^2 \tag{23}$$

Equations (20) through (22) allow the calculation of the mean turbulent skin-friction over the entire body or wing area. The skin-friction axial force coefficient on each component is then:

$$C_{A_f} = C_{f_\infty} \frac{A_{wet}}{A_{ref}} \tag{23}$$

where A_{wet} is the surface area of the component in question.

For most flows, a portion of the flow is laminar. An approximation to the mean skin- friction coefficient for laminar flow can be obtained from[70]

$$C_{f_l} = \frac{1.328}{\sqrt{R_e}} \tag{24}$$

Here the Reynolds number is based on the distance where transition occurs rather than the reference length, as was the case for Equation (22).

The point where transition occurs is dependent on many factors. Experience has shown, for flight vehicles, a transition Reynolds number of 1 x 10^6 for the body and 0.5 x 10^6 for the wings gives acceptable numbers. For wind tunnel models without a trip, a transition Reynolds number of 3 to 5 million is more reasonable due to a smooth surface. If a boundary layer trip is used, the entire configuration component should have turbulent flow.

2.8 LIFTING SURFACE THEORY[71]

Lifting Surface Theory refers to the solution of the flow over a three dimensional wing where the distribution of pressure is allowed to vary in both the spanwise and chordwise direction. The fundamental equation is the three dimensional perturbation equation, here written in rectangular coordinates, as:

$$(1-M_\infty^2)\ \Phi_{xx} + \Phi_{yy} + \Phi_{zz} = 0 \tag{25}$$

The Flow tangency boundary condition requires:

$$\left.\begin{aligned} \Phi_z &= \frac{\partial z_u}{\partial x}\ at\ z = 0^+ \\ \Phi_z &= \frac{\partial z_l}{\partial x}\ at\ z = 0^- \end{aligned}\right\} for\ (x,y)\ on\ S \tag{25a}$$

If the wing thickness is neglected and we limit ourselves to missiles, then wing chamber can also be neglected. Then the boundary conditions in Equation (25a) become:

$$\Phi_z = -\alpha \tag{25b}$$

for both the upper and lower surfaces.

In addition to this boundary condition, the Kutta condition (which requires the velocity on the upper and lower surfaces at the trailing edge to be equal) is also imposed for subsonic flow.

The assumptions involved in the Lifting Surface Theory, as applied to most missile configurations, are therefore small perturbations in the flow due to the presence of the wing and the thickness and chamber effects are zero or small compared to angle of attack effects.

Equation (25) may be simplified somewhat by using Prandtl-Glauert rule (72) to relate the compressible subsonic normal force or pitching moment to the incompressible case. That is:

$$(C_N)_{M_\infty, AR, \alpha} = \frac{(C_N)_{0, AR, \alpha}}{\sqrt{1 - M_\infty^2}} \tag{26}$$

$$(C_M)_{M_\infty, AR, \alpha} = \frac{(C_M)_{0, AR, \alpha}}{\sqrt{1 - M_\infty^2}}$$

Using the above relations, the normal force and pitching moment on a given wing at any subsonic Mach number may be found by calculating the aerodynamics of the same wing at zero Mach number. Figure 2-9 is a representation of the wing planform parameters.

For $M_\infty = 0$, Equation (25) reduces to La Places equation

$$\nabla^2 \Phi = 0 \tag{27}$$

with boundary condition (25b).

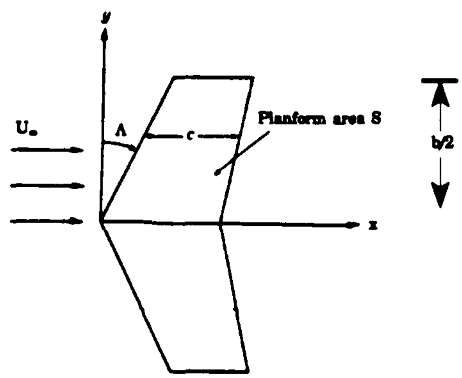

FIGURE 2-9. WING PLANFORM PARAMETERS

There are many methods to solve Equation (27). The one used here is that of Chadwick et al.[71] which closely follows Ashley et al.[72]. The velocity potential Φ is given by:

$$\Phi(x,y,z) = -\frac{1}{8\pi}\iint_S \frac{\Delta C_p(x_1,y_1)}{(y-y_1)^2+z^2}\, z\left[1+\frac{x-x_1}{\sqrt{(x-x_1)^2+(y-y_1)^2+z^2}}\right]dx_1 dy_1 \quad (28)$$

Here, x_1, y_1 are coordinates of an element of the lifting surface that has a differential pressure coefficient of ΔC_p between the lower and upper surfaces at this point (x_1, y_1). It is required to determine the pressure loading over the entire surface. Following Chadwick[71], Equation 28 is first differentiated with respect to z and the limit as $z \to 0$ taken. The result is then equated to the boundary condition, Equation (25b) to obtain:

$$\alpha(x_1,y_1) = \frac{1}{8\pi}\iint \frac{\Delta C_p(x_1,y_1)}{(y-y_1)^2}\left[1+\frac{x-x_1}{\sqrt{(x-x_1)^2+(y-y_1)^2}}\right]dx_1 dy_1 \quad (29)$$

The cross on the y_1 integral indicates a singularity at $y = y_1$, in which case Manglers principal-value technique[72] can be applied. The details of the solution of the integral Equation (29) for ΔC_p (x,y) will not be repeated here as they are given in detail in many references (see for example, Chadwick.[71]) Worthy of note, however, is the fact that Equation (29) is an integral equation for which the wing loading ΔC_p is to be found as a linear function of angle of attack. This wing loading is first approximated by a series expansion with a set of unknown coefficients of number equal to the number of surface elements on the wing planform. That allows each ΔC_p to be influenced by all other elements of the wing. The unknown coefficients in each ΔC_p series are found by solution of an inverse matrix. ΔC_p (x,y) is then calculated.

Once the span loading ΔC_p (x,y) is known over the entire wing surface, the normal force at a given spanwise location is:

$$C_n = \frac{1}{c}\int_{x_{LE}}^{x_{TE}} \Delta C_p dx \quad (30)$$

The total normal force for the entire wing is:

$$C_N = \frac{2}{S_{ref}}\int_0^{b/2} cC_n dy \quad (31)$$

The pitching moment of a given airfoil section, about the point where the wing leading edge intersects the body, is then (positive leading edge up):

$$C_m = -\frac{1}{c\ell_{ref}} \int_{x_{LE}}^{x_{TE}} x \Delta C_p dx \tag{32}$$

The total pitching moment becomes:

$$C_M = \frac{2}{S_{ref}} \int_0^{b/2} c C_m dy \tag{33}$$

If it is desired to calculate the pitching moment about some other reference point, then

$$C_{M_0} = C_M + C_N \frac{x_0}{\ell_{ref}} \tag{34}$$

where x_0 is the distance from the reference point to the juncture of the wing leading edge with the body. The center of pressure of an airfoil section is:

$$x_{CP} = -\frac{C_m}{C_n} \tag{35}$$

or of the entire wing

$$x_{CP} = -\frac{C_M}{C_N} \tag{36}$$

Finally, the spanwise center of pressure of a wing semispan is:

$$y_{CP} = \frac{\int_0^{b/2} c C_n y dy}{\int_0^{b/2} c C_n dy} \tag{37}$$

Equations (30), (31), (32), (33), and (37) can be solved by numerical quadrature, such as Simpson's rule, with special attention given to the leading edge singularity.

It should also be mentioned that if one is interested in dynamic derivatives[73], these aerodynamics can be obtained by a modification to the boundary condition, Equation (25a). That is, for rolling and pitching motions, the angle of attack in Equation (25a) is replaced by:

$$\alpha(x,y) = \alpha_o + \frac{py}{V_\infty} + \frac{q(x - x_{ref})}{V_\infty} \tag{38}$$

Equation (27) is a linear partial differential equation so that solutions can be combined together in a linear fashion. This means, for roll damping, simply set $\alpha_o = q = 0$ and the boundary condition is

$$\alpha(x,y) = \frac{py}{V_\infty} \tag{38a}$$

Likewise, for pitching damping, $\alpha_0 = p = 0$ and

$$\alpha(x,y) = \frac{q(x-x_{ref})}{V_\infty} \tag{38b}$$

2.9 THREE DIMENSIONAL THIN WING THEORY[72]

Three Dimensional Thin Wing Theory (TDTWT) is quite similar to lifting surface theory (LST) in the sense the same perturbation Equation (25) is used. The only difference is that TDTWT is normally used to represent the supersonic flow solutions of Equation (25) versus LST the subsonic solutions. Since, for supersonic flow, solutions to Equation (25) are hyperbolic versus elliptic for the subsonic case, they generally are easier to obtain. This is because no upstream influence is felt by a disturbance at a given point on the wing surface. In contrast, the subsonic solutions required a matrix inversion at each wing element to determine the unknown coefficients used to determine the pressure differential from lower to upper surfaces. On the other hand, the assumptions of TDTWT are the same as for LST. They both assume small perturbations in an isentropic flow. The isentropic flow assumption means no shock waves are allowed.

In contrast to the body solutions generated by Van Dyke, adequate wing solutions can be obtained at higher Mach numbers. This is because of the low slopes present on most wing planforms (thickness is generally very small), the wing frontal area is generally less than 10 percent of the body frontal area, and in the region of leading edge bluntness, where perturbation theory is invalid, modified Newtonian Theory is used for wave drag calculation.

The most general boundary conditions for Equation (25) in supersonic flow are the flow tangency condition specified by

$$\frac{w(x,y)}{V_\infty} = \Phi_z = \frac{\partial F}{\partial X} = \left(\frac{dz}{dx}\right)_{x,y} + \alpha + \frac{py}{V_\infty} + \frac{q(x-x_{ref})}{V_\infty} + \dot{\alpha}t \tag{39}$$

and the perturbation velocities must vanish upstream from the point where the disturbance originates. Mathematically, this can be stated in the form

$$u(o^-,y,z) = v(o^-,y,z) = w(o^-,y,z) = 0 \tag{40}$$

Since Equation (25) is linear, individual solutions can be added together. This allows individual treatment of the Equation (39) boundary condition for drag, lift, roll and pitch damping computations. For wave drag calculations, only the first term of Equation (39) is retained and the other terms are set to zero. For lift calculations, the angle of attack α is retained and the other terms set to zero. For roll damping, the third term of Equation (29) is retained and the other terms set to zero. For pitching rate, the q term of Equation (39) is retained and the other terms set to zero. Finally, for a constant vertical acceleration, the last term is retained and the other four terms set to zero. Pitch damping moment, $C_{M_q} + C_{M_{\dot{\alpha}}}$, normally refers to the sum of the terms due to a constant pitch rate and constant vertical acceleration.

The solution to Equation (25), using the first term of Equation (39) as the boundary condition, will give the axial force coefficient of a sharp wing. If the leading edge is blunt, MNT is used in conjunction with perturbation theory. The general solution to Equation (25) is[72]:

$$\Phi\ (x,y,0) = -\frac{w(x,y)}{\pi}\int\int_{s}\frac{dx_1 dy_1}{\sqrt{(x-x_1)^2-\beta^2(y-y_1)^2}} \tag{41}$$

The pressure coefficient at any point on the wing surface is

$$C_p = -2\Phi_x(x,y,o) \tag{42}$$

The perturbation velocity Φ_x, at a given point p, is dependent on the location of the point with respect to the line of sources and sinks which generates the wing leading edge or other discontinuity and whether this point is in a subsonic or supersonic flow region. For example, referring to Figure 2-10A, if point P is at P_1, and the wing generator is a subsonic source or sink line (SOSL), then

$$\Phi_x = -\frac{2w(x_{p1},y_{p1})}{\pi\beta\sqrt{\eta^2-1}}\cosh^{-1}\sqrt{\frac{n^2-1}{\sigma^2-1}} \tag{43}$$

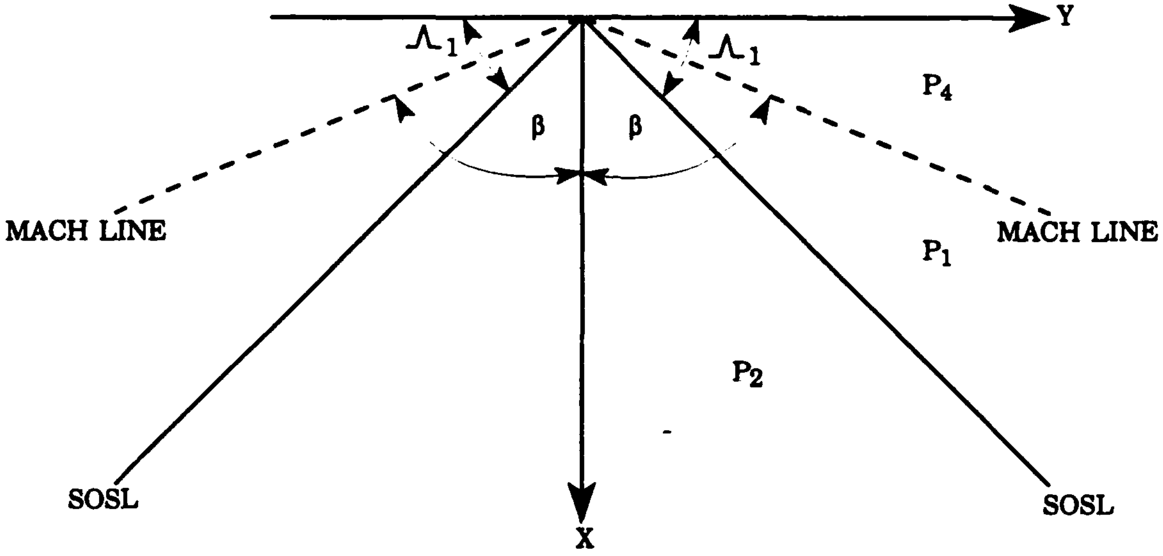

FIGURE 2-10A. TRIANGULAR SURFACE SYMMETRIC ABOUT X AXIS FOR SUBSONIC SOSL

where w is determined from the boundary condition and is (for the airfoil section at $y = y_{p1}$):

$$w(x_{p1}, y_{p1}) = \left.\frac{dz}{dx}\right|_{x=x_{p1}}$$

In Equation (43), the definitions

$$\eta = \frac{k}{\beta}$$

$$k = \tan \Lambda \qquad (43a)$$

$$\sigma = \frac{k y_p}{x_p}$$

have been used. If P = P_2, the induced velocity at P_2 due to a given SOSL is:

$$\Phi_x = -\frac{2w(x_{p2}, y_{p2})}{\pi\beta\sqrt{\eta^2-1}} \cosh^{-1}\sqrt{\frac{\eta^2-\sigma^2}{1-\sigma^2}} \qquad (44)$$

At the wing tip, there is an additional disturbance within the Mach line emanating from the tip leading edge (Figure 2-10B). The induced velocity in this region, P = P_3 is:

$$\Phi_x = -\frac{w(x_{p3}, y_{p3})}{\pi\beta\sqrt{\eta^2-1}} \cosh^{-1}\left[\frac{\eta^2+|\sigma|}{\eta(|\sigma|+1)}\right] \qquad (45)$$

The absolute value of σ is taken because σ is actually negative for the point P_3 . The induced velocity at any point, say P = P_4, outside of the Mach lines emanating from the beginning of the SOSL is zero since this point is out of the zone of influence.

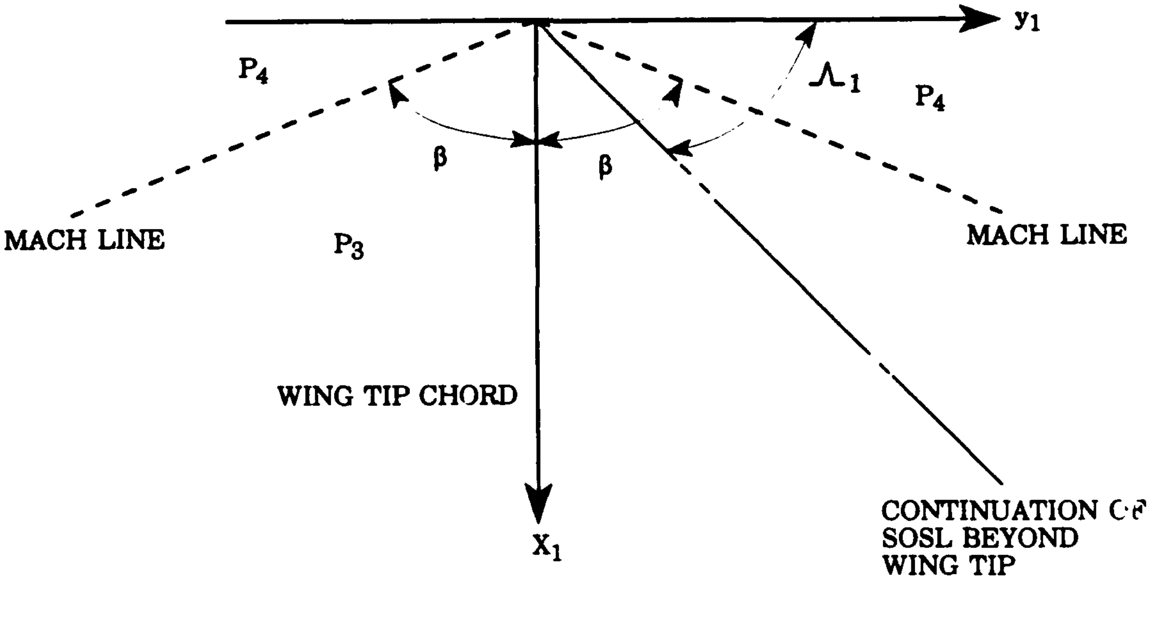

FIGURE 2-10B. WING TIP EFFECTS FOR SUBSONIC SOSL

If the wing generator is supersonic, the Mach lines from point 0 in Figure 2-11A lie behind the SOSL. If in Figure 2-11A, $P = P_1$, then the induced velocity at P_1 due to the disturbance caused by the SOSL is :[73]

$$\Phi_x = -\frac{w(x_{p1}, y_{p1})}{\beta\sqrt{1-\eta^2}} \tag{46}$$

If $P = P_2$, the induced velocity is

$$\Phi_x = -\frac{w(x_{p2}, y_{p2})}{\pi\beta\sqrt{1-\sigma^2}}\left[\pi - 2\sin^{-1}\sqrt{\frac{\eta^2-\sigma^2}{1-\sigma^2}}\right] \tag{47}$$

Referring to Figure 2-11B, the additional induced velocity inside the area bounded by the tip and the Mach line emanating from the tip ($P = P_3$) is:

$$\Phi_x = -\frac{w(x_{p3}, y_{p3})}{\pi\beta\sqrt{1-\eta^2}}\cos^{-1}\left[\frac{|\sigma|+\eta^2}{\eta(1+|\sigma|)}\right] \tag{48}$$

Again if $P = P_4$, the point is out of the zone of influence of the SOSL and thus the induced velocity is zero.

The induced velocity at a given point on any wing geometry can now be computed by the proper superposition of the triangular SOSL shown in Figures 2-10 and 2-11. This is because of the linear nature of the governing flow-field Equation (1). As an example of how the above superposition principle works, consider the wing shown in Figure 2-12. For simplicity, the slopes χ_1 and χ_2 are constant. The wing AHJD can be represented by the superposition of five SOSL. The first has the planform AEH and source intensity:

$$w(x_p, y_p) = V_\infty \chi_1 \tag{49}$$

where χ_1 is the slope of the segment AB. The second has the planform BIF and intensity

$$w(x_p, y_p) = (\chi_2 - \chi_1) V_\infty \tag{50}$$

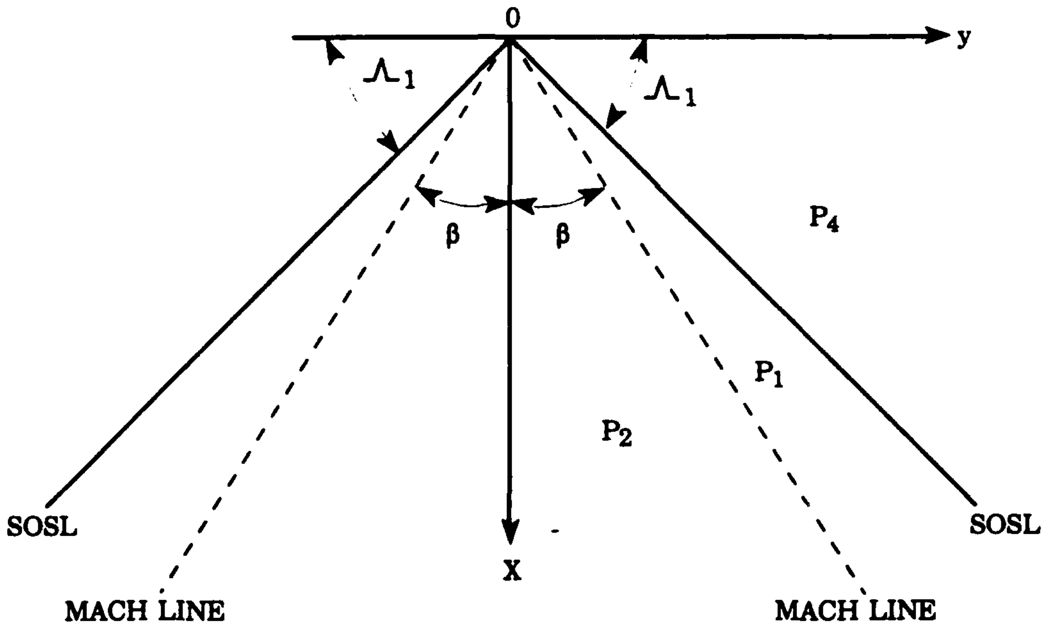

FIGURE 2-11A. TRIANGULAR SURFACE SYMMETRIC ABOUT X-AXIS FOR SUPERSONIC SOSL

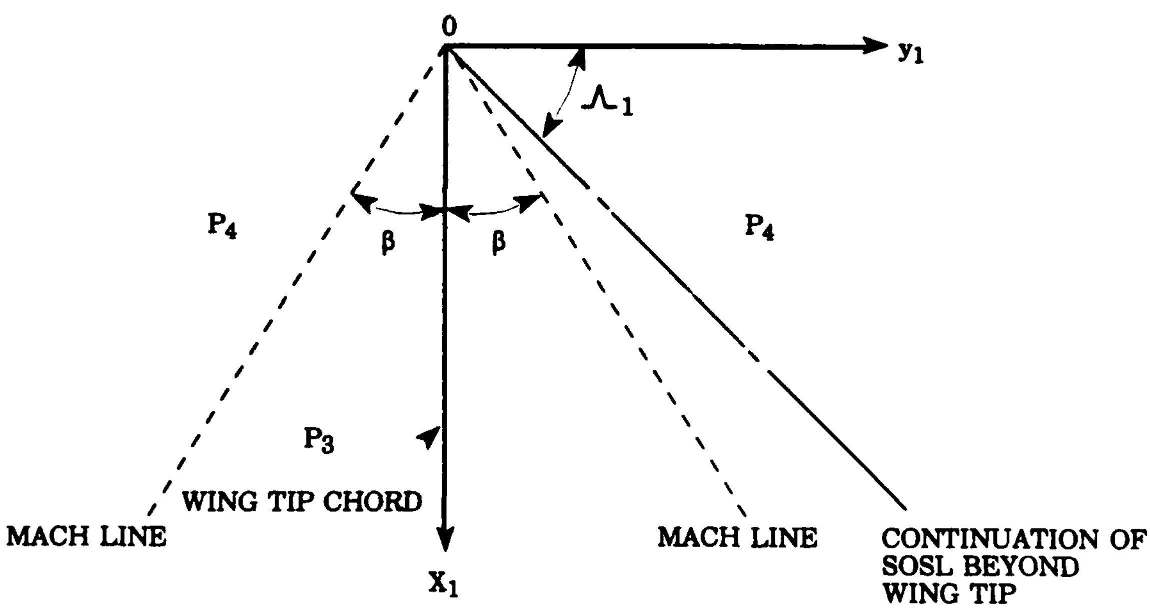

FIGURE 2-11B. WING TIP EFFECTS FOR SUPERSONIC SOSL

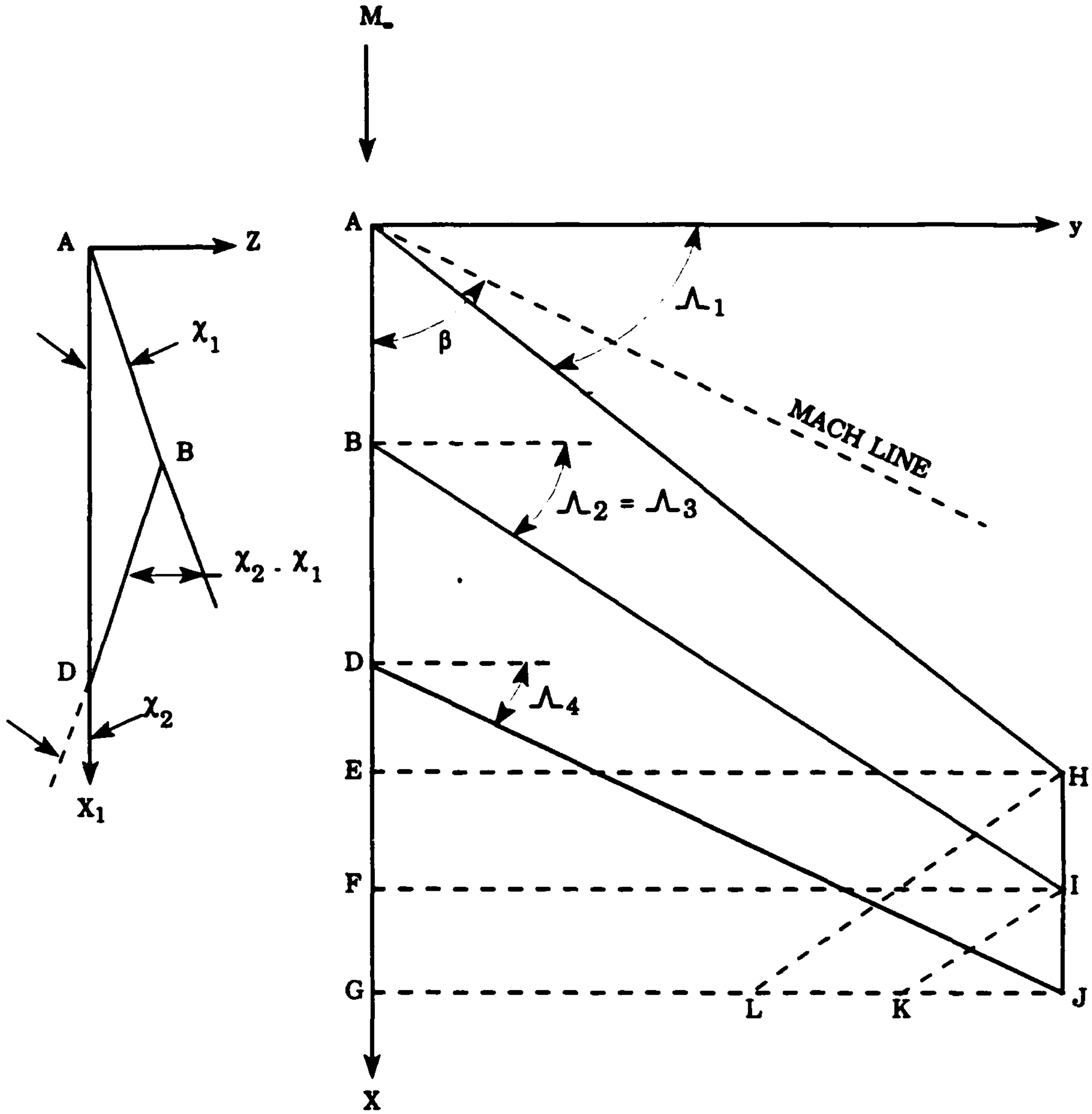

FIGURE 2-12. LINEAR SUPERPOSITION OF TRIANGULAR SOURCE AND SINK DISTRIBUTIONS

and the third the planform DJG and intensity

$$w(x_p, y_p) = -\chi_2 V_\infty \tag{51}$$

The other two SOSL represent the tip effects. They are the planforms HJL and IJL and have source intensities of opposite signs than those representing the wing.

The above procedure can be applied to a wing of general planform. The only difference is that for each point in question, the slope is not constant as was the case in the simplified example. Then for some general point located on the wing surface, the total induced velocity due to all sources and sinks is found by applying one of the Equations (43) through (48) for each SOSL. The particular equation applied depends upon the location of the point relative to the SOSL and the Mach line as discussed earlier. These individual contributions are then summed to get the total induced velocity. Knowing the total induced velocity at a point allows one to calculate the pressure coefficient at the given point by Equation (42).

The pressure coefficient can be calculated at a given number of spanwise and chordwise locations. The drag of a given airfoil section at the spanwise station $y = y_A$ is then

$$C_d = \frac{2}{c(y_A)} \int_0^{c(y_A)} C_p(x, y_A)\, w(x, y_A)\, dx \tag{52}$$

The total drag for one fin of semispan b/2 is then:

$$C_D = \frac{1}{S_w} \int_0^{b/2} C_d c(y)\, dy \tag{53}$$

where $S_w = b/2(c_r + c_t)$. For cruciform fins, the total drag coefficient is:

$$C_D = \frac{4}{S_W} \int_0^{b/2} C_d c(y)\, dy \tag{54}$$

If it is desired to base the drag coefficient on the body cross-sectional area, the Equation (54) must be multiplied by the factor S_w/S_{ref}.

Equations (52) and (54) can be integrated by numerical quadrature if the generators of the wing surface are supersonic. If the generators are subsonic, linear theory indicates the pressure coefficients go to infinity at the wing generators. Physically, this cannot be true which means that for a subsonic SOSL, linear theory is not valid at the SOSL. The reason is that the velocity perturbations in the vicinity of the discontinuities are no longer small, violating one of the assumptions in linear theory. However, the velocity perturbations are small a slight distance from the SOSL so that linear theory can be applied. Numerical experiments indicated a distance of five thousandths of the chord length from the SOSL is sufficient and the value of pressure calculated at this point can be assumed to exist up to the SOSL.

The analysis using TDTWT has been illustrated for the axial force computation using the first term of the boundary condition of Equation (39). A very similar process is used for the lift, roll and pitch damping computations. The reader is referred to references 74 through 86 for the theoretical derivations and to Moore et al [2,4] for the practical application of the theories for these force or moment components. Time will not permit the many applications of TDTWT.

2.10 SLENDER BODY AND LINEAR THEORY FOR INTERFERENCE LIFT COMPUTATION[87]

The method almost universally used for including interference between the various missile components into approximate aeroprediction codes is that due to Pitts, et al.[87] There are three primary types of interference lift (note that lift and normal force are used interchangeably here) to be concerned with. These are the effects on the wing due to the presence of the body, the effect on the body due to the presence of a wing, and finally, the effect on an aft lifting surface due to wing or body shed vortices. Wing to wing or shock wave interference will not be discussed at present.

To better understand the interference lift components, it is instructive to examine the total normal force of a configuration as defined by Pitts et al.[87] This is given by

$$\begin{aligned} C_N = C_{N_B} &+ \left[\left(K_{W(B)} + K_{B(W)}\right)\alpha + \left(k_{W(B)} + k_{B(W)}\right)\delta\right]\left(C_{N_\alpha}\right)_W \\ &+ \left[\left(K_{T(B)} + K_{B(T)}\right)\alpha\right]\left(C_{N_\alpha}\right)_T + C_{N_{T(V)}} + C_{N_{B(V)}} \end{aligned} \tag{55}$$

The first term in Equation 55 is the normal force of the body alone including the linear and nonlinear components; the second term is the contribution of the wing (or canard) including interference effects and control deflection; the third term is the contribution of the tail including interference effects and control deflection; and the last term is the negative downwash effect on the tail or body due to wing shed or body shed vortices. The K's represent the interference of the configuration with respect to angle of attack, and the k's represent the interference with respect to control deflection. Each of these interference factors is estimated[2] by slender body or linear theory.[87] As such, they are independent of angle of attack.

The various interference factors, as defined by slender body theory (SBT), are[87]:

$$K_{W(B)} = 2/\pi \left\{ \frac{(1+r^4/s^4)\left[\frac{1}{2}\tan^{-1}\frac{1}{2}(s/r-r/s)+\pi/4\right]}{(1-r/s)^2} - \frac{r^2/s^2[(s/r-r/s)+2\tan^{-1}(r/s)]}{(1-r/s)^2} \right\} \tag{56}$$

$$K_{B(W)} = (1+r/s)^2 - K_{W(B)} \tag{57}$$

$$\begin{aligned} k_{W(B)} = \frac{1}{\pi^2}\Bigg\{ & \frac{\pi^2}{4}\frac{(s/r+1)^2}{(s/r)^2} + \frac{\pi[(s/r)^2+1]^2}{(s/r)^2(s/r-1)^2}\sin^{-1}\left[\frac{(s/r)^2-1}{(s/r)^2+1}\right] \\ & - \frac{2\pi(s/r+1)}{s/r(s/r-1)} + \frac{[(s/r)^2+1]^2}{(s/r)^2(s/r-1)^1}\left(\sin^{-1}\left[\frac{(s/r)^2-1)}{(s/r)^2+1}\right]\right)^2 \\ & - \frac{4(s/r+1)}{s/r(s/r+1)}\sin^{-1}\left[\frac{(s/r)^2-1}{(s/r)^2+1}\right] + \frac{8}{(s/r-1)^2}\log\left[\frac{(s/r)^2+1}{2s/r}\right]\Bigg\} \end{aligned} \tag{58}$$

$$k_{B(W)} = K_{W(B)} - k_{W(B)} \tag{59}$$

Figure 2-13 plots the interference lift factors given by Equations (56) through (59) as a function of the body radius to wing semispan plus body radius ratio (r/s).

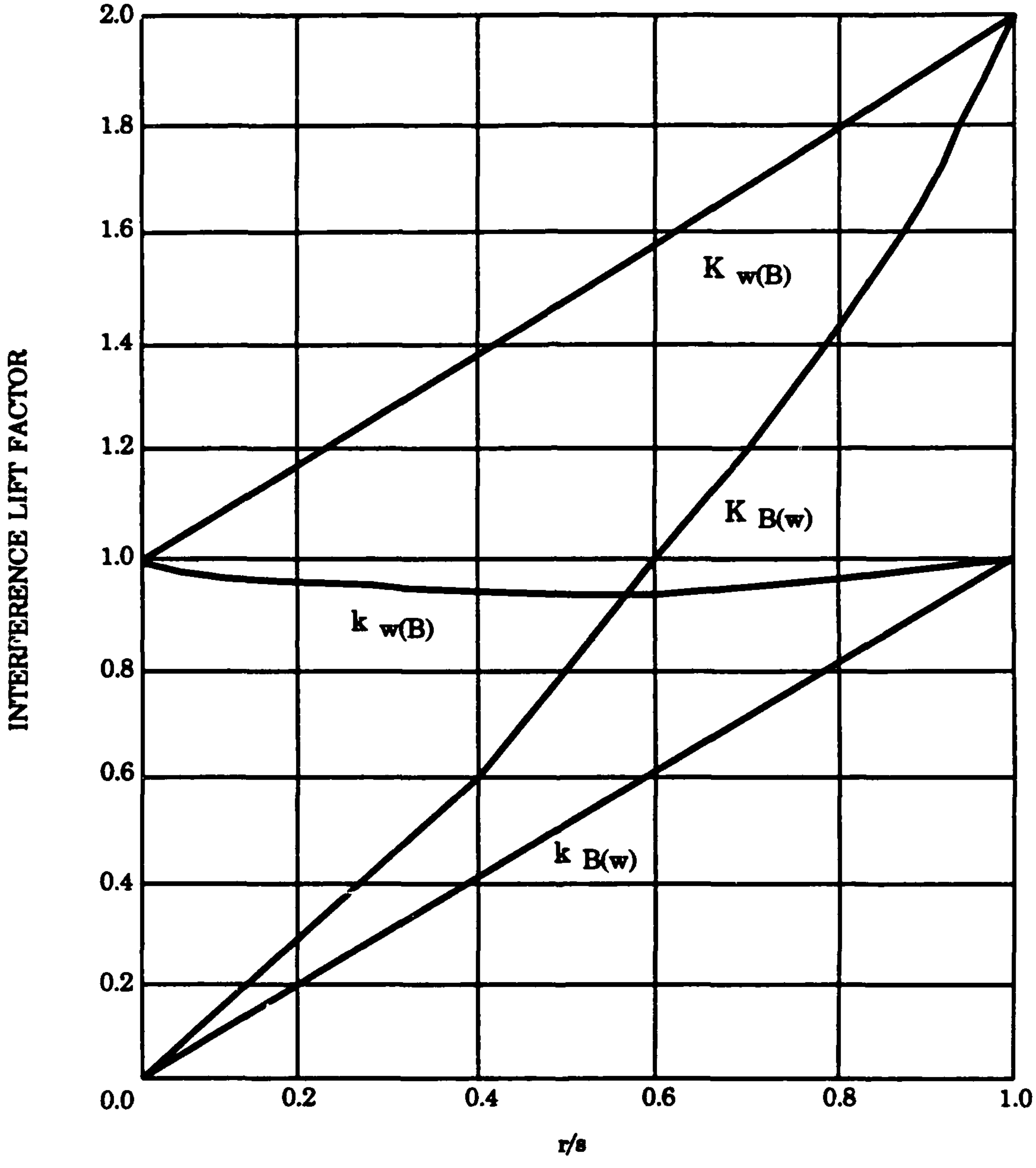

FIGURE 2-13. SLENDER BODY THEORY INTERFERENCE LIFT FACTORS

As the Mach number increases supersonically, SBT gives values of $K_{B(W)}$ which are too high if the wing is near the missile rear. This is because much of the carryover lift onto the body is actually lost to the wake of the vehicle. Figure 2-14 illustrates this for the no afterbody, infinite afterbody, and short afterbody cases. Linear theory formulations are available for the infinite and no afterbody cases to replace Equation 57 if the parameter

$$\beta AR(1+\lambda)\,[1/(m\beta)+1]>4 \tag{60}$$

Moore[2] then linearly interpolated between the infinite and no afterbody cases as a function of the area covered by the Mach lines to obtain $K_{B(W)}$ for the short afterbody case.

Strictly speaking, the methodology discussed here is limited to slender bodies with triangular planforms of low aspect ratio. Experience has shown, that if the correct value of wing-alone lift is computed, the interference factors can give very reasonable results for wings which do not have triangular planforms or even have low aspect ratio. Moore[2] showed how an engineering estimate of interference lift could be obtained, even for planforms such as that shown in Figure 2-15A. The actual SBT configuration is that shown in Figure 2-15B. Since most of the interference lift occurs near the wing body juncture, reference (2) used approximations given by Equation (61)

$$\begin{aligned}
[K_{B(W)}]_{II} &= [K_{B(W)}]_I G \\
[K_{W(B)}]_{II} &= 1 + ([K_{W(B)}]_I - 1)\,G \\
[k_{W(B)}]_{II} &= 1 + ([k_{W(B)}]_I - 1)\,G \\
[k_{B(W)}]_{II} &= ([k_{W(B)}]_I - [k_{W(B)}]_I)\,G
\end{aligned} \tag{61}$$

to estimate the interference factors of the wing in Figure 2-15A. G in Equation (61) is the ratio of the root chord of the wing for which the interference factor is desired to that of the wing that slender body theory assumes. That is

$$G = \frac{(c_r)_{II}}{(c_r)_I}$$

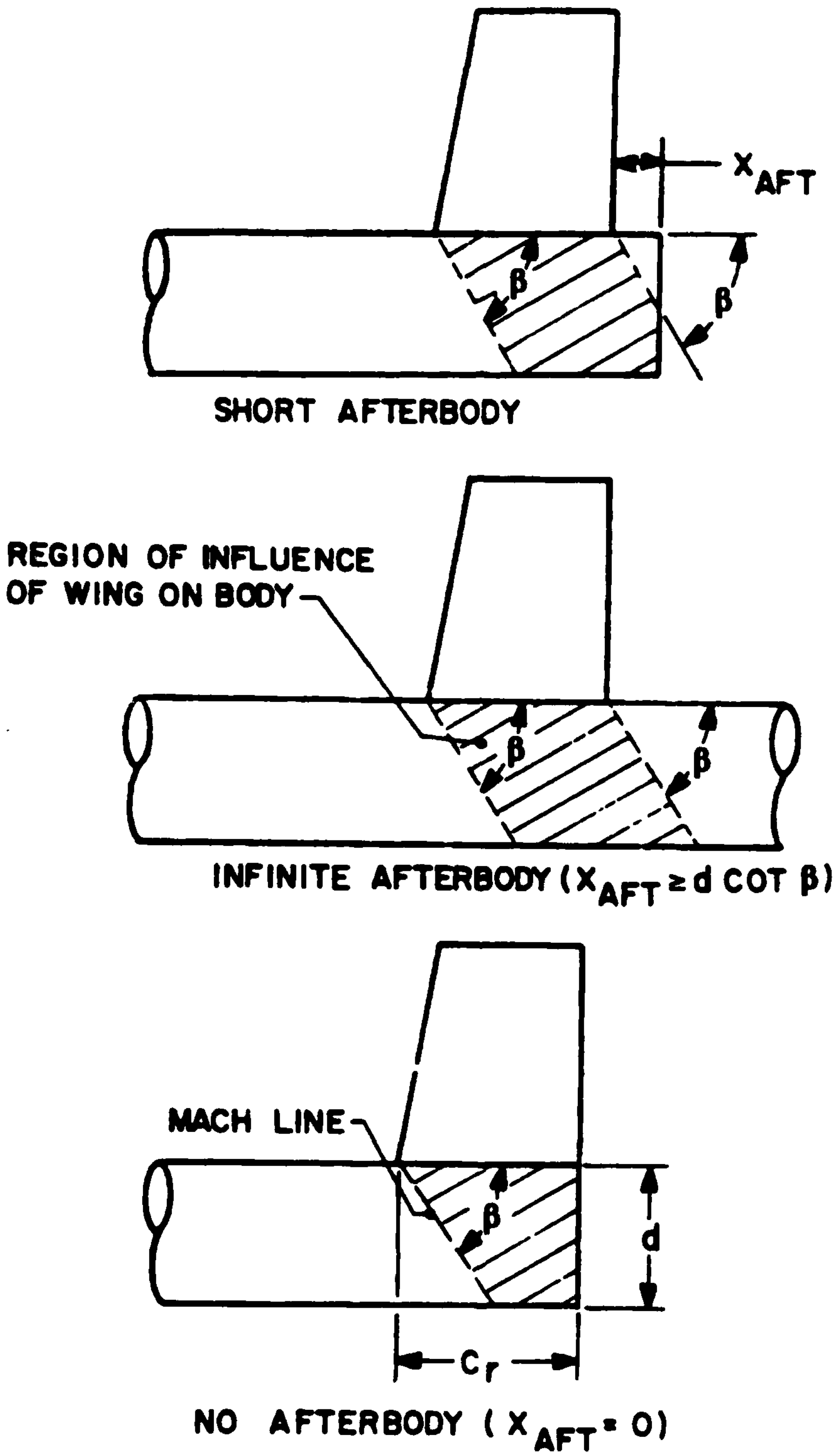

FIGURE 2-14. DETERMINATION OF $K_{B(W)}$ FOR HIGH-ASPECT-RATIO RANGE AT SUPERSONIC SPEEDS

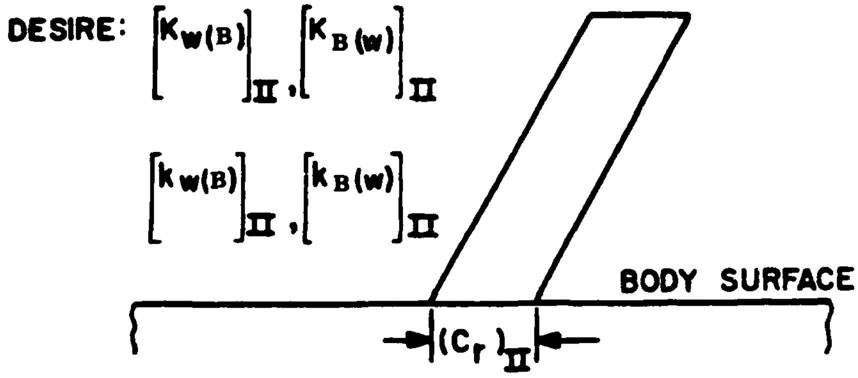

FIGURE 2-15A. WING FOR WHICH INTERFERENCE LIFT IS DESIRED

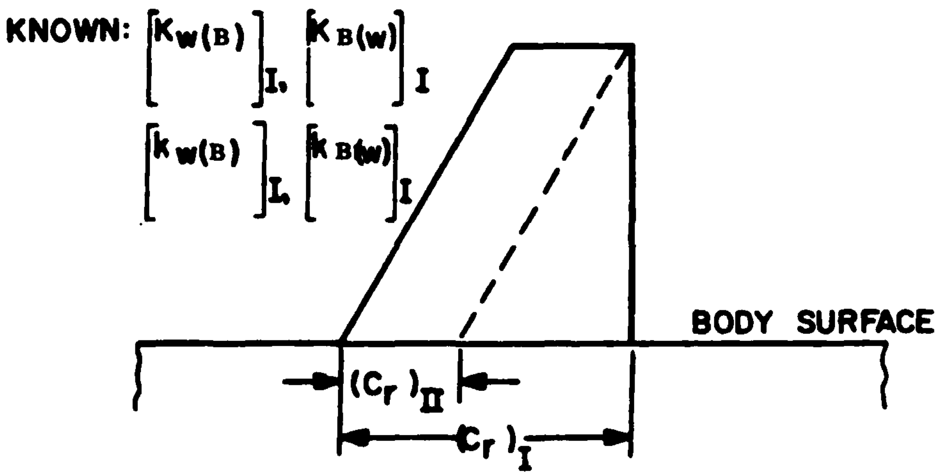

FIGURE 2-15B. ASSUMED SLENDER BODY REPRESENTATION

The last two terms of Equation (55) are also interference terms. $C_{N_{T(V)}}$ is the lift on the tail caused by the vortices shed by the wing or canard upstream. $C_{N_{B(V)}}$ is the negative lift on the afterbody due to wing shed vortices. These terms are also calculated analytically and are given by:

$$C_{N_{T(V)}} = \frac{(C_{N_\alpha})_W (C_{N_\alpha})_T [K_{W(B)} \sin\alpha + k_{W(B)} \sin\delta_W]\, i\, (s_T - r_T) A_W}{2\pi (AR)_T (f_W - r_W) A_{ref}} \tag{62}$$

$$C_{N_{B(V)}} = \frac{-4\Gamma}{A_W V_\infty}\left[\frac{f_W^2 - r_W^2}{f_W} - f_T + \frac{r_T^2}{\sqrt{f_T^2 + h_T^2}}\right] \tag{63}$$

Here i is the tail interference factor given by Pitts et al[87] and Γ is the strength of the wing shed vortex.

2.11 EMPIRICAL METHODS[2,4,6]

It is fair to wonder why approximate aeroprediction codes are defined as semiempirical with all the theoretical methods discussed so far. The truth is, that while these methods allow the individual component forces and moments to be calculated fairly rigorously at a given Mach number or angle of attack, there are still many conditions where the analytical methods presented previously are either not applicable or the difficulty in applying then is not worth the effort. In those cases, empirical methods are generally used. The combination of theoretical and empirical techniques in a code is thus why they are called semiempirical codes. A few examples where empirical methods are used are transonic aerodynamics, body alone subsonic aerodynamics, rotating band or protuberance aerodynamics, and base drag of the body and lifting surfaces. There are actually analytical methods available for transonic aerodynamic computations. However, most of the methods are inconsistent from a computational standpoint with the approximate codes. What is done in many cases, is to use the sophisticated analytical tools[2,4,6] to estimate the transonic aerodynamics, as a function of key geometric parameters, then to include these into an engineering code in a table lookup fashion. Obviously, for a vehicle that spends a large portion of its time in the transonic flow region, $0.8 < M_\infty < 1.2$, it would be justifiable to use a more sophisticated estimation process.

The base drag empirical method will be discussed in more detail in the next section of the report, which deals with some of the newer nonlinear methods developed in the past three years.

3.0 NEW APPROXIMATE AERODYNAMIC METHODS

This part of the report will deal with many of the new aerodynamic prediction methods developed over the past 3 years. These methods include extension of the SOSET to include real gas effects (including two new nonlinear angle-of-attack pressure predictors), an improved version of the Modified Newtonian Theory (IMNT), and improvements to the Allen and Perkins viscous crossflow theory; also included are a new nonlinear wing-alone method, new nonlinear wing body and body wing interference methods due to angle of attack, a new nonlinear wing body interference method due to control deflection, a method for treating nonlinear wing tail interference, and an improved base drag prediction model.

These new methods and improvements were directed at three weak areas in the NSWCDD Aeroprediction Code of 1981 (AP81): (1) limited Mach number and inability to compute temperatures at the surface for aeroheating calculations, (2) lack of nonlinear lift capability except for the body alone, and (3) base drag methodology that was not robust enough in terms of including fin effects.

3.1 SOSET EXTENDED TO REAL GASES[89, 90]

The main reason the fourth version[7] of the aeroprediction code was limited to Mach number 8 was that, above $M_\infty = 6$ real gas effects start becoming important but, can still be neglected at $M_\infty = 8$. However, as Mach number increases substantially above $M_\infty = 6$, the need to include real gas effects into the aeroprediction code increases if one is interested in inviscid surface temperatures. If one is only interested in forces and moments, real gas effects have a slight effect on the pitching moment, but only second-order effects on axial and normal force[88]. However, one of the key issues in high-speed vehicles is aerodynamic heating, material selection, and insulation. Any excess weight can have a strongly adverse impact on vehicle performance. Thus, a simple yet accurate method of estimating vehicle surface temperature (inviscid) for use in heat transfer analysis is needed.

Figure 3-1[89] is an illustration of the importance of real gas effects. It plots the static temperature behind a normal shock for both perfect and real gases at an altitude of 170,000 ft. At this altitude, the speed of sound is approximately 1100 ft/sec and the freestream air temperature is approximately 283°K. The normal shock would occur in the vicinity immediately ahead of the blunted portion of a seeker or the missile nose. Note that the temperatures of interest to tactical weapons aerodynamicists can be very high, for high Mach number conditions assuming a perfect gas. Also shown on the figure are the real gas results[92]. Note, in particular, the plot of T_R/T_P, the ratio of the real gas to perfect gas temperature. For Mach numbers of 6 or less, this ratio is unity or near unity. This is the reason that aerodynamic computations below $M_\infty = 6$ could neglect real gas effects with little error. However, as M_∞ goes above $M_\infty = 6$, the error in temperature using the perfect gas assumption becomes increasingly large. This is of particular importance to materials and structures engineers designing the system to withstand these temperatures. Also shown in Figure 3-1 is the melting point of typical structural materials used in present-day missile design. The actual-use temperature is less than the melting-point temperature. For missiles that fly at any appreciable time above the maximum-use temperature of a given material, some form of active cooling or insulation would be required. This means additional dead weight and, hence, less performance for the missile. It is therefore obvious that a reasonably accurate estimate of temperature is essential for the design of the seeker and the structure of the weapon. To meet the need for a fairly accurate method of predicting surface temperature, SOSET was extended to include real gas effects. In so doing, new approximate methods were developed for angle of attack pressure prediction and an improved version of MNT was derived. These new methods will be briefly described.

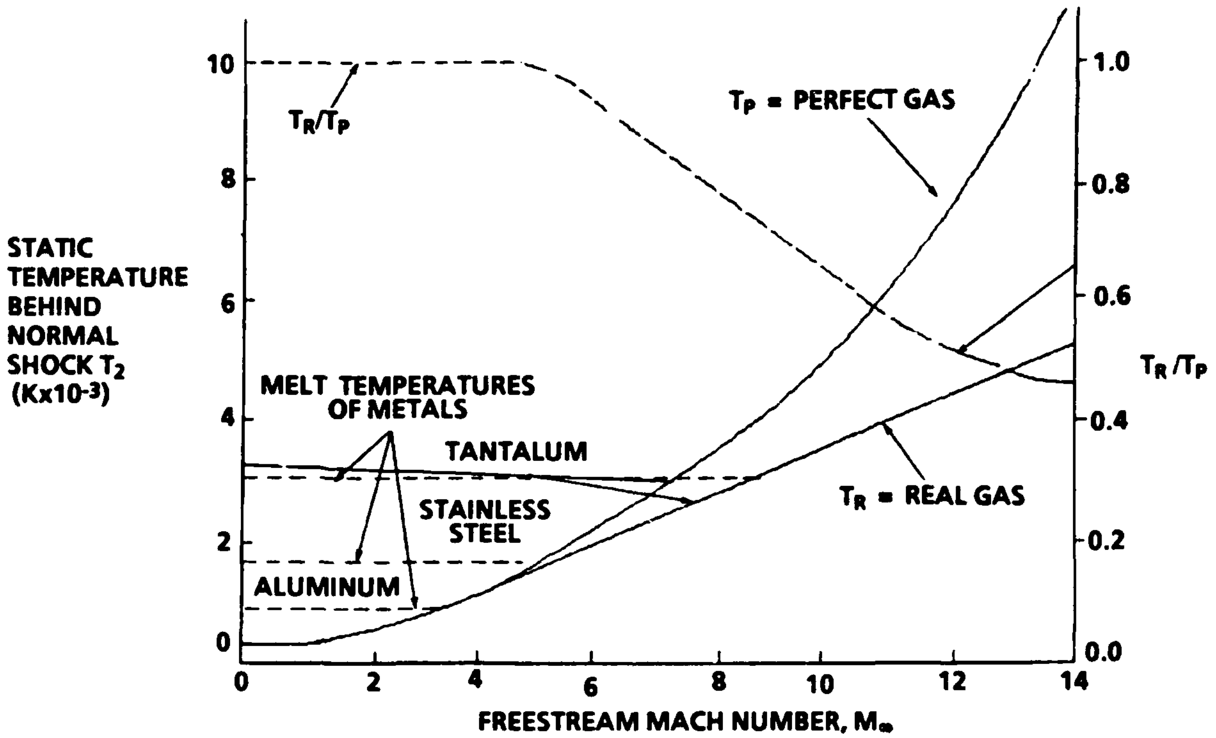

FIGURE 3-1. TEMPERATURE BEHIND A NORMAL SHOCK AS A FUNCTION OF FREESTREAM MACH NUMBER (H = 170kft)

SOSET and MNT for perfect gases were discussed in 2.1 and 2.3, respectively. Refer to 2.1 for the SOSET methodology and to Moore, et al.[89, 90] for the extension to real gases. It is noted that to extend SOSET to real gases requires several things: (1) a cone solution for real gases (p_c); (2) a Prandtl-Meyer Expansion (PME) for real gases (p_2); (3) a derivation of a new pressure derivative $(\partial p/\partial s)_2$, where the perfect-gas assumption has not been made; and (4) a way to compute temperature given values of pressure.[89] After the real-gas pressure derivative $(\partial p/\partial s)_2$ was derived and checked, it was found that $(\partial p/\partial s)_2$ became negative for many cases, causing one to choose between the Generalized Shock Expansion Theory (GSET where $\eta = 0$) and the tangent cone theory ($\eta = \infty$). In comparisons of the pressure prediction to full Euler computations, it was found that a better way to implement the shock expansion theory for M $\geq$ 6 was to redefine Equation (10) as

$$p = p_c - (p_c - p_2)\,\eta_1 \tag{64}$$

with η_1 being an input parameter chosen by the user. It was found that a value of $\eta_1 = 0$ gave slightly better pressure predictions for slightly blunt configurations, whereas a value of $\eta_1 = 1$ gave better accuracy where bluntness was large. Thus, final implementation of SOSET in AP93 is Equation (64), with η_1 as an input, p_c the real gas tangent cone pressure, and p_2 the real-gas value of pressure computed from a Prandtl-Meyer expansion.

To compute inviscid temperatures (and other properties) along the surface of a pointed or blunt body, the constancy of entropy along the surface for perfect, frozen, or equilibrium chemically reacting flows is used. Knowing the value of entropy and pressure from the pointed cone solution[92] or the normal shock solution for a blunt body[93], one can then use the thermofit equations of Tannehill and Mugge[94] and Srinivasen, et al.,[95] to determine other properties, i.e.,

$$\left.\begin{aligned} T &= T(p,S) \\ \rho &= \rho(p,S) \\ a &= a(p,S) \\ e &= e(p,S) \end{aligned}\right\} \tag{65}$$

The remaining properties at the body surface can be found from standard thermodynamic relationships, i.e.,

$$\left.\begin{gathered} h = e + p/\rho \\ H_0 = \left(\frac{\gamma_\infty R}{\gamma_\infty - 1}\right) T_{0_\infty} = constant \\ V = \sqrt{2(H_0 - h)} \\ M = V/a \\ \gamma = \frac{a^2 \rho}{p} \\ Z = \frac{p}{\rho R T} \end{gathered}\right\} \tag{66}$$

In the process of computing surface properties, three new pressure prediction methods were derived. The first of these was to give an improved pressure coefficient prediction on the blunt nose of a missile configuration over that provided by the MNT. If the pressure coefficient of MNT is defined as

$$(C_p)_{MNT} = C_{p_0} \sin^2 \delta_{eq} \tag{67}$$

then the nose pressure on the blunt nose part of a missile is given by

$$C_p = (C_p)_{MNT} - \Delta C_p \tag{68}$$

ΔC_p of equation (68) is defined by

$$\Delta C_p = k \cos^m (\delta eq) \ [\cos \delta eq - \cos(\delta eq)_m] \tag{69}$$

where $(\delta \text{ eq})_m = 25.95$ deg, m = 2.78, and

$$k = 2.416 C_{p_o} + 4.606 \left[0.1507 C^2_{p_o} + \frac{1.124}{M_\infty^2} C_{p_o} \right]^{1/2}$$

Figure 3-2 shows the results of the Improved Modified Newtonian theory (IMNT) of Equations (68) and (69), compared to Equation (67) alone, and a full numerical solution of the Euler equations[67] for a hemispherical forebody at $M_\infty = 10$. The IMNT gives up to 7 percent improvement in pressure compared to the MNT. Even past the match point (δeq < 25.95 deg), the IMNT gives good agreement with the numerical solution down to δeq values of 10 deg. This level of accuracy in pressure prediction will also translate into more accurate drag computations, particular on bodies with large bluntness.

The other two pressure prediction formulas have to do with calculating the pressure on a point behind the blunt nose portion of the body but at an angle of attack. These are

$$C_p(\alpha,\phi) = C_{p_{\alpha=0}} - (2\alpha)\sin(2\theta)\cos(\phi) + (F\cos^2\theta)\alpha^2 + (4/3\sin(2\theta)\cos(\phi))\alpha^3 \tag{70}$$

where

$$F = (2 - \frac{1}{\beta})(1 - \tan^2\theta_c) - (2 + \frac{2}{\beta})\sin^2\phi$$

and

$$C_p(\alpha,\phi) = C_{p_{\alpha=0}} - \frac{(2\alpha)\sin(2\theta)\cos(\phi)}{3} \tag{71}$$

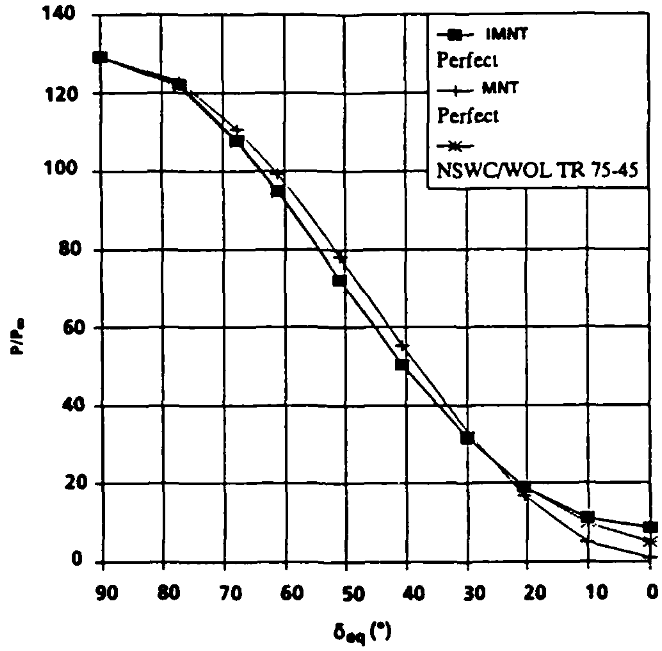

FIGURE 3-2. SURFACE PRESSURE DISTRIBUTION OVER A HEMISPHERICAL FOREBODY AT $M_\infty = 10$

Equation (70) is used for pointed body configurations, as well as for blunt body configurations in the windward plane area ($60° < \phi \leq 180°$). Equation (71) is used in the leeward plane ($\phi \leq 60°$) for configurations with blunt noses. In Equation (70), $(C_p)_{\alpha=0}$ is the pressure coefficient at $\alpha = 0$, which comes from Equation (64). Figure 3-3 is an example of the application of Equation (70) to a cone along with the associated inviscid surface temperatures. The approximate results are close to the exact cone solution.[97]

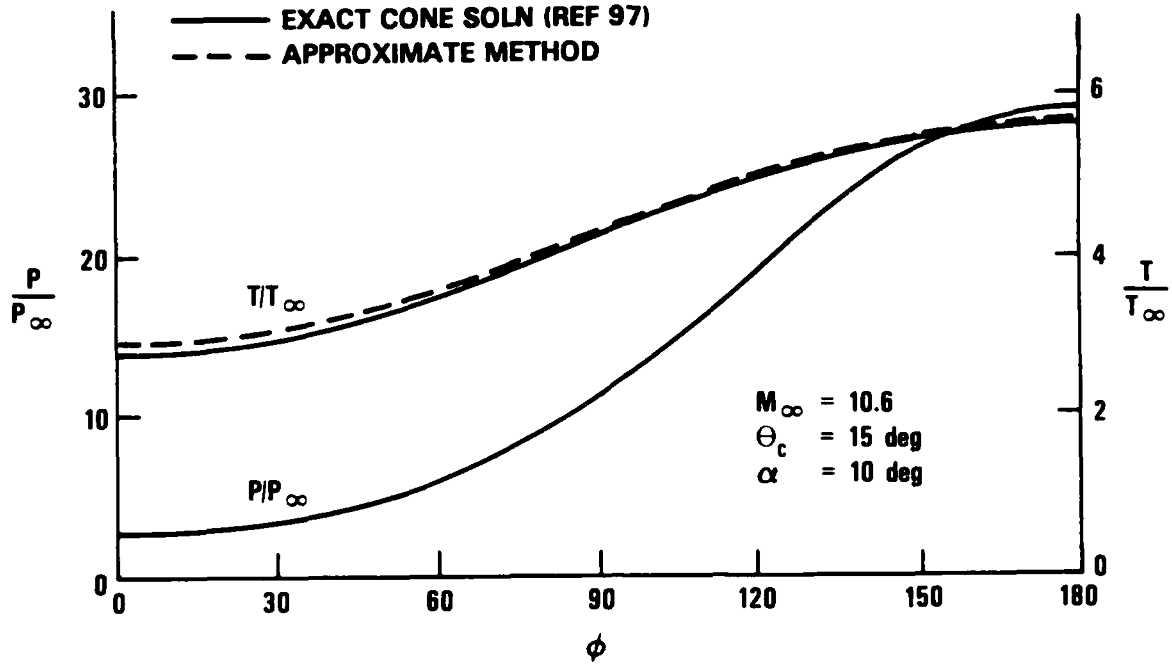

FIGURE 3-3. PERFECT-GAS COMPARISON OF EXACT AND APPROXIMATE CONE SOLUTIONS

Figure 3-4 presents the comparison of the present methodology for predicting inviscid surface temperatures on a 20-percent blunt cone at α = 10 deg and M_∞ = 15. These results are compared to a full numerical solution of the Euler equations (ZEUS)[22] for both perfect and real gases. The real-gas temperatures are substantially lower than the perfect-gas results and also agree with the full Euler solution except in the vicinity of the overexpansion region past the blunt tip. Figure 3-3 uses most of the theory developed for the approximate methodology in Equations (64) through (71), along with the assumptions used in computing temperature.

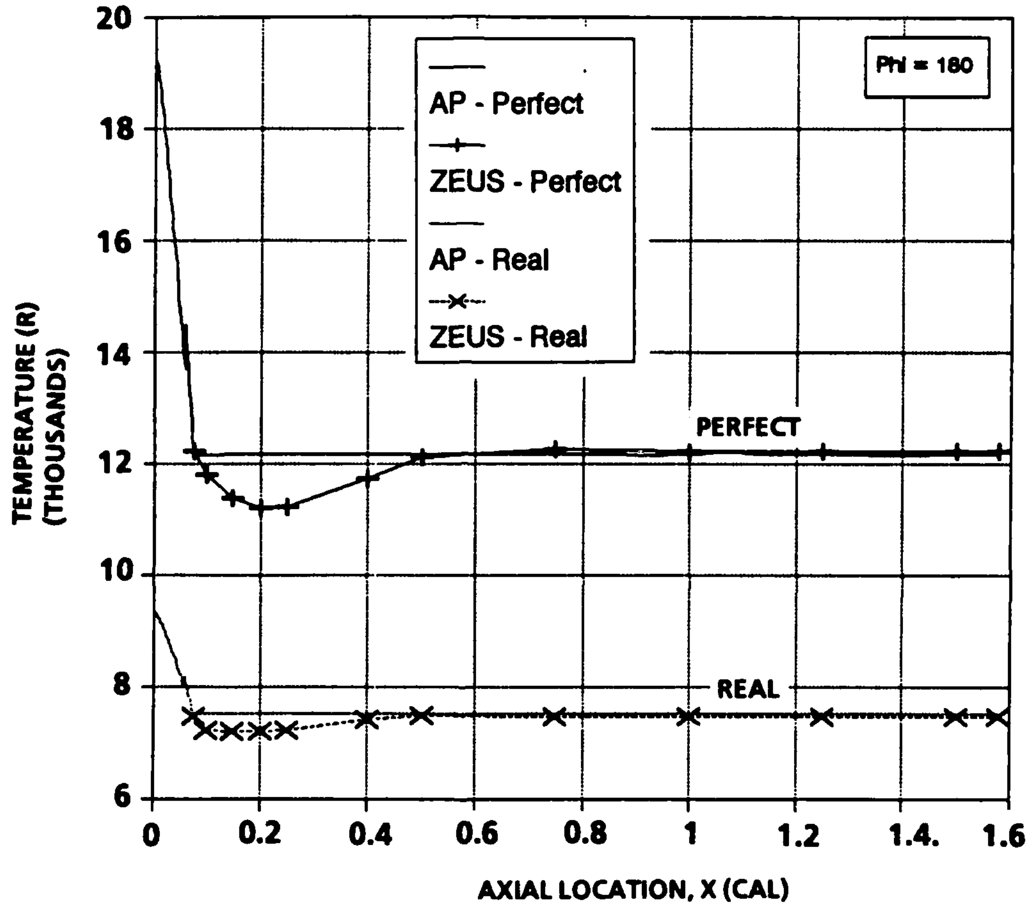

FIGURE 3-4. COMPARISON OF APPROXIMATE AND EXACT TEMPERATURE IN WINDWARD PLANE OF A 20 PERCENT BLUNT CONE (M_∞ = 15, α = 10 DEG)

3.2 AEROHEATING[98]

The AP93 methodology computes boundary layer heating information in the form of a heat transfer rate, $\dot{q}_w$; a heat transfer coefficient, H; and a recovery temperature (adiabatic wall temperature), T_{aw}, at each computational point.[98] These variables are related as shown in Equation (72).

$$H = \frac{\dot{q}_w}{T_{aw} - T_w} \tag{72}$$

T_W is the wall temperature. For high-temperature flows, the heat transfer coefficient is often expressed in terms of enthalpies.

$$H_1 = \frac{\dot{q}_w}{h_{aw} - h_w} \tag{73}$$

At temperatures above about 1500°R, Equation (73) is the more rigorously correct of the two. The heat transfer is normalized as shown in Equations (72) and (73) because the coefficients H and H_1 remain fairly constant over a wide range of wall temperatures, even though the actual heat transfer rate, $\dot{q}_w$, may vary significantly. Thus, since T_{aw} and h_{aw} are not functions of wall temperature, once a heating computation is performed for a given Mach number/altitude combination, it need not be repeated simply because of changes in wall conditions. This weak coupling greatly simplifies the problem of tracking the time-dependent thermal response of a surface exposed to boundary layer heating. The aerodynamic solution may be obtained first with a code such as AP93, and the results stored in tabular form as functions of a Mach number, altitude, and angle of attack. This information can then be accessed by an independent algorithm to compute the time-varying heat transfer rates and the resulting integrated surface temperature history along any given trajectory that lies within the limits of the data matrix.

The only departure from the use of true inviscid surface conditions as boundary layer edge properties occurs in the case of blunt bodies. The curvature of the detached bow shocks associated with these configurations creates an entropy layer near the body surface. The inviscid solution would give a uniform boundary layer edge entropy over the entire body equal to that behind a normal shock at the free-stream Mach number, since this is the entropy along the inviscid streamline that wets the body surface. In reality, because of the finite thickness of the boundary layer, the true edge entropy is that which exists at some point in the entropy layer located at a distance above the surface equal to the local boundary layer thickness. This entropy value is determined by an iterative mass balance technique.[98]

Once appropriate boundary layer edge conditions are determined, a series of specialized analytical relations are used to determine the aerodynamic heating at various locations. At the nose tip stagnation point, a simplified version of the Fay-Riddell formula[99] gives

$$\dot{q}_w = 0.763 Pr^{-0.6} \sqrt{\rho_0 \mu_0} \sqrt{\frac{dV_e}{dx}} (h_{aw} - h_w) \quad (74)$$

The stagnation point velocity gradient, dV_e/dx, is determined from the Newtonian theory, assuming a spherical nose tip. At the nose tip, the flow will always be laminar.

If control surfaces are present, the viscous heating along their leading edge stagnation lines is determined by the Beckwith and Gallagher swept-cylinder relations[100] modified to include real-gas effects.[101] For the laminar case,

$$\dot{q}_{w,l} = 0.57 Pr^{-0.6} \sqrt{\rho_0 \mu_0} \sqrt{\frac{dV_e}{dx}} (h_{aw} - h_w) (\cos\Lambda)^{1.1} \quad (75)$$

where Λ is the leading edge sweep angle and dV_e/dx is the stagnation line velocity gradient derived from Newtonian theory, assuming, a cylindrical leading edge. For turbulent flow,

$$\dot{q}_{w,t} = 1.04 Pr^{-0.6} \frac{(\rho^* \mu^*)^{0.8}}{(\mu_0)^{0.6}} (V_p \sin\Lambda)^{0.6} \left(\frac{du_e}{dx}\right)^{0.2} (h_{aw} - h_w) \quad (76)$$

where V_p is the flow velocity parallel to the leading edge stagnation line and the (*) superscript denotes evaluation at a reference enthalpy given by[102]

$$h^* = 0.5 (h_w + h_e) + 0.22 (h_{aw} - h_e) \quad (77)$$

The (e) subscript denotes evaluation at the boundary layer edge. The laminar or turbulent status of the flow is determined by comparison of the Reynolds number, based on the leading edge diameter, to user-specified upper and lower limits. If Re_D is below the lower limit, laminar values are used. If Re_D is above the upper limit, fully turbulent flow is assumed. For intermediate values of Re_D , a linear combination of laminar and turbulent values is computed.

For points on the body, the Eckert reference enthalpy flat plate formulation is used.[103] For laminar flow,

$$\dot{q}_{w,l}=0.332\,(Pr^{*})^{-0.667}\frac{\rho^{*}V_{e}}{\sqrt{\dfrac{Re^{*}}{N_{l}}}} \tag{78}$$

and for the turbulent case,

$$\dot{q}_{w,t} = 0.185\,(Pr^{*})^{-0.667}\frac{\rho^{*}V_{e}}{\left[\ln\dfrac{Re^{*}}{N_{t}}\right]^{2.584}} \tag{79}$$

N_l and N_t are transformation factors that allow for the approximation of three-dimensional (3-D) effects. They are equal to three and two, respectively. The laminar or turbulent flow character, is determined as before by comparing the local Reynolds number, based on boundary layer running length, to user-specified upper and lower limits.

Heating rates on the surfaces of wings, fins, or canards are determined by using Equations (78) and (79) but in this case, N_l and N_t are both equal to one because of the two-dimensional (2-D) nature of the flow. The degree of turbulence is determined in the same manner as for the body.

An example of the new aeroheating method is given in Figure 3-5. Figure 3-5 shows the heat transfer rate on a 15 degree half angle cone with a nose radius of 1.1 inches as a function of distance along the axis of symmetry. Conditions considered are M_∞ = 10.6 and angle of attack 10 degrees. Comparisons are made with a more complicated approximate technique[104] that uses streamline tracking combined with the axisymetric analog to model 3-D effects. Experimental data are also shown[105] along with the results from the MINIVER[101] code used in a tangent cone mode. AP 93 and MINIVER tend to under predict the data by about 10 - 15 percent, a performance that is credible considering the simplified nature of the solution. Note that the AP 93 gives improved results over MINIVER in the vicinity of the stagnation region due to the more accurate calculation of entropy at the edge of the boundary layer and more accurate real gas properties.

3.3 BASE DRAG

The AP81 estimated base drag using a composite of empirical data for the body alone. Also, an approximation was made for the effect of angle-of-attack, fin location, and fin thickness effects as a function of Mach number based on a limited amount of data. As a result, a request was made to the National Aeronautics and Space Administration, Langley Research Center (NASA/LRC) to perform additional wind tunnel tests, where additional base pressure measurements could be taken to try and quantify the effects mentioned, plus those due to control deflection.

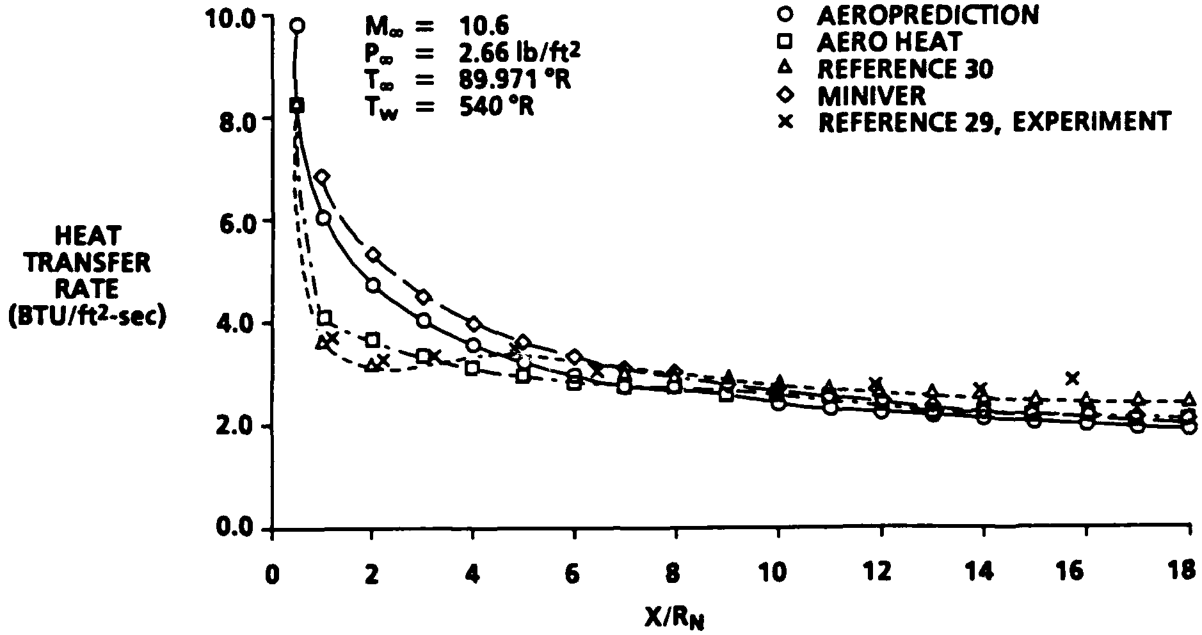

FIGURE 3-5. WINDWARD PLANE HEAT TRANSFER RATES FOR 1.1-IN. NOSE RADIUS, 15-DEG HALF-ANGLE CONE AT α = 10 DEG

Wilcox was the chief engineer for the tests that were conducted and reported.[106, 107] Eighty-nine base pressure taps were placed around a 7.2 caliber, 5-inch diameter body with a side mounted sting. These taps were placed every 22.5 deg in circumferential location and at several radii from the body centroid toward the outer edge. The configuration matrix of data taken is shown in Table 3-1. The base pressure measured at each of the 89 orifice locations was then averaged over its incremental base area to get the average base pressure at each condition, of Table 3-1. Based on these average base pressure measurements at each test condition, changes in base pressure, and hence, base drag because of a particular physical model change, or flight condition change could be readily computed by simply subtracting the two data points.

TABLE 3-1. CONFIGURATION INDEX

Config	Fins Off	t/c 0.05	t/c 0.10	t/c 0.15	x/c 0	x/c 1.0	x/c 2.0	δ 0	δ 10	δ 20	α (M_∞ = 2.0)	α ($M_\infty \geq$ 2.5)
1	X										Sweep	Sweep
2				X	X			X			0,5,10	0
3				X	X				X		0,5,10	0
4				X	X					X	0,5,10	0
5			X		X			X			0,5,10	0
6			X		X				X		0,5,10	0
7			X		X					X	0,5,10	0
8		X			X			X			0,5,10	0
9		X			X				X		0,5,10	0
10		X			X					X	0,5,10	0
11		X				X		X			0,5,10	0
12			X			X		X			0,5,10	0
13				X		X		X			0,5,10	0
14				X			X	X			0,5,10	0
15			X				X	X			0,5,10	0
16		X					X	X			0,5,10	No data

Using the process described, along with a wind tunnel data base not available when AP81 was developed,[108] a new empirical estimate of base pressure coefficient C_{p_B} was derived. This new estimate is shown in Figure 3-6 and compared to the AP81 value of C_{p_B}. The two curves are similar, with the AP93 slightly higher than AP81 for $M_\infty \leq 1.5$ and slightly lower than AP81 for $M_\infty \geq 3.0$. Body-alone angle-of-attack effects on base pressure are then estimated by

$$\left(C_{p_B}\right)_{NF,\alpha} = \left(C_{p_B}\right)_{NF,\alpha=0}\left[1+0.01F_1\right] \tag{80}$$

Here, $\left(C_{p_B}\right)_{NF,\alpha=0}$ comes from Figure 3-6 and F_1, the increase due to angle of attack from Figure 3-7. Boattail and power-on effects on base drag are estimated as present in AP81.

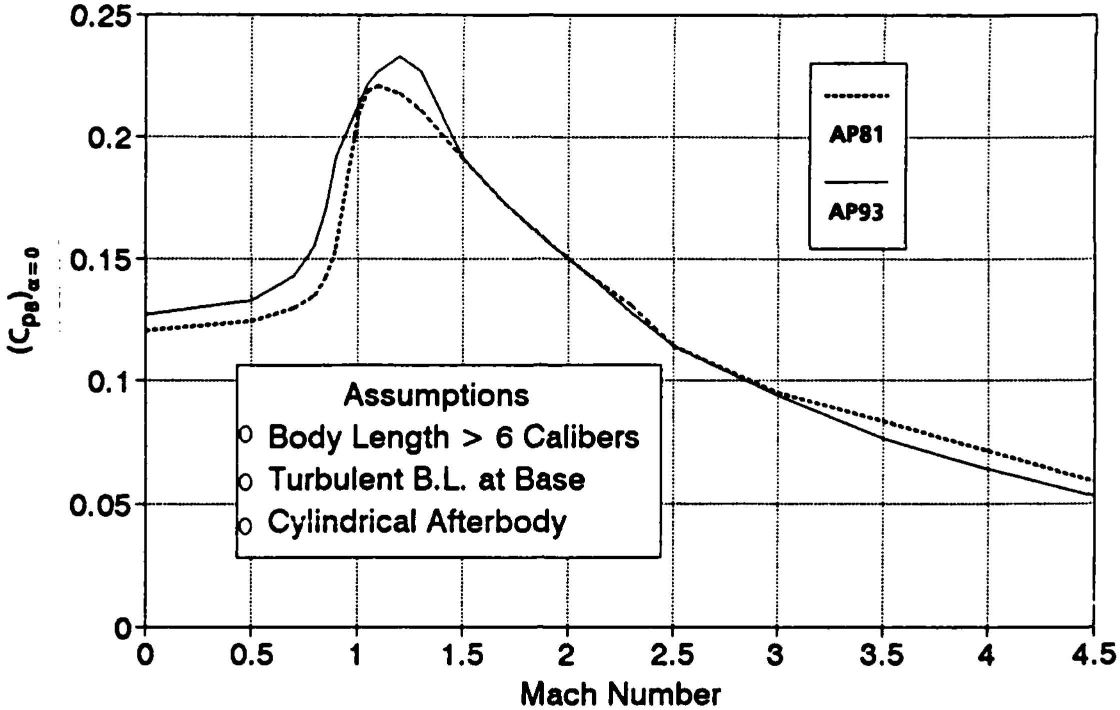

FIGURE 3-6. MEAN BODY-ALONE BASE PRESSURE COEFFICIENT USED IN AP81 AND AP93

At this point, it is worth noting that, while the databases of Moore, et al., and Butler, et al., helped to improve the estimate of base pressure as a function of Mach number and angle of attack for the body alone,[106, 107, 108] additional data are still needed for $\alpha \leq 15$ deg at all Mach numbers. This need is indicated by the dotted lines in Figures 3-7, which are extrapolations from data available for $\alpha \geq 15$ deg and engineering judgement. This same statement will also be even more true for fin effects due to control deflection and angle of attack, as will be discussed in the following paragraphs.

The total body base pressure coefficient for fins located flush with the base is

$$(C_{p_B})_{\alpha,\delta,t/c,x/c=0} = [1+0.01F_2](C_{p_B})_{NF,\alpha=0} + 0.01F_3(t/d) \tag{81}$$

where $(C_{p_B})_{NF,\alpha=0}$, F_2, and F_3 come from the AP93 curve of Figures 3-6, 3-8, and 3-9 respectively.

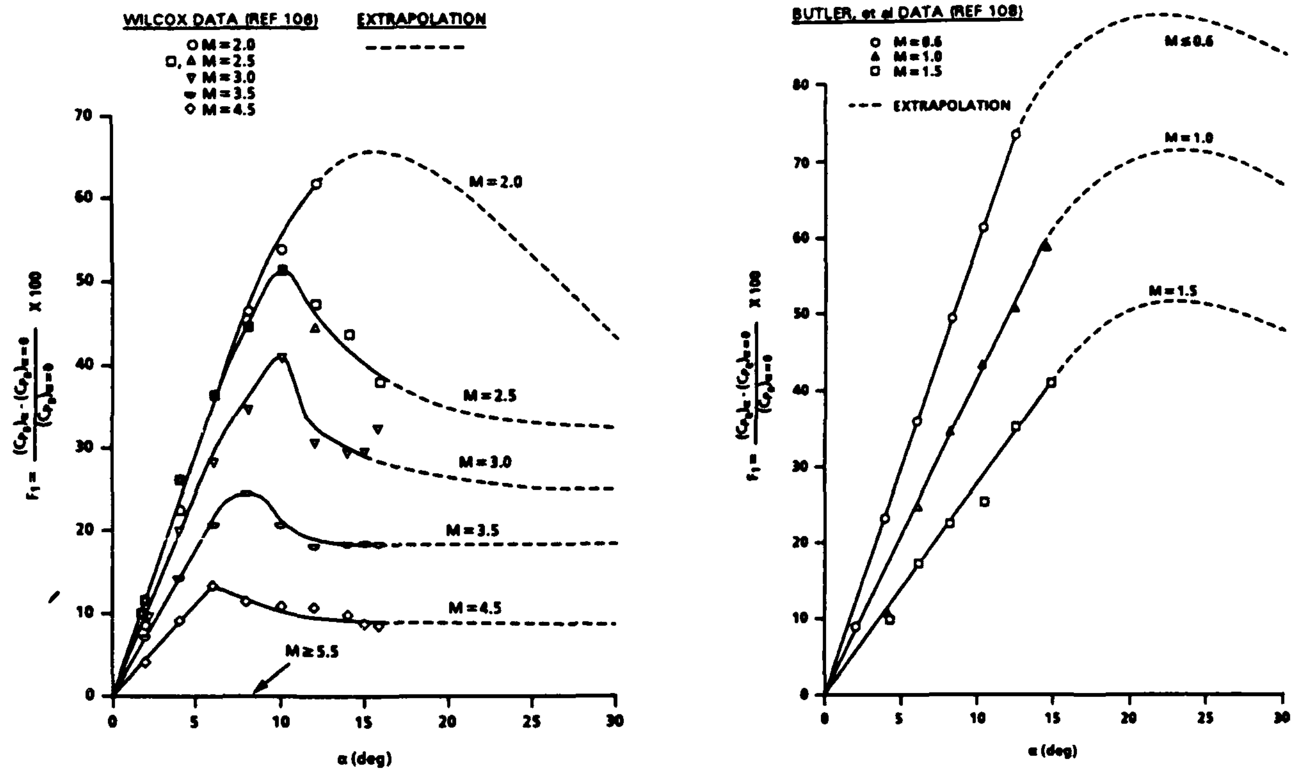

A. ($M_\infty \geq 2$)　　B. ($M_\infty < 2$)

FIGURE 3.7. PERCENT INCREASE IN BODY-ALONE BASE PRESSURE COEFFICIENT DUE TO ANGLE OF ATTACK

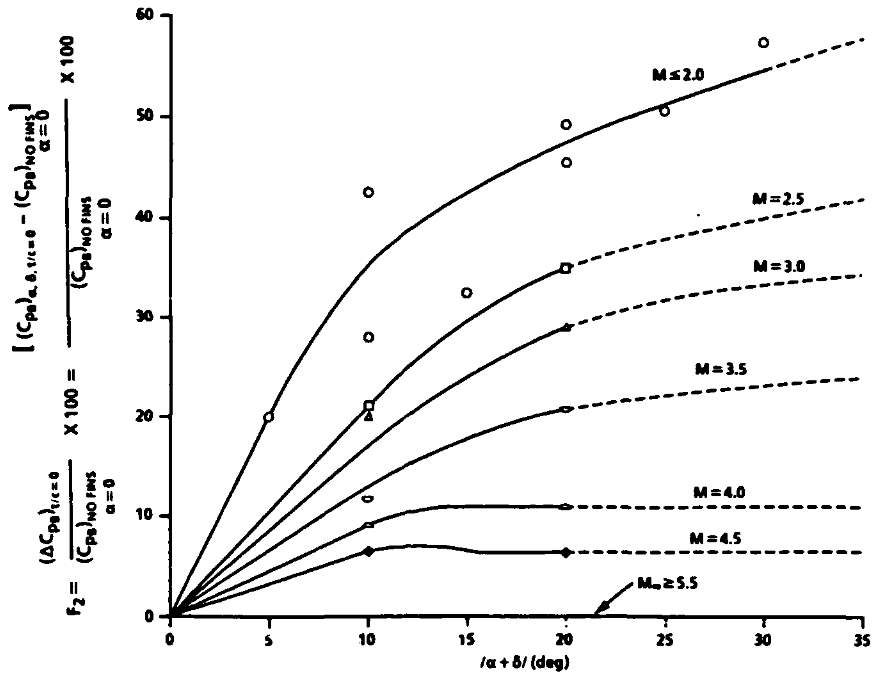

FIGURE 3-8. PERCENT INCREASE IN BASE PRESSURE COEFFICIENT DUE TO COMBINED EFFECTS OF ANGLE OF ATTACK AND CONTROL DEFLECTION (t/c ≈ 0)

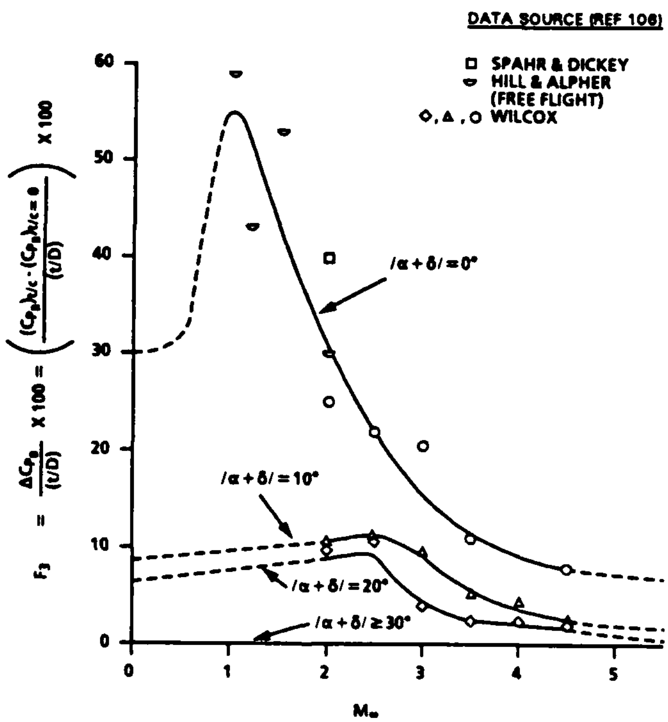

FIGURE 3-9. ADDITIONAL PERCENT INCREASE IN BASE PRESSURE COEFFICIENT DUE TO FIN THICKNESS AT VARIOUS VALUES OF $|\alpha + \delta|$

In Figure 3-8, no data were taken for $M_\infty < 2$,[106, 107] and none could be found in the literature. Hence, the data for $M_\infty = 2$ are assumed to apply for $M_\infty < 2$ as well. While this is a big assumption, it is believed to be better than neglecting the base pressure effect due to control deflection and angle of attack, which other engineering aerodynamics codes do. It is also worth noting that Figure 3-9 indicates what is intuitively obvious: for small control deflections and angles of attack, fin thickness effects are important in base pressure estimation, whereas for large values of α and δ, the additional change in C_{P_B} due to fin thickness is minimal.

The final parameter to define the effect on base pressure is fin location relative to the body base. This is done through Equation (82), where

$$(C_{P_B})_{\alpha,\delta,t/c,x/c} = (C_{P_B})_{NF,\alpha} + 0.01(\Delta C_{P_B})_{\alpha,\delta,t/c,x/c} \tag{82}$$

Here $(C_{P_B})_{NF,\alpha}$ is the body-alone base pressure coefficient at a given angle of attack given by Equation (80) and $(\Delta C_{P_B})_{\alpha,\delta,t/c,x/c}$ is the total change due to the presence of fins at a given α, δ, t/c, and x/c. An example of $(\Delta C_{P_B})_{\alpha,\delta,t/c,x/c}$ is given in Figure 3-10 for $M_\infty = 2.0$ and $|\alpha + \delta| = 10$ deg. Moore, et al., showed other curves for this parameter.[106] Figure 3-10 shows that the change in base pressure due to all variables present varies from that at x/c = 0, where the fins dominate to that of the body alone where the fins have no effect (x/c ≈ 2.5).

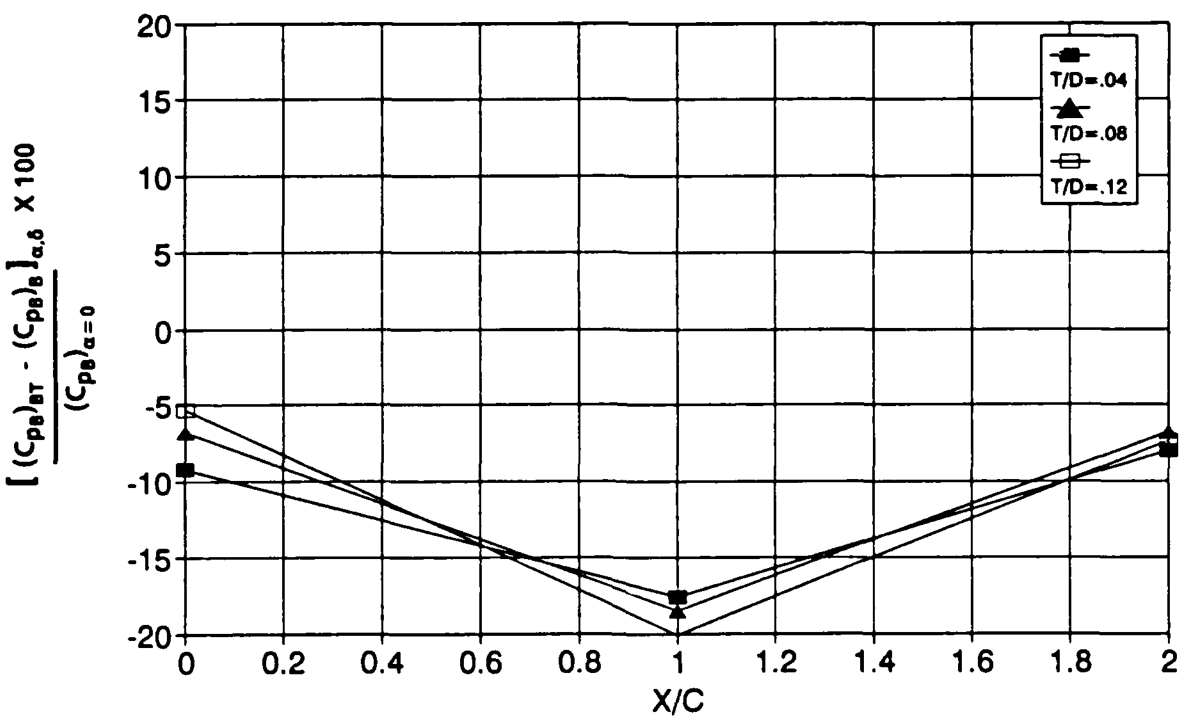

FIGURE 3-10. PERCENT INCREASE IN BASE PRESSURE COEFFICIENT DUE TO FIN LOCATION $|\alpha + \delta| = 10$ DEG, $M_\infty = 2.0$

3.4 IMPROVED METHOD FOR BODY-ALONE NORMAL FORCE AND CENTER OF PRESSURE[109, 110]

The normal-force coefficient of the body alone is estimated by [109]

$$C_N = C_{N_L} + C_{N_{NL}} \tag{83}$$

where C_{N_L} is the linear term and $C_{N_{NL}}$ the nonlinear term. The linear term is predicted in AP81 by either SOSET, second-order Van Dyke combined with MNT, or empirical depending on the Mach number range.[1, 6] The nonlinear term is estimated by the Allen-Perkins viscous crossflow theory.[34] No changes were made in the linear term of Equation (83) in AP93 from AP81. Three changes in the nonlinear term of Equation (83) were made for the AP93.

The nonlinear term of Equation (83) is[69]

$$C_{N_{NL}} = \eta C_{d_c} \sin^2\alpha \frac{A_p}{A_{ref}} \tag{84}$$

The first change from AP81 is in the value of η. AP81 used an incompressible value of η with no account of compressibility effects, although compressibility effects have been clearly shown.[111] The compressibility effect is shown in Figure 3-11A along with the line drawn to represent the data. This line is defined as

$$\begin{aligned} \eta &= \left(\frac{1-\eta_0}{1.8}\right) M_N + \eta_0 \qquad && for\ M_N \le 1.8 \\ \eta &= 1 && for\ M_N > 1.8 \end{aligned} \tag{85}$$

where η_0 is the incompressible value of η ($M_N = 0$) used in AP81[1].

The second change is in the value of the crossflow drag coefficient used. This value was changed to allow the effect of transition on the body surface to affect the value chosen. This affects the value of C_{d_c} for M_N values of 0.5 and less. Also, the value of C_{d_c} is slightly lower for $0.6 \le M_N \le 2.2$ than that used in AP81. This is based on the large NASA Tri-Service Data Base.[112] The new value of C_{d_c} used in AP93 is given in Figure 3-11B. If the flow on the body is a combination of laminar and turbulent (the case for most conditions), a value somewhere in between the two values on the Figure 3-11B curve for $M_N \leq 0.5$ will be computed. If X_L defines the length of laminar flow on the body and X_T is the total length, then for $M_N \leq 0.5$,

$$C_{d_c} = 1.2 - \left(\frac{X_L}{X_T}\right) 0.8 \tag{86}$$

Thus, if $X_L = 0$ so the flow over the body is fully turbulent, a value of $C_{d_c} = 1.2$ will be computed, whereas a value of 0.4 will be picked if the flow is fully laminar.

The third change made in AP93 was in the center-of-pressure location. AP81 used a weighted average of the normal force center of pressure of the linear term and nonlinear term, where the nonlinear term X_{cp} was at the centroid of the planform area in the crossflow plane and the X_{cp} of the linear term was computed theoretically or empirically. Both of these values were held constant as angle of attack increased, the only change being from the changing values of the normal-force terms of Equation (83). In numerical experiments using the NASA Tri-Service Missile Data Base, it was found that the assumption of a constant value of center of pressure with angle of attack was not completely correct. It is suspected that as angle of attack increases, the center of pressure of the linear term of Equation (83) changes and can no longer be assumed to be constant. An empirical way to represent this change with Mach number is given in Figure 3-11C. This change is effective for $\alpha \geq 10$ deg. Between $\alpha = 0$ and 10 deg, the correction is implemented in a linear fashion between zero at $\alpha = 0$ to its full value at $\alpha = 10$ deg.

Figure 3-12 is an example of the normal-force and center-of-pressure comparisons of the AP81, AP93, and experimental data. The data are for a 12.33-caliber tangent-ogive cylinder configuration with a 3.0-caliber nose.[112] The improvements made in AP93 give significantly better results on both C_N and X_{cp} as a function of angle of attack.

3.5 WING-ALONE NONLINEAR NORMAL FORCE AND CENTER OF PRESSURE

One of the major reasons the AP81 gave poor results at $\alpha > 10$ deg for many missile configurations was the failure to include nonlinearities in wing lift. Using NASA and ONR Data Bases[113, 114] a semiempirical method was developed for the nonlinear wing-alone normal-force term analogous to the body-alone Equations (83) and (84).[109,110] The nonlinear term of wing-alone lift, therefore, can be defined as

$$C_{N_{NL}} = f(M_N, AR, \Lambda) \left(\frac{A_p}{A_{ref}}\right) \sin^2\alpha \tag{87}$$

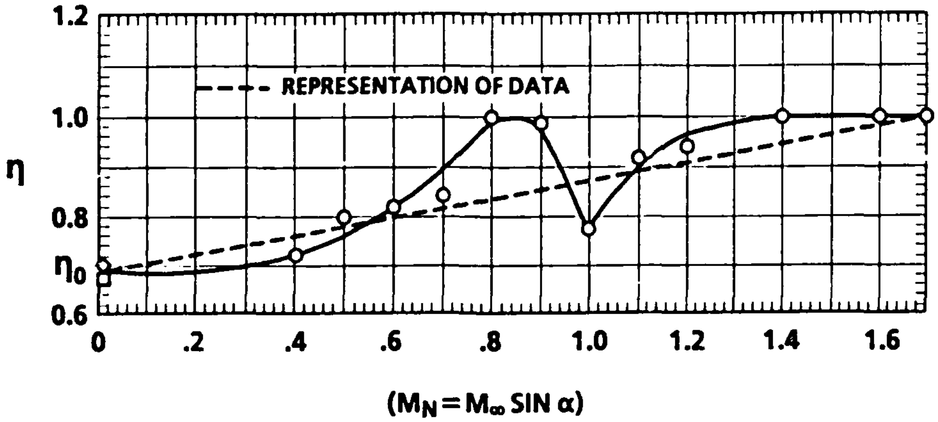

FIGURE 3-11A. COMPRESSIBILITY EFFECTS ON CROSSFLOW DRAG PROPORTIONALITY FACTOR

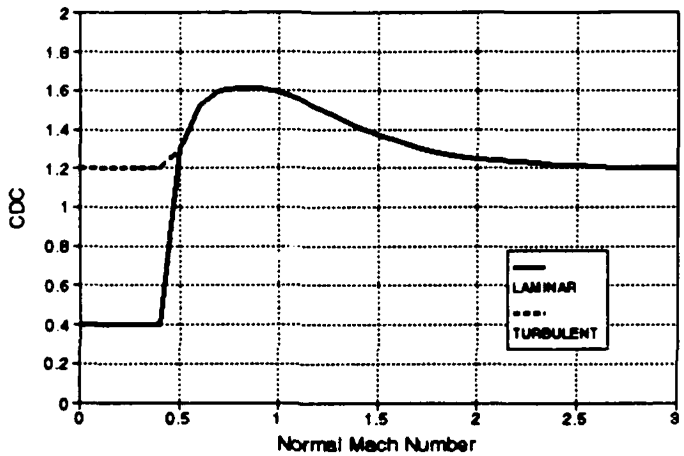

FIGURE 3-11B. CROSSFLOW DRAG COEFFICIENT FOR AN OGIVE-CYLINDER CONFIGURATION

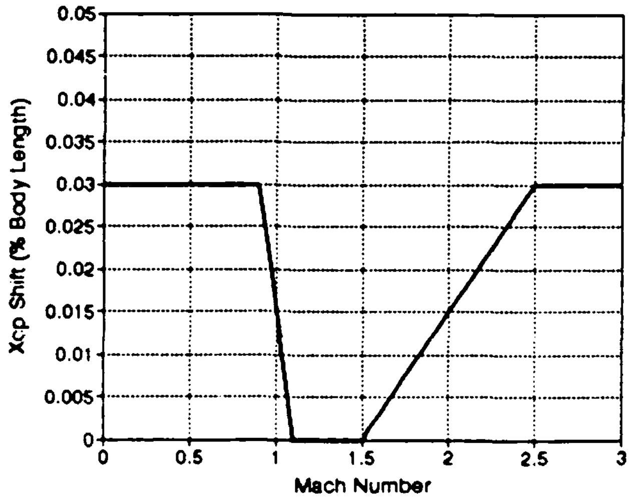

FIGURE 3-11C. CENTER-OF-PRESSURE SHIFT IN BODY-ALONE NORMAL FORCE FOR $\alpha \geq 10$ DEG

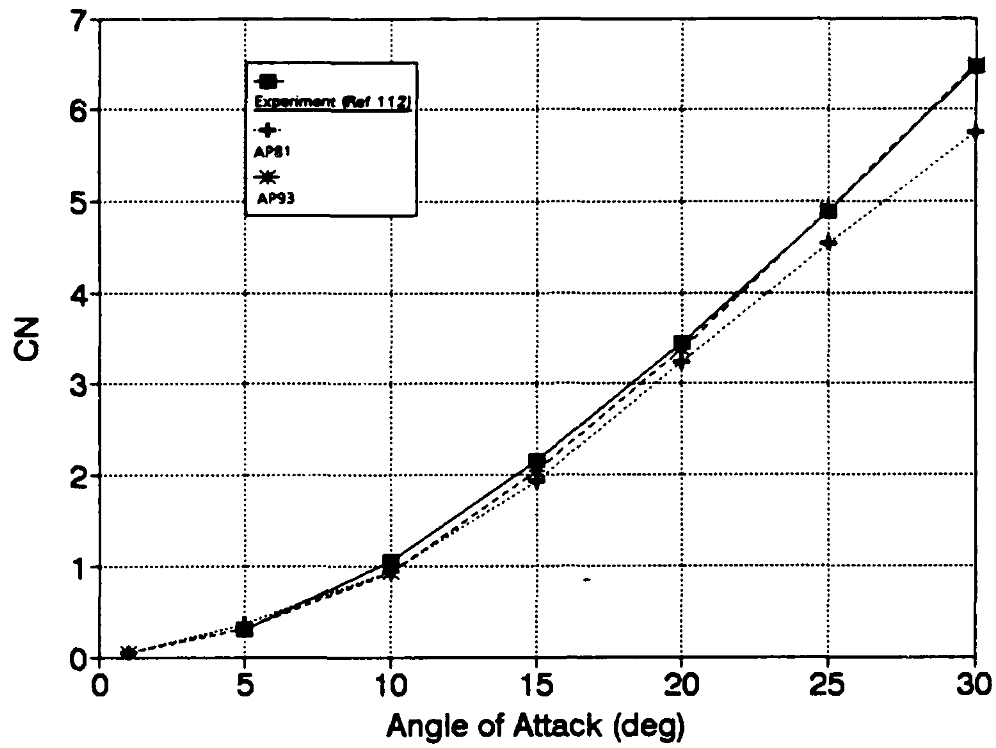

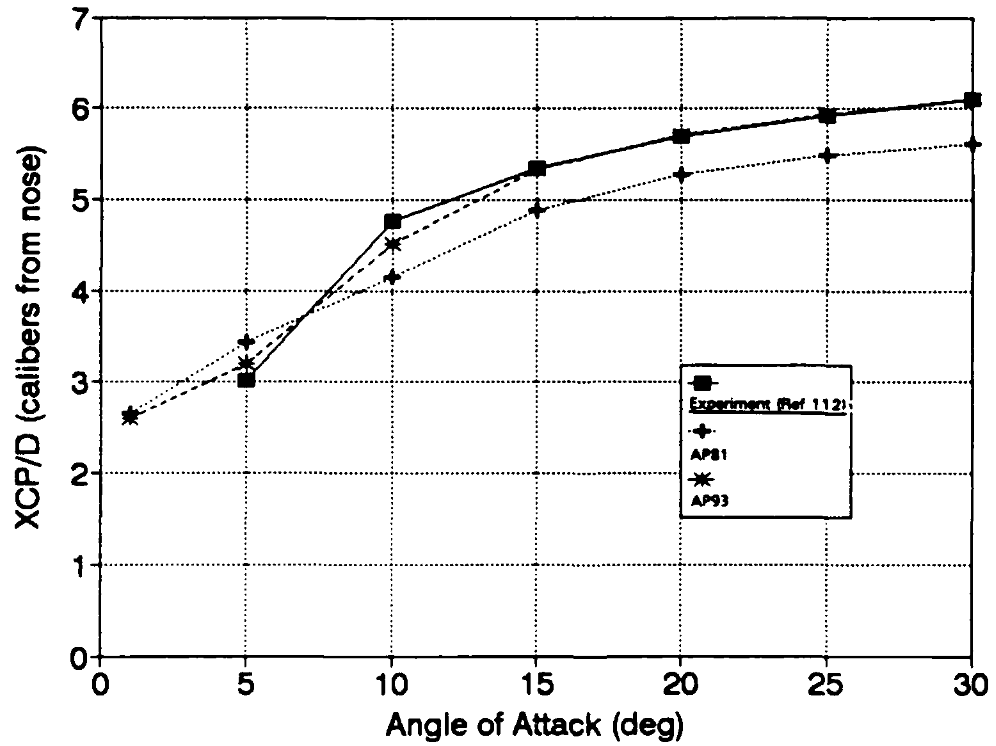

FIGURE 3-12. BODY-ALONE NORMAL-FORCE COEFFICIENT AND CENTER OF PRESSURE (M_{∞} = 3.5)

Here, $f(M_N, AR, \lambda)$ is analogous to the ηC_{d_c} of the body alone in Equation (84). Since the total wing-alone normal force is known for a given AR, M_∞, λ, and α,[113, 114] and the linear value of lift is known from the 3-D thin-wing theory or lifting surface theory from AP81; the nonlinear normal force of the wing alone is

$$C_{N_{NL}}\ (M_N, AR, \lambda) = C_N\ (M_N, AR, \lambda) - C_{N_L}\ (M_N, AR, \lambda) \tag{88}$$

Using the data of References 113 and 114, Equation (88) values were generated and a parameter k_1 defined as

$$k_1 = \frac{C_{N_{NL}}(M_N, AR, \lambda)}{\sin^2\alpha} \tag{89}$$

was generated. Tables of k_1 for both high and low Mach numbers are given in Tables 3-2 and 3-3. The total wing-alone normal force in AP93 is therefore

$$C_{N_w} = C_{N_L} + k_1 \sin^2\alpha \frac{A_w}{A_{ref}} \tag{90}$$

The second term of Equation (90) was neglected in AP81.

The center of pressure of the wing-alone lift was assumed to vary quadratically between its linear theory value at $\alpha = 0$ to the centroid of the planform area (adjusted for thickness effects) at $\alpha = 60$ deg.

Defining the center of pressure of the wing-alone linear term as A and the center of pressure of the nonlinear term as B (both in percent of mean geometric chord), then the center of pressure of the wing lift is

$$(X_{cp})_w = A + \frac{1}{36}|\alpha_w|[B - A] + \frac{1}{5400}\alpha_w^2[A - B] \tag{91}$$

α_w is the total angle of attack in degrees on the wing. Figure 3-13 gives an example of the AP93 methodology compared to AP81 and experimental data. This particular case shows significant improvement in the wing-alone normal force of the AP93 versus AP81 when compared to the experiment. However, no improvement in center of pressure is obtained because $\lambda = 0$ and the centroid of the planform area is the same as experimental data suggest.

TABLE 3-2. VALUES OF k_1 FOR LOW MACH NUMBER

$AR \leq 0.5;\ M_\infty < 4.0$

λ/M_∞	0.0	0.5	1.0	1.5	2.0	2.5	3.0	3.5	4.0	4.5
0.0	1.55	1.57	1.60	1.60	1.51	1.25	0.92	0.56	0.29	0.16
0.5	2.84	2.90	2.82	2.30	1.35	1.00	0.80	0.64	0.47	0.33
1.0	2.37	2.45	2.43	2.31	1.50	1.05	0.90	0.75	0.61	0.48

$AR = 1.0;\ M_\infty < 3.5$

λ/M_∞	0.0	0.5	1.0	1.5	2.0	2.5	3.0	3.5	4.0	4.5
0.0	1.32	1.48	1.46	0.99	0.40	0.22	0.12	0.09	0.09	0.11
0.5	2.44	2.45	1.85	0.70	0.31	0.19	0.20	0.26	0.36	0.43
1.0	1.20	1.22	1.10	0.50	0.45	0.50	0.65	0.78	0.88	0.94

$AR \geq 2.0;\ M_\infty < 3.5$

λ/M_∞	0.0	0.5	1.0	1.5	2.0	2.5	3.0	3.5	4.0	4.5
0.0	-1.80	-1.84	-1.95	-1.50	-0.20	0.00	0.10	0.20	0.25	0.30
0.5	-1.80	-1.84	-1.95	-1.50	-0.20	0.30	0.41	0.60	0.72	0.80
1.0	-1.45	-1.47	-1.35	-0.70	0.20	0.60	0.83	0.98	1.09	1.15

TABLE 3-3. VALUES OF k_1 FOR HIGH MACH NUMBER

$AR \leq 0.5;\ M_\infty \geq 4.0$

$\lambda/M_\infty \sin\alpha$	0.0	0.5	1.0	1.5	2.0	2.5	3.0	3.5	4.0	4.5	5.0	5.5	6.0
0.0	-1.60	-0.98	0.23	0.55	0.71	0.82	0.89	0.92	0.95	0.95	0.95	0.95	0.95
0.5	-0.87	-0.24	0.33	0.60	0.73	0.82	0.89	0.92	0.95	0.95	0.95	0.95	0.95
1.0	-0.31	0.09	0.46	0.68	0.78	0.87	0.91	0.93	0.95	0.95	0.95	0.95	0.95

$AR = 1.0;\ M_\infty \geq 3.5$

$\lambda/M_\infty \sin\alpha$	0.0	0.5	1.0	1.5	2.0	2.5	3.0	3.5	4.0	4.5	5.0	5.5	6.0
0.0	-0.39	-0.39	-0.29	0.06	0.29	0.48	0.60	0.69	0.75	0.81	0.86	0.91	0.94
0.5	0.14	0.17	0.29	0.46	0.63	0.76	0.85	0.90	0.93	0.95	0.95	0.95	0.95
1.0	0.30	0.50	0.86	0.93	0.94	0.95	0.95	0.95	0.95	0.95	0.95	0.95	0.95

$AR \geq 2.0;\ M_\infty \geq 3.5$

$\lambda/M_\infty \sin\alpha$	0.0	0.5	1.0	1.5	2.0	2.5	3.0	3.5	4.0	4.5	5.0	5.5	6.0
0.0	-0.25	-0.05	0.20	0.50	0.80	0.95	0.95	0.95	0.95	0.95	0.95	0.95	0.95
0.5	0.02	0.29	0.80	0.98	0.98	0.97	0.97	0.96	0.95	0.95	0.95	0.95	0.95
1.0	0.66	1.02	1.15	1.18	1.15	1.09	1.02	0.96	0.95	0.95	0.95	0.95	0.95

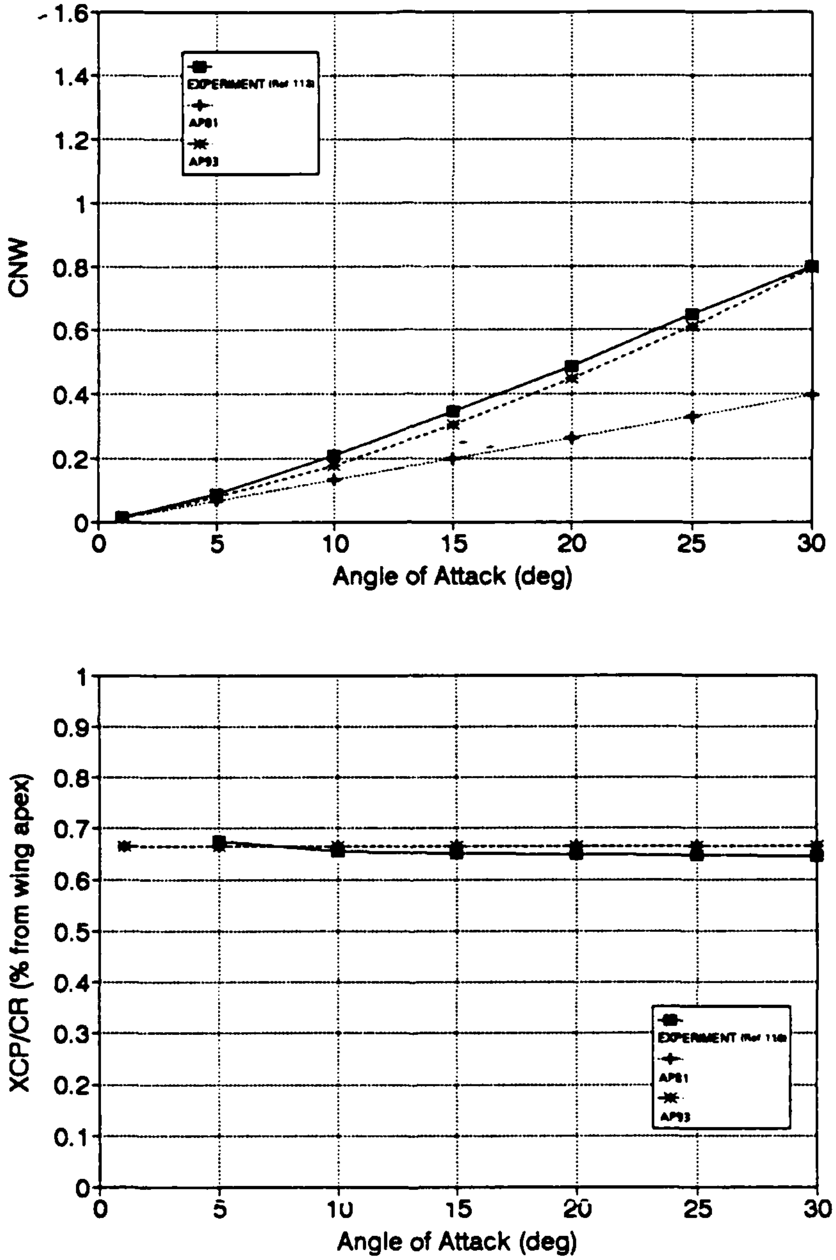

FIGURE 3-13. WING-ALONE NORMAL-FORCE COEFFICIENT AND CENTER OF PRESSURE (AR = 0.5, λ = 0.0, M_∞ = 1.6)

3.6 WING-BODY AND BODY-WING NONLINEAR INTERFERENCE FACTORS DUE TO ANGLE OF ATTACK [109, 110]

The total configuration normal-force coefficient at a given angle of attack, control deflection and Mach number is given by Equation (55) repeated here for convenience:

$$C_N = C_{N_B} + \left[\left(K_{W(B)} + K_{B(W)}\right)\alpha + \left(k_{W(B)} + k_{B(W)}\right)\delta_W\right]\left(C_{N_\alpha}\right)_W + \left[\left(K_{T(B)} + K_{B(T)}\right)\alpha + \left(k_{T(B)} + k_{B(T)}\right)\delta_T\right]\left(C_{N_\alpha}\right)_T + C_{N_{T(V)}} \quad (55)$$

Moore, et al., found that the wing-body interference factor $K_{W(B)}$ had the qualitative behavior as shown in Figure 3-14.[109] At low angles of attack, slender-body theory appeared to be a good estimate of $K_{W(B)}$. This estimate was adjusted slightly for $M_\infty \le 1.5$ by an amount $\Delta K_{W(B)}$. At some angle of attack defined as α_c, $K_{W(B)}$ seemed to decrease in a nearly linear fashion. The rate of this decrease was a function of Mach number: the higher the Mach number, the larger the rate of decrease. At some point defined as α_D, the $K_{W(B)}$ appeared to reach a minimum and remain about constant. As a result of this analysis, a mathematical model was derived to define $K_{W(B)}$ in terms of its slender-body theory value $[K_{W(B)}]_{SB}$ and an empirical correction derived from several databases.[112, 113, 114] This model given in Figure 3-14 is

$$K_{W(B)} = \left[K_{W(B)}\right]_{SB} + \left[\Delta K_{W(B)}\right]_{\alpha=0}\left(\frac{r/s}{0.5}\right) \quad for\ \alpha \le \alpha_c$$

$$K_{W(B)} = \left[K_{W(B)}\right]_{SB} + \left\{\left[\Delta K_{W(B)}\right]_{\alpha=0} + \frac{dK_{W(B)}}{d\alpha}(\alpha - \alpha_c)\right\}\left(\frac{r/s}{0.5}\right) \quad for\ \alpha_c \le \alpha \le \alpha_D \quad (92)$$

$$K_{W(B)} = \left[K_{W(B)}\right]_{SB} + \left\{\left[\Delta K_{W(B)}\right]_{\alpha=0} + \frac{dK_{W(B)}}{d\alpha}(\alpha_D - \alpha_c)\right\}\left(\frac{r/s}{0.5}\right) \quad for\ \alpha > \alpha_D$$

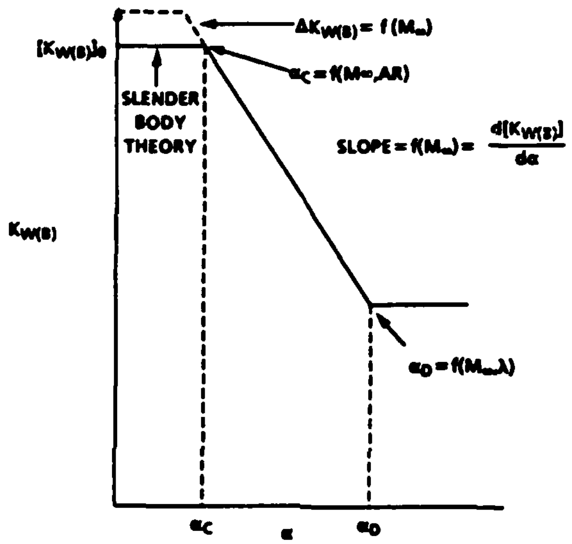

GENERAL EQUATION:

$$K_{W(B)} = \left[K_{W(B)}\right]_{SB} + \left[\Delta K_{W(B)}\right]_{\alpha=0} \frac{r/s}{0.5} \quad \text{for } \alpha \le \alpha_c$$

$$K_{W(B)} = \left[K_{W(B)}\right]_{SB} + \left[\Delta K_{W(B)}\right]_{\alpha=0} \frac{r/s}{0.5} + \left(\frac{dK_{W(B)}}{d\alpha}\right) \frac{(\alpha-\alpha_c)(r/s)}{0.5} \quad \text{for } \alpha_c \le \alpha \le \alpha_D$$

$$K_{W(B)} = \left[K_{W(B)}\right]_{SB} + \left\{\left[\Delta K_{W(B)}\right]_{\alpha=0} + \frac{dK_{W(B)}}{d\alpha}(\alpha_D-\alpha_c)\right\}\left(\frac{r/s}{0.5}\right) \quad \text{for } \alpha > \alpha_D$$

FIGURE 3-14. QUALITATIVE BEHAVIOR OF WING-BODY INTERFERENCE FACTORS AS A FUNCTION OF ANGLE OF ATTACK

The empirical corrections to $K_{W(B)}$ are also in a form that can be defined mathematically as opposed to a table lookup procedure. These equations for

$$[\Delta K_{W(B)}]_{\alpha=0},\ \frac{dK_{W(B)}}{d\alpha},\ \alpha_C,\ \alpha_D$$

are as follows:

$\underline{[\Delta K_{W(B)}]_{\alpha=0}}$

$$[\Delta K_{W(B)}]_{\alpha=0}=0.22 \qquad for\ M_\infty\le 1.0$$

$$[\Delta K_{W(B)}]_{\alpha=0}=-0.44[M_\infty-1.5] \qquad for\ 1.0<M_\infty\le 1.5 \tag{93}$$

$$[\Delta K_{W(B)}]_{\alpha=0}=0 \qquad for\ M_\infty>1.5$$

$\underline{d[K_{W(B)}]\ /\ d\alpha}$

$$\frac{d[K_{W(B)}]}{d\alpha} = -(0.00283M_\infty + 0.025) \tag{94}$$

$\underline{\alpha_C}$

$\underline{M\le 2.0}$

$$\alpha_C = 12.5 - 1.06M_\infty - 2.59M^{SCALESYM502}_{SCALESYM50\infty} \qquad for\ AR\le 0.5$$

$$\alpha_C = 12.5 - 6.25M_\infty \qquad for\ AR=1.0 \tag{95}$$

$$\alpha_C = 4.5 + 2.25M_\infty - 2.25M^{SCALESYM502}_{SCALESYM50\infty} \qquad for\ AR\ge 2.0$$

$\underline{M_\infty>2.0}$

$\alpha_C=0$

$\underline{\alpha_D}$

$$\alpha_D = 33.3 - 8.19M_\infty + 0.82M_\infty^2 \qquad for\ \lambda = 0$$

$$\alpha_D = 25.3 - 6.62M_\infty + 0.66M_\infty^2 \qquad for\ \lambda = 1.0$$

$$\alpha_D = [\alpha_D]_{\lambda=1.0} + \lambda[(\alpha_D)_{\lambda=0} - (\alpha_D)_{\lambda=1.0}] \qquad for\ 0<\lambda<1.0 \tag{96}$$

The semi-empirical model for $K_{B(W)}$ was also defined in terms of its slender body or linear theory value, plus a correction due to nonlinearities associated with angle of attack. The mathematical model for $K_{B(W)}$ was defined as [109]

$$K_{B(W)} = [K_{B(W)}]_{\substack{SB \\ LT}} + \frac{r/s}{0.5}\left\{[\Delta K_{B(W)}]_{\alpha=0} + \frac{d[K_{B(W)}]}{d\alpha}|\alpha|\right\} \tag{97}$$

Unfortunately, a mathematical model for $[\Delta K_{B(W)}]_{\alpha=0}$ and $d[K_{B(W)}]/d\alpha$ was difficult to define because of the variability of the constants as a function of the parameters of interest. As a result, a three-parameter table lookup for these two parameters is used in AP93 based on the data in Table 3-4. The parameters in the table lookup include M_∞, λ, and AR. Linear interpolation is used.

In Equations (92) and (96), the factor

$$\frac{r/s}{0.5}$$

appears. This is because the NASA Tri-Service Missile Data Base is based on $r/s = 0.5$, and Pitts, et al., indicates that the aerodynamics vary linearly with r/s.[87] This assumption is inherent in the semiempirical models for $K_{W(B)}$ and $K_{B(W)}$.

TABLE 3-4. DATA FOR BODY-WING NONLINEAR SEMIEMPIRICAL INTERFERENCE MODEL

Data for $[\Delta K_{B(W)}]_{\alpha=0}$

Aspect Ratio	Taper Ratio	Mach Number ≤ 0.6	0.8	1.2	1.5	2.0	2.5	3.0	3.5	≥ 4.5
≤ 0.25	0, 0.5, 1.0	-0.1	-0.1	0.5	0.6	0.7	0.8	0.7	0.5	0.3
0.5	0.5	-0.28	-0.1	0.13	0.11	0.05	-0.02	-0.06	0	0
1.0	0.5	-0.26	-0.2	0.15	0.21	0.15	0	0	0	0
≥ 2.0	0.5	-0.13	-0.04	0.12	0.43	-0.16	0	0.37	-0.08	-0.16
0.5	0	-0.3	-0.06	0.26	0.28	0.17	0.12	0.14	0	0
≥ 2.0	0	-0.2	-0.1	0.12	0.52	0.12	0.15	0.22	-0.06	-0.22
0.5	1.0	-0.16	0.08	0.26	0.14	-0.12	0	-0.05	-0.10	0
≥ 2.0	1.0	-0.2	-0.1	0.12	0.45	-0.02	0.11	0.28	-0.17	-0.3

Data for $d[K_{B(W)}]/d\alpha$

Aspect Ratio	Taper Ratio	Mach Number ≤ 0.6	0.8	1.2	1.5	2.0	2.5	3.0	3.5	≥ 4.5
≤ 0.25	0, 0.5 1.0	0.018	0.013	-0.010	-0.023	-0.013	-0.022	-0.031	-0.025	-0.031
0.5	0.5	0.019	0.010	-0.008	-0.010	-0.013	-0.013	-0.013	-0.012	-0.012
1.0	0.5	0.013	0.010	-0.007	-0.013	-0.020	-0.017	-0.012	-0.012	-0.012
≥ 2.0	0.5	0.010	0.011	0	-0.013	-0.010	-0.017	-0.040	-0.012	-0.012
0.5	0	0.033	0.022	0	-0.007	-0.010	-0.008	-0.014	-0.012	-0.012
≥ 2.0	0	0.010	0.010	-0.007	-0.020	-0.011	-0.020	-0.023	-0.012	-0.012
0.5	1.0	0.019	0	-0.019	-0.010	-0.007	-0.013	-0.014	-0.012	-0.012
≥ 2.0	1.0	0.010	0.01	-0.007	-0.017	0	-0.017	-0.026	-0.012	-0.012

In examining cases where r/s is small, it was found that at high angles of attack, the wing-alone solution was not recovered properly through the process, Equations (92) and (97). To remedy this situation, the AP93 nonlinear interference factors were blended into those predicted by slender-body or linear theory as r/s became small. The specific equations used to do this are

<u>For r/s ≥ 0.25</u>

$$K_{W(B)} = \left[K_{W(B)}\right]_{AP93}$$
$$K_{B(W)} = \left[K_{B(W)}\right]_{AP93} \qquad (98a)$$

<u>For 0.05 < r/s < 0.25</u>

$$K_{W(B)} = \left[K_{W(B)}\right]_{SBT} - \left(\left[K_{W(B)}\right]_{SBT} - \left[K_{W(B)}\right]_{AP93}\right)(r/s - 0.05)/0.2$$
$$K_{B(W)} = \left[K_{B(W)}\right]_{\substack{SBT\\LT}} - \left(\left[K_{B(W)}\right]_{\substack{SBT\\LT}} - \left[K_{B(W)}\right]_{AP93}\right)(r/s - 0.05)/0.2 \qquad (98b)$$

<u>For r/s ≤ 0.05</u>

$$K_{W(B)} = \left[K_{W(B)}\right]_{SBT} \; ; \; K_{B(W)} = \left[K_{B(W)}\right]_{\substack{SBT\\LT}} \qquad (98c)$$

In essence, the model represented by Equations (98a) through (98c) uses the nonlinear interference factors for r/s values greater than 0.25; they use a blend of slender-body or linear theory and the nonlinear values of interference factors for r/s values between 0.05 and 0.25. They also use the slender-body or linear theory values for r/s values less than 0.05. Hence, when the body vanishes (r/s = 0), the wing-alone solution will be automatically recovered in a smoother and more accurate way.

Figure 3-15 is an example of the normal force on the wing in the presence of the body and the normal force on the body in the presence of the wing using AP93 theory, the AP81 theory, and compared to experimental data. Note that

$$C_{N_{W(B)}} = C_{N_W} K_{W(B)}$$
$$C_{N_{B(W)}} = C_{N_W} K_{B(W)} \qquad (99)$$

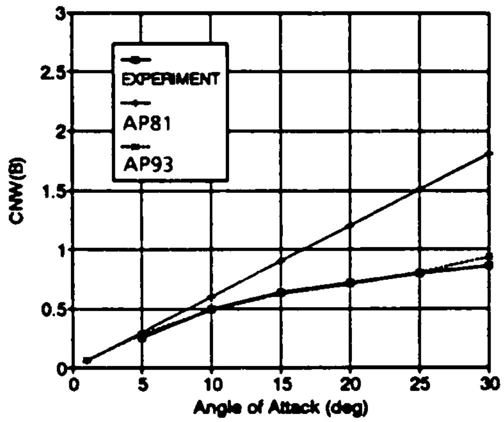

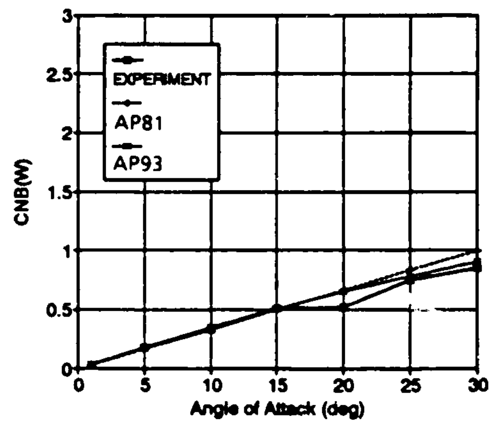

FIGURE 3-15. WING-BODY AND BODY-WING INTERFERENCE AS A FUNCTION OF α (AR = 2.0, λ = 0, M_∞ = 1.2)

Hence, Figure 3-15 is actually a representation of the normal-force coefficient on the wing and additional normal force on the body due to the wing. Thus, Equation (99) is a representation of the accuracy of not only $K_{W(B)}$ and $K_{B(W)}$, but C_{N_W} in conjunction with the interference factors. This is a more true indication of the accuracy of the code because there are actually two of the component force terms that make up Equation (39). As seen in Figure 3-15, the AP93 methodology is clearly superior to the AP81 theory as angle of attack increases.

The center of pressure of the new value of normal force of the wing in the presence of the body estimated by Equation (92) is assumed to remain at the values of the wing-alone solution of AP93 given by Equation (91). The center of pressure of the additional lift on the body due to the presence of the wing is estimated using the AP81 method, which is either slender-body or linearized theory. These values are modified for short afterbodies.[2]

In exercising the AP93 on missile configurations in the transonic speed regime ($0.6 \le M \le 2.0$), it was found that some of the nonlinear lift associated with small aspect ratio fins ($AR \le 1.4$) was lost due to shock-wave formation. An empirical approach in the AP81 accounted for a certain amount of linear lift loss. This appeared to be satisfactory for the larger aspect ratio fins, where the nonlinear normal-force term with angle of attack was negative. However, when the fins have a positive nonlinear normal force due to angle of attack, some of this force appears to be lost with shock waves. This loss was estimated empirically as a function of Mach number and angle of attack for a wing that had an area-to-body reference area of about one. These data for ΔC_N losses due to compressibility effects are given in Table 3-5. A two parameter linear interpolation is made from Table 3-5 for a given M_∞ and α to compute ΔC_N. ΔC_N is further degraded for taper ratio for values of $\lambda < 0.5$. The specific equations for ΔC_N are

$$
\begin{aligned}
\Delta C_{N_{B(W)}} &= -(\Delta C_N)\frac{A_W}{A_{ref}} && \text{for } \lambda \ge 0.5 \\
\Delta C_{N_{B(W)}} &= -(\Delta C_N)\left(\frac{A_W}{A_{ref}}\right)\left(\frac{\lambda}{0.5}\right) && \text{for } 0.1 \le \lambda \le 0.5 \qquad (100) \\
\Delta C_{N_{B(W)}} &= -0.2\Delta C_N\left(\frac{A_W}{A_{ref}}\right) && \text{for } \lambda \le 0.1
\end{aligned}
$$

TABLE 3-5. LOSS OF WING NONLINEAR NORMAL FORCE DUE TO SHOCK-WAVE EFFECTS IN TRANSONIC FLOW

	$\alpha + \delta$ |, deg|								
M_∞	0	5	10	15	20	25	30	35	≥ 40
≤ 0.4	0.0000	0.0000	0.0000	0.0000	0.0000	0.0000	0.0000	0.0000	0.0000
0.6	0.0000	0.0000	0.0000	0.0000	-0.0220	-0.2060	-0.6890	-0.9500	-1.300
0.8	0.0000	0.0000	0.0000	0.0000	-0.0531	-0.2200	-0.7100	-1.010	-1.400
1.2	0.0000	0.0000	-0.0093	-0.0293	-0.1651	-.04167	-0.7629	-1.070	-1.500
1.5	0.0000	0.0000	-0.0653	-0.1111	-0.1556	-0.4444	-0.7000	-1.070	-1.500
2.0	0.0000	0.0000	-0.0076	-0.0376	-0.1502	-0.1142	-0.0951	-0.0700	- 0.0500
≥2.5	0.0000	0.0000	0.0000	0.000	0.0000	0.0000	0.0000	0.0000	0.0000

3.7 NONLINEAR WING-BODY INTERFERENCE FACTOR DUE TO CONTROL DEFLECTION[8]

Initially, it was planned to use slender-body theory for the interference factors $k_{W(B)}$ and $k_{B(W)}$, as currently done in AP81. This plan was based on results comparing computations (using Equations (55) where all the nonlinearities are included) with experimental data at $\delta = 0$ for both body-tail and wing-body-tail or dorsal-body-tail configurations.[109] These comparisons were good and seemed to indicate that new technology was superior to existing engineering approaches. However, when results were examined for configurations that had control deflections on either the aft or forward lifting surface, they were found to be not as good as desired. This led to the conclusion that nonlinear interference factors, due to control deflection, were also required to improve the performance of AP93 when compared to experimental data.

The approach taken was to use the AP93 with the non-linearities of wing-alone, wing-body, and body-wing interference effects due to angle of attack included, use the slender-body estimates of $k_{W(B)}$ and $k_{B(W)}$ for control deflection, and derive empirical modifications to $k_{W(B)}$ based on numerical experiments compared to actual missile data. Because $k_{W(B)}$ appears in the vortex lift on the tail due to canard or wing shed vortices, the numerical experiments were conducted with canard body-tail configurations.

Referring to Equation (55), the vortex normal-force coefficient on the tail is[87]

$$C_{N_{T(V)}} = \frac{\left(C_{N_\alpha}\right)_W \left(C_{N_\alpha}\right)_T \left[K_{W(B)} \sin\alpha + F k_{W(B)} \sin\delta_W\right] i\left(s_T - r_T\right) A_W}{2\pi\,(AR)_T \left(f_W - r_W\right) A_{ref}} \qquad (101)$$

Equation (101) has a factor F that multiplies the term due to control deflection in the wing-tail vortex lift. This factor is needed in addition to the nonlinearity for $k_{W(B)}$, partly because the negative afterbody lift due to control deflection is not presently modeled in either AP81 or AP93. This term is defined by Equation (63).

The main reason this term was not included in the AP81 code was that it required an estimate of f_T, which is the position of the canard shed vortex at the tail. Also, Nielsen, et al., indicated that this term was generally much smaller than that computed by Equation (101).[114] To account for this term, a vortex tracking algorithm or an empirical correction to the term in Equation (101) is needed. For angles of attack much greater than 25 or 30 deg, a vortex tracking algorithm may be needed. However, up to α of about 30 deg, a nonlinear model of interference effects resulting from control deflection was developed by defining $k_{W(B)}$ as a function of angle of attack and Mach number and F as a function of Mach number and angle of attack.

Using the work of Nielsen, et al., McKinney, and Smith, et al., for low Mach number,[114, 115, 117] a semiempirical nonlinear model for $k_{W(B)}$ and the parameter F were derived from numerical experiments. The mathematical model for $k_{W(B)}$ is based on slender-body theory similar to $k_{W(B)}$ and $k_{B(W)}$ and modified for angle of attack or control deflection. In general, it was found that

$$k_{W(B)} = C_1 (M)[k_{W(B)}]_{SB} + C_2(|\alpha_W|, M_\infty)$$
$$F = C_3(M, |\alpha_W|) \tag{102}$$

More specifically, $k_{W(B)}$, C_1, C_2, and F are defined in Figure 3-16 for Mach numbers where data are available. For Mach numbers less than 0.8 and greater than 4.6, the equations derived for those conditions have been used. The current method for using the empirical estimate for $k_{W(B)}$ from Figure 3-16 is to linearly interpolate between Mach numbers for a given value of α, δ, and M_∞.

The model in Figure 3-16 has a lot of similarities to the nonlinear $K_{W(B)}$ model already discussed: at low angle of attack, slender-body theory gives a reasonable estimate of $k_{W(B)}$. However, as angle of attack increases, $k_{W(B)}$ decreases up to low supersonic Mach numbers. For higher supersonic Mach numbers, $k_{W(B)}$ actually increases at higher angles of attack, presumably due to compressibility effects. Also, for low angles of attack, a value of F near one is found for the vortex lift model, indicating again reasonable accuracy of the theory in reference 87. However, as angle of attack is increased, F increases above one for many Mach numbers. That is, Equation (101) gives values of $C_{N_{T(V)}}$ too small due to control deflection of a forward surface. As already mentioned, this is most probably due to the neglect of the effect on the afterbody Equation (63), which accounts for a greater percentage of the afterbody effect compared to the Equation (101) results, as angle of attack increases.

$\underline{M \le .8}$

If $|\alpha_w| \le 24.0 \rightarrow k_{w(B)} = 1.4[k_{w(B)}]_{SB}$
If $|\alpha_w| > 24.0 \rightarrow k_{w(B)} = 1.4\,[.000794\,|\alpha_w|^2 - .0933\,|\alpha_w| + 2.71]$
$F = 1.1$

$\underline{M = 1.1}$

If $|\alpha_w| \le 15.0 \rightarrow k_{w(B)} = 1.3[k_{w(B)}]_{SB}$
If $|\alpha_w| > 15.0 \rightarrow k_{w(B)} = 1.3\,[.00087\,|\alpha_w|^2 - .0825\,|\alpha_w| + 1.98]$
$F = 1.1$

$\underline{M = 1.5}$

If $|\alpha_w| \le 10.0 \rightarrow k_{w(B)} = .9[k_{w(B)}]_{SB}$
If $|\alpha_w| > 10.0 \rightarrow k_{w(B)} = .9[k_{w(B)}]_{SB} - .015[|\alpha_w| - 10.0]$
If $|\alpha_w| \le 20.0 \rightarrow F = .8$
If $|\alpha_w| > 20.0 \rightarrow F = .8 + .10[|\alpha_w| - 20.0]$

$\underline{M = 2.0}$

If $|\alpha_w| \le 10.0 \rightarrow k_{w(B)} = .9[k_{w(B)}]_{SB}$
If $|\alpha_w| > 10.0 \rightarrow k_{w(B)} = .9[k_{w(B)}]_{SB} - .005[|\alpha_w| - 10.0]$
If $|\alpha_w| \le 20.0 \rightarrow F = .8$
If $|\alpha_w| > 20.0 \rightarrow F = .8 + .17[|\alpha_w| - 20.0]$

$\underline{M = 2.3}$

If $|\alpha_w| \le 20.0 \rightarrow k_{w(B)} = .9[k_{w(B)}]_{SB}$
If $|\alpha_w| > 20.0 \rightarrow k_{w(B)} = .9[k_{w(B)}]_{SB} - .005[|\alpha_w| - 20.0]$
If $|\alpha_w| \le 30.0 \rightarrow F = .9$
If $|\alpha_w| > 30.0 \rightarrow F = .9 + .15[|\alpha_w| - 30.0]$

$\underline{M = 2.87}$

If $|\alpha_w| \le 20.0 \rightarrow k_{w(B)} = .9[k_{w(B)}]_{SB}$
If $|\alpha_w| > 20.0 \rightarrow k_{w(B)} = .9[k_{w(B)}]_{SB} - .005[|\alpha_w| - 20.0]$
If $|\alpha_w| \le 30.0 \rightarrow F = .9$
If $|\alpha_w| > 30.0 \rightarrow F = .9 + .17[|\alpha_w| - 30.0]$

$\underline{M = 3.95}$

$k_{w(B)} = .8[k_{w(B)}]_{SB}$
If $|\alpha_w| \le 40.0 \rightarrow F = 0.9$
If $|\alpha_w| > 40.0 \rightarrow F = 0.9 + .4[|\alpha_w| - 40.0]$

$\underline{M \ge 4.6}$

If $|\alpha_w| \le 20.0 \rightarrow k_{w(B)} = 0.75[k_{w(B)}]_{SB}$
If $|\alpha_w| > 20.0 \rightarrow k_{w(B)} = 0.75[k_{w(B)}]_{SB} + .01[|\alpha_w| - 20.0]$
If $|\alpha_w| \le 35.0 \rightarrow F = .9$
If $|\alpha_w| > 35.0 \rightarrow F = .9 + .3[|\alpha_w| - 35.0]$

where $\alpha_w = \alpha + \delta$

FIGURE 3-16. NONLINEAR WING-BODY INTERFERENCE MODEL DUE TO CONTROL DEFLECTION

4.0 SUMMARY OF METHODS IN 1993 VERSION OF NSWCDD AEROPREDICTION CODE (AP93) AND COMPARISON WITH EXPERIMENT[8, 109]

The methods used for computing forces and moments in the AP93 are summarized in Tables 4-1, 4-2, and 4-3. Note that the code can now be useful for computing aerothermal information as well as forces and moments. This means the code now has five uses:

a. Providing inputs to flight dynamics models that estimate range or miss distance

b. Assessing static stability of various missile configurations

c. Assessing various design parameters in terms of optimizing the configuration

d. Assessing structural integrity using the loads portion of the code

e. Assessing aerothermal aspects of a design using the heat transfer coefficients at high Mach numbers.

As seen in Tables 4-1, 4-2, and 4-3, there are many methods that go into the overall makeup of a component build up code, such as the APC. The past 20 years have shown that this type of code can be quite useful when used in preliminary or conceptual design studies to provide down selection on many configuration alternatives in a fairly accurate and cost-effective manner. Most of the methods listed in the tables have been briefly summarized in sections of the report.

Several different complete missile configurations have been considered in the validation of the AP93 code compared to experimental data.[8, 109] A sample of several of the flight conditions on a few of the configurations considered will be given here. Also, there will be comparisons with AP81 or other SOTA aeroprediction codes when such results are available in the literature. Funds were not available to do a thorough comparison.

The first case for comparison of the AP93 and AP81 is the configuration shown in Figure 4-1A. The body shown has a three-caliber tangent ogive nose with a total length of 12.33 calibers. It has aspect ratio 2.0 tails and 0.1 dorsals. Mach numbers of 4.5 and 10 are considered, and comparisons are made with the ZEUS code. Results of these comparisons in terms of normal force coefficient and center of pressure as a function of angle of attack are shown in Figure 4-1B. Center of pressure results show the AP93 within two percent of the body length compared to the ZEUS computations at all angles of attack considered. On the other hand, the AP81 center of pressure results differ by as much as 8 percent of the body length from the ZEUS code. In examining normal force coefficient comparisons, it is seen that at Mach 4.5 the AP93 is within 5 percent of the ZEUS code, whereas the AP81 results are low by as much as 30 percent due to the omission of nonlinear wing-alone and interference lift. At M = 10, the normal force of AP93 is within 13 percent of the ZEUS code, whereas the AP81 results are off by as much as 40 percent.

TABLE 4-1. AP93 METHODS FOR BODY-ALONE AERODYNAMICS

Component/ Mach Number Region	Subsonic $M_\infty < 0.8$	Transonic $0.8 \leq M_\infty < 1.2$	Low Supersonic $1.2 \leq M_\infty \leq 2.4$	High Supersonic $2.4 < M_\infty \leq 6.0$	Hypersonic $M_\infty > 6.0$
Nose Wave Drag	-	Semiempirical based on Euler Solutions	Second-Order Van Dyke plus MNT	SOSET plus IMNT	SOSET plus IMNT Modified for Real Gases
Boattail or Flare Wave Drag	-	Wu and Aoyoma	Second-Order Van Dyke	SOSET	SOSET for Real Gases
Skin Friction Drag	Van Driest II				
Base Drag	Improved Empirical Method				
Aeroheating Information	-	-	-	-	SOSET plus IMNT for Real Gases
Inviscid Lift and Pitching Moment	Empirical	Semiempirical based on Euler Solutions	Tsien First-Order Crossflow	SOSET	SOSET for Real Gases
Viscous Lift and Pitch Moment	Improved Allen and Perkins Crossflow				

TABLE 4-2. AP93 METHODS FOR WING-ALONE AND INTERFERENCE AERODYNAMICS

Component/ Mach Number Region	Subsonic $M_\infty < 0.8$	Transonic $0.8 \le M_\infty < 1.2$	Low Supersonic $1.2 \le M_\infty \le 2.4$	High Supersonic $2.4 < M_\infty \le 6.0$	Hypersonic $M_\infty > 6.0$
Wave Drag	–	Empirical	Linear Theory plus MNT	Shock Expansion (SE) plus MNT Along Strips	SE plus MNT for Real Gases Along Strips
Skin Friction Drag	Van Driest II				
Trailing Edge Separation Drag	Empirical				
Body Base Pressure Caused by Tail Fins	Improved Empirical				
Inviscid Lift and Pitching Moment • Linear • Nonlinear	 Lifting Surface Theory Empirical	 Empirical Empirical	 3DTWT Empirical	 3DTWT or SE Empirical	 3DTWT or SE Empirical
Wing-Body, Body-Wing Interference • Linear • Nonlinear	 Slender-Body Theory or Linear Theory Modified for Short Afterbodies Empirical				
Wing-Body Interference due to δ • Linear • Nonlinear	 Slender-Body Theory Empirical				
Wing Tail Interference	Line Vortex Theory with Empirical Modifications for $k_{W(B)}$ Term and Nonlinearities				
Aeroheating	None Present				SE plus MNT for Real Gases

TABLE 4-3. AP93 METHODS FOR DYNAMIC DERIVATIVES

Component/Mach Number Region	Subsonic $M_\infty < 0.8$	Transonic $0.8 \le M_\infty < 1.2$	Low Supersonic $1.2 \le M_\infty \le 2.4$	High Supersonic $2.4 < M_\infty \le 6.0$	Hypersonic $M_\infty > 6.0$
Body Alone	Empirical				
Wing and Interference Roll Damping Moment	Lifting Surface Theory	Empirical	Linear Thin Wing Theory	Linear Thin Wing Theory or Strip Theory	
Wing Magnus Moment	Assumed Zero				
Wing and Interference Pitch Damping Moment	Lifing Surface Theory	Empirical	Linear Thin Wing Theory	Linear Thin Wing Theory or Strip Theory	

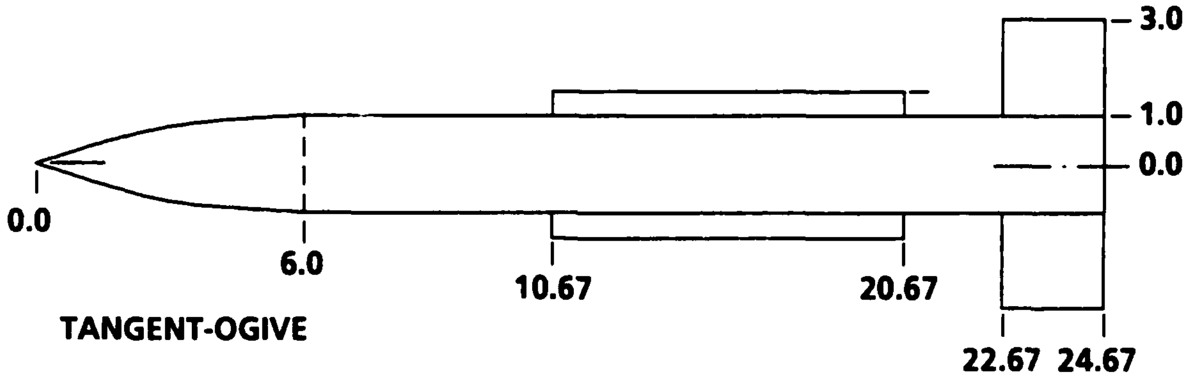

FIGURE 4-1A. BODY-DORSAL-TAIL CONFIGURATION USED FOR COMPARING ZEUS, IAP, AND OAP COMPUTATIONS

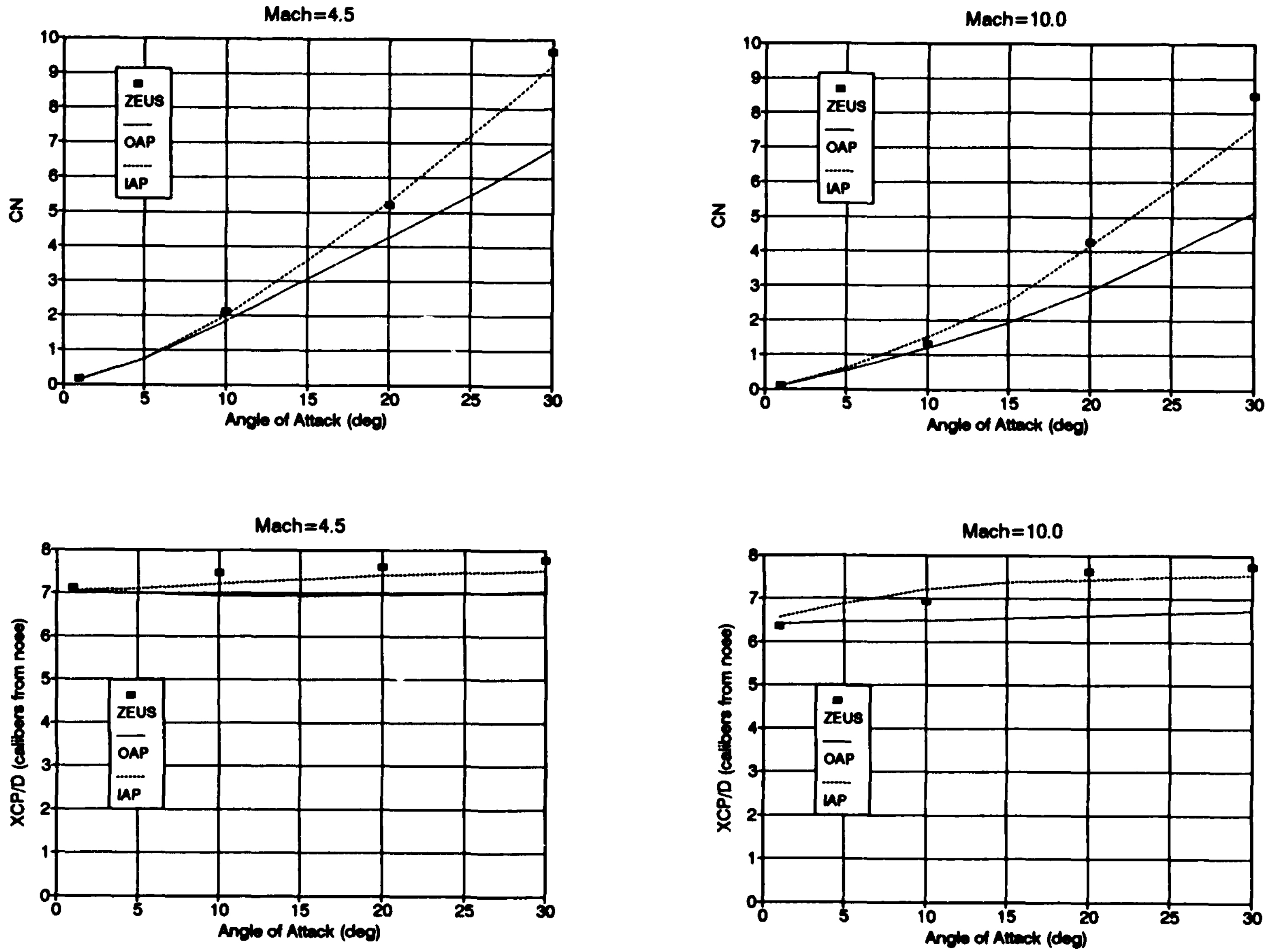

FIGURE 4-1B. COMPARISON OF PRESENT NORMAL FORCE COEFFICIENT AND CENTER OF PRESSURE COMPUTATIONS WITH THE ZEUS CODE FOR THE DORSAL-BODY-TAIL CONFIGURATION OF FIGURE 4-1

The second configuration, Figure 4-2A, is taken from Howard and Dunn.[118] The dorsals have an aspect ratio of 0.12 and tail surfaces have an aspect ratio of 4. The aeroprediction code will not handle the configuration as shown at the top of Figure 4-2A. Experience has shown it necessary to keep the lifting surface area, centroid of area, span, taper ratio, and aspect ratio the same in the configuration modification process. This means the tip and root chord of the dorsal and tail surfaces had to be adjusted with these constraints in mind. The new adjusted configuration is shown at the bottom of Figure 4-2A. Hence, this configuration has all parameters outside the empirical data base for use in the AP93 including Mach number, aspect ratio, body configuration, and r / s.

Howard and Dunn showed only normal force coefficient results for the body-tail and body-dorsal-tail configurations at $M = 0.1$.[118] Results of the AP81, AP93, and Missile DATCOM are shown in Figure 4-2B compared to experiment for both the body-tail and body-dorsal-tail configurations. For the wing-body case, the AP93, and Missile DATCOM produce almost identical results; both show higher C_N values than experiment, particularly at low angles of attack. It is not clear why this discrepancy exists. The AP81 results, which have the older values of C_{d_c} and no nonlinear wing lift, show even higher results than either the AP93 or Missile DATCOM.

The body-dorsal-tail configuration results of Figure 4-2B show that the AP93 is clearly superior to both the AP81 and Missile DATCOM. Normal force errors of the AP93 are less than 5 percent at all conditions, whereas errors of the AP81 and Missile DATCOM are as high as 40 and 50 percent, respectively. The fundamental reason for the AP93 success is the nonlinear wing-alone normal force and interference factor methodology. At $\alpha = 30°$, the body-dorsal and dorsal-body contributes about ⅔ of the total configuration normal force.

The third configuration for validation of the new semiempirical methodology is shown in Figure 4-3A. This configuration also differs substantially from the geometry characteristics from which the new semiempirical methodology was derived. The body is 21.2 versus 12.33 calibers long with a 2-caliber Von Karman versus a 3-caliber tangent-ogive nose. The dorsals and tail surfaces have aspect ratios of 0.36 and 2.14, respectively, both at the outer edge of the data base.

Wind tunnel data exist for both the body-tail and body-dorsal-tail configuration for Mach numbers of 2.3 to 4.6 and at several roll orientations.[119] Comparisons are made at $\phi = 0°$ roll and at Mach numbers of 2.3 and 4.6 for both the body-tail and body-dorsal-tail configurations. Results of these comparisons are shown in Figure 4-3B for the body-tail and Figure 4-3C for the body-dorsal-tail. The AP93 results are within the expected accuracy bounds on normal force, center of pressure, and pitching moment. While AP81 results are not shown for clarity, significant improvements in normal force for both body-tail and body-dorsal-tail configurations occur with less significant improvements in center of pressure. As noted in the comparisons, the AP93 is slightly superior to Missile 3 for most pitching moments[22] and the two codes (AP93 and Missile 3) are about equal in normal force prediction.

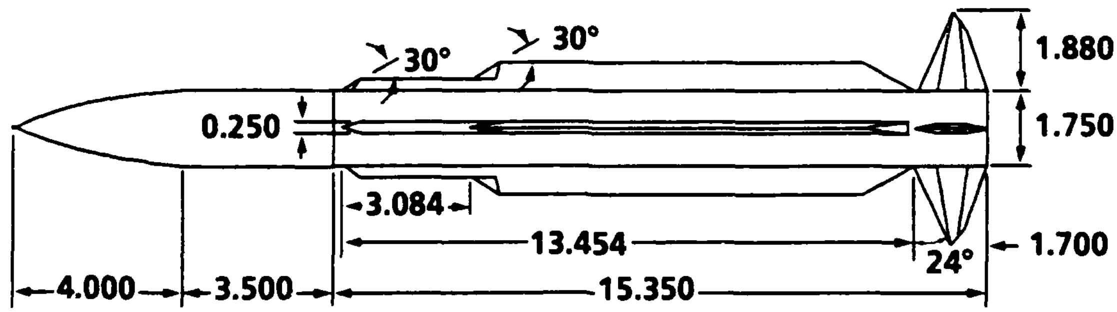

CONFIGURATION TESTED IN WIND TUNNEL (FROM REFERENCE 29 WHERE DIMENSIONS ARE IN INCHES)

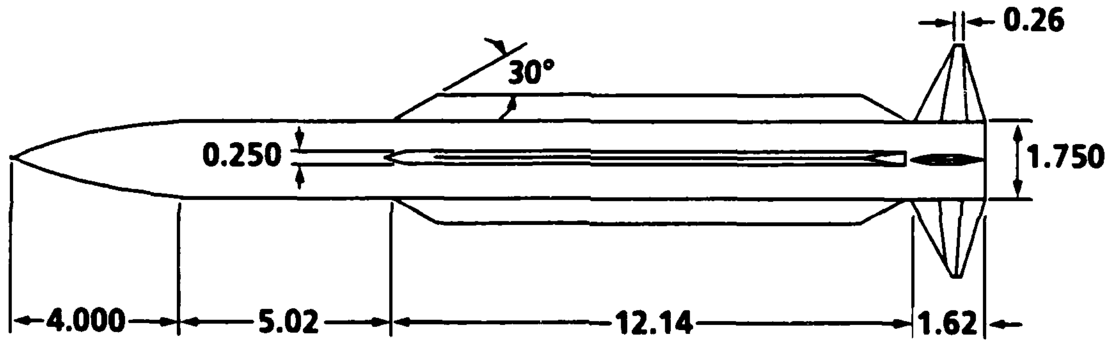

MODIFIED CONFIGURATION USED IN AEROPREDICTION COMPUTATIONS

PARAMETERSFOR BOTH MODELS

$(AR)_T = 4.0$	$b_t = 3.76$ in.	$\lambda_T = .16$	$(\Lambda_{LE})_T = 24°$	$A_T = 3.54$ in.^{2}
$(AR)_D = .12$	$b_D = 1.32$ in.	$\lambda_D = .77$	$(\Lambda_{LE})_D = 60°$	$A_D = 14.2$ in.^{2}

FIGURE 4-2A. CONFIGURATION USED FOR COMPARISON WITH MISSILE DATCOM AND EXPERIMENT

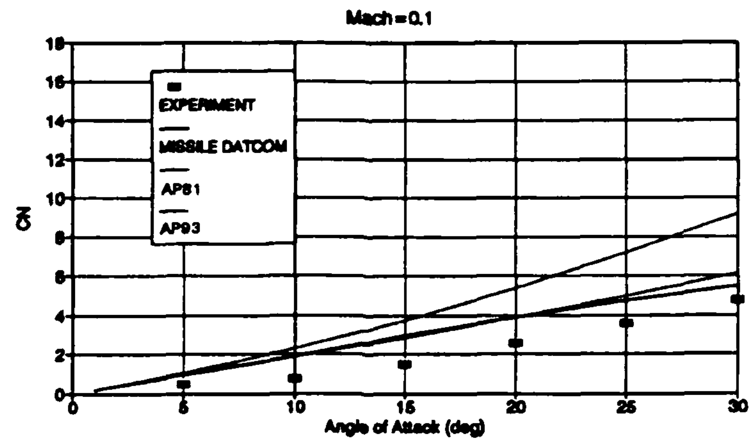

BODY-TAIL

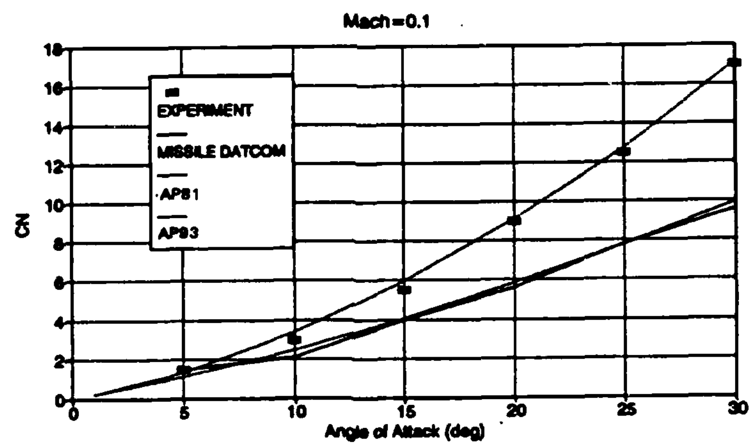

DORSAL-BODY-TAIL

FIGURE 4-2B. COMPARISON OF PRESENT NORMAL FORCE COEFFICIENT WITH THAT PREDICTED BY MISSILE DATCOM AND EXPERIMENT FOR CONFIGURATION OF FIGURE 4-2A

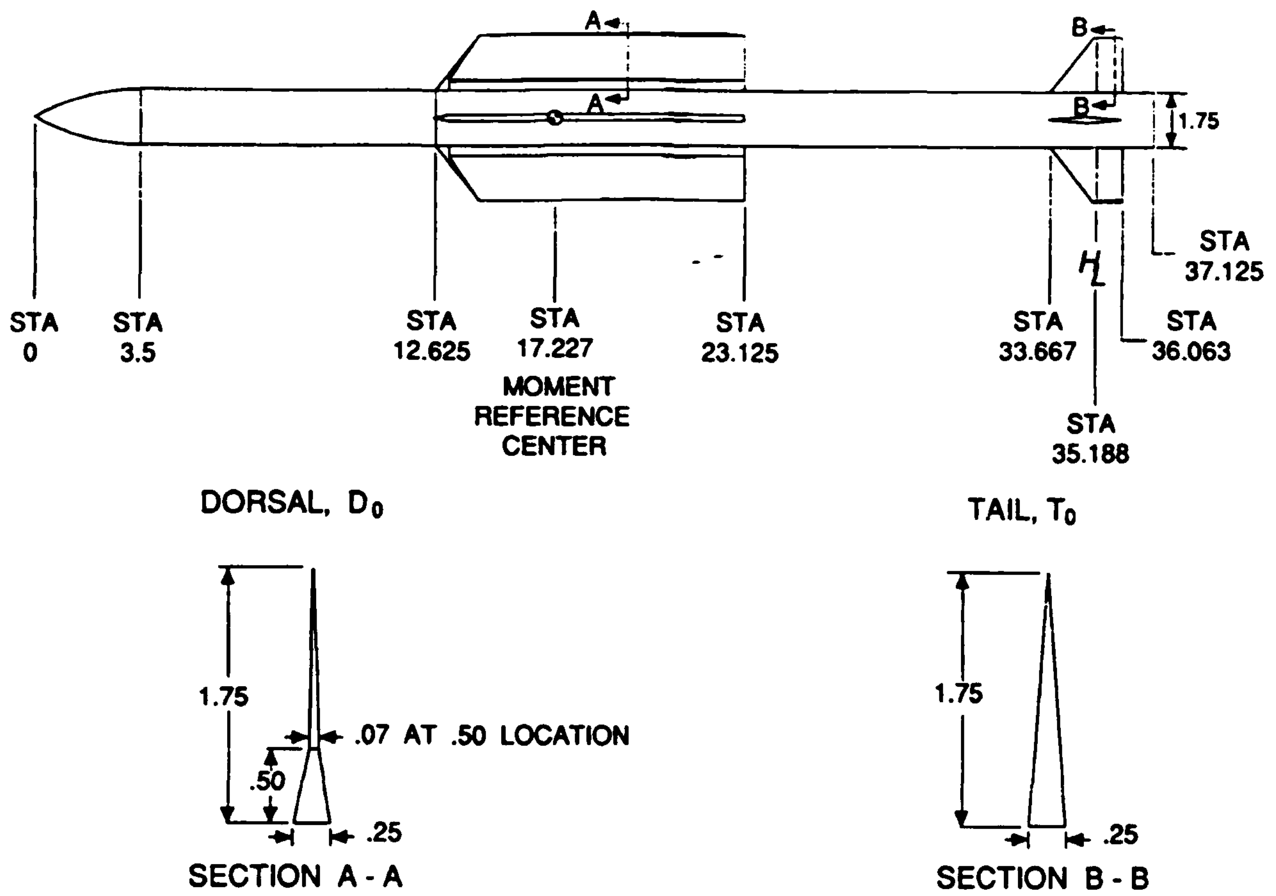

FIGURE 4-3A. DORSAL-BODY-TAIL CONFIGURATION USED FOR COMPARING MISSILE 3, AP93, AND AP81 COMPUTATIONS

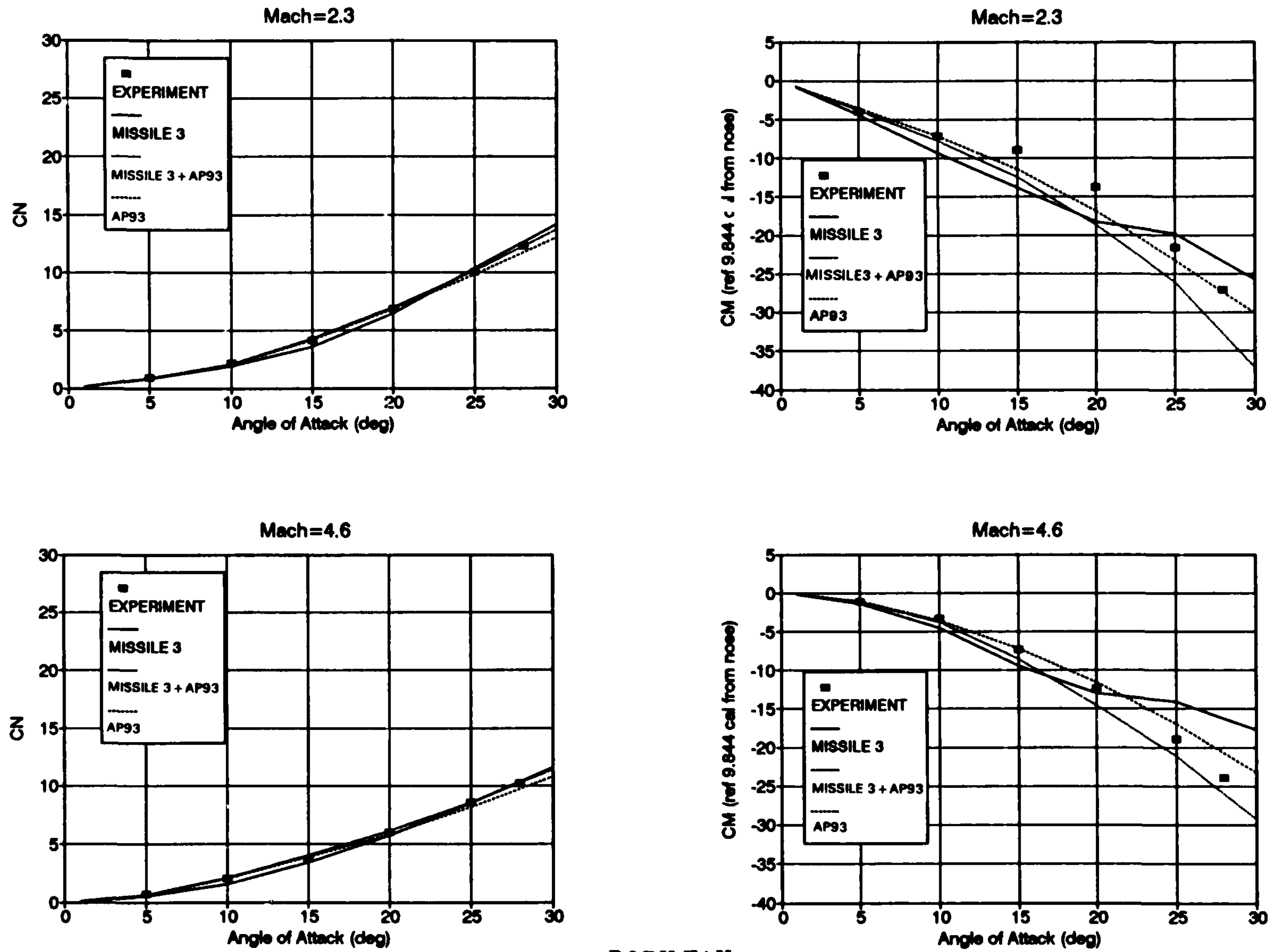

BODY-TAIL

FIGURE 4-3B. COMPARISON OF PRESENT NORMAL FORCE COEFFICIENT AND PITCHING MOMENT COEFFICIENTS WITH MISSILE 3 ON THE CONFIGURATION OF FIGURE 4-3A (BODY-TAIL PORTION OF)

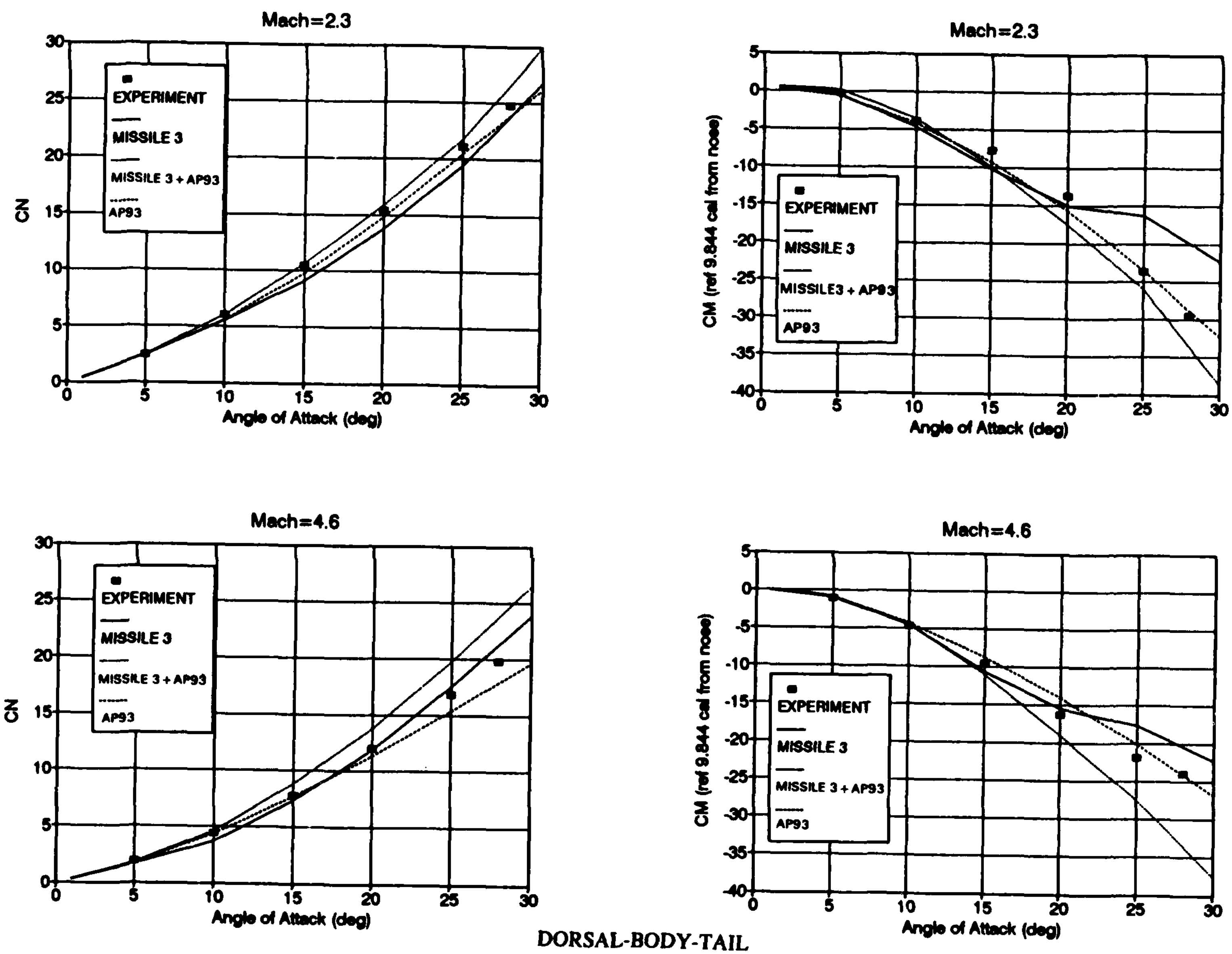

FIGURE 4-3C. COMPARISON OF PRESENT NORMAL FORCE COEFFICIENT AND PITCHING MOMENT COEFFICIENTS WITH MISSILE 3 ON CONFIGURATION OF 4-3A

A fourth case considered is the canard-body-tail case shown in Figure 4-4A.[120] The configuration is somewhat of an extreme case for the body-alone aerodynamics because it is a hundred percent blunt and is about 22.3 calibers long. The configuration tested in the wind tunnel has hangers attached to the body for aircraft carry and launch. However, tests were conducted with and without the hangers, and the results showed that C_N and C_M were unchanged but C_A was increased with the hangers present. The AP93 and AP81 theoretical computations are compared to the corrected data of Groves and Fournier,[120] where the hangers have been omitted. Results are given in Figures 4-4B through 4-4I for Mach numbers of 0.8, 2.86, and 4.63 and at canard deflections of 0, 10, and 20 deg. Examining Figures 4-4B through 4-4I, it is shown that AP93 gives good agreement with experimental data under almost all conditions. Significant improvements of the AP93 over the AP81 are seen at the lower Mach numbers and at the higher Mach number, higher angle-of-attack conditions.

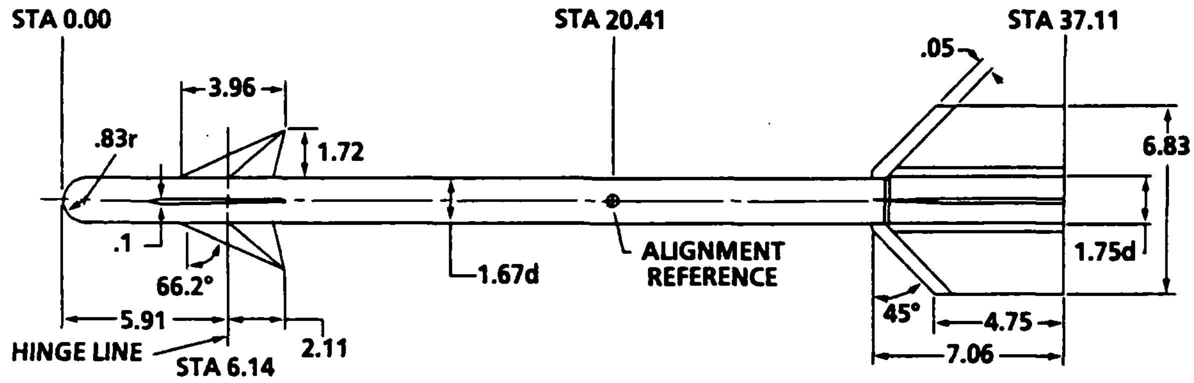

FIGURE 4-4A. CANARD-BODY-TAIL CONFIGURATION USED IN VALIDATION PROCESS[120]

In analyzing why this improvement occurs at those conditions, it is noted that the aspect ratio of the tail surfaces of the configuration of Figure 4-4A is about 0.87 and that of the canard is about 1.7. Examining Tables 4-2 and 4-3, the nonlinearity in wing-alone lift is small for Mach numbers greater than about 1.5. As normal Mach number increases, $[M_\infty \sin(\alpha + \delta)]$ and Mach numbers exceed about 3.5 to 4.0, nonlinearity due to compressibility becomes important. As long as the aerodynamics are fairly linear, the AP81 gives good results up to moderate angles of attack. However, when nonlinearities are present, the AP93 shows significant improvement. This improvement is the greatest on the Figure 4-4A configuration at low Mach number because the nonlinear normal-force term on the canards is negative, whereas that of the tails is positive. The combination produces a strong couple in terms of the pitching moment as evidenced by Figures 4-4A through 4-4I. A good nonlinear capability, such as that present in the AP93, is absolutely essential to get accurate stability and control information for these cases. Just examining Figure 4-4B, the center of pressure of the AP81 at $\alpha = 20$ deg differs from the experimental data by -9.4 percent of the body length versus 1.3 percent for the AP93.

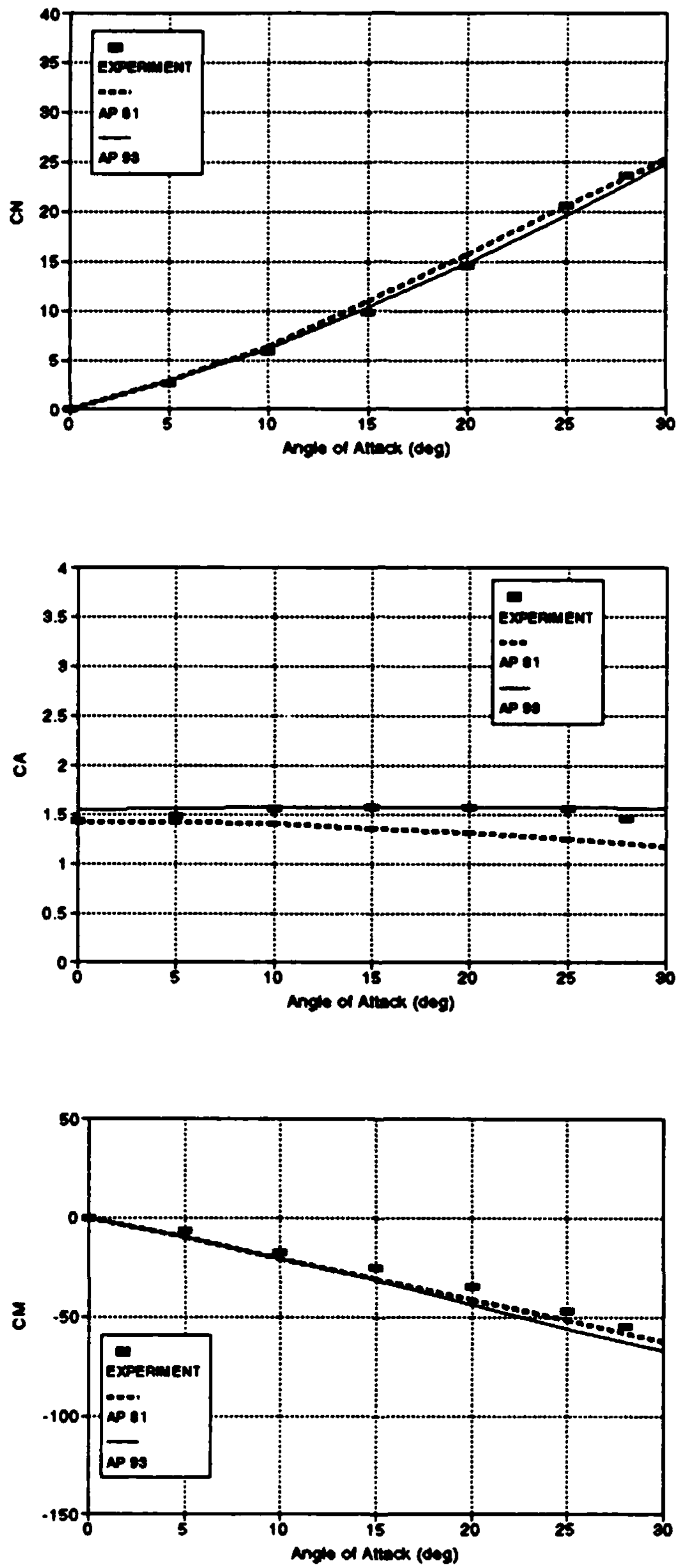

FIGURE 4-4B. NORMAL- AND AXIAL-FORCE AND PITCHING MOMENT COEFFICIENTS FOR CONFIGURATION OF FIGURE 4-4A ($M_\infty = 2.86$, $\delta = 0°$)

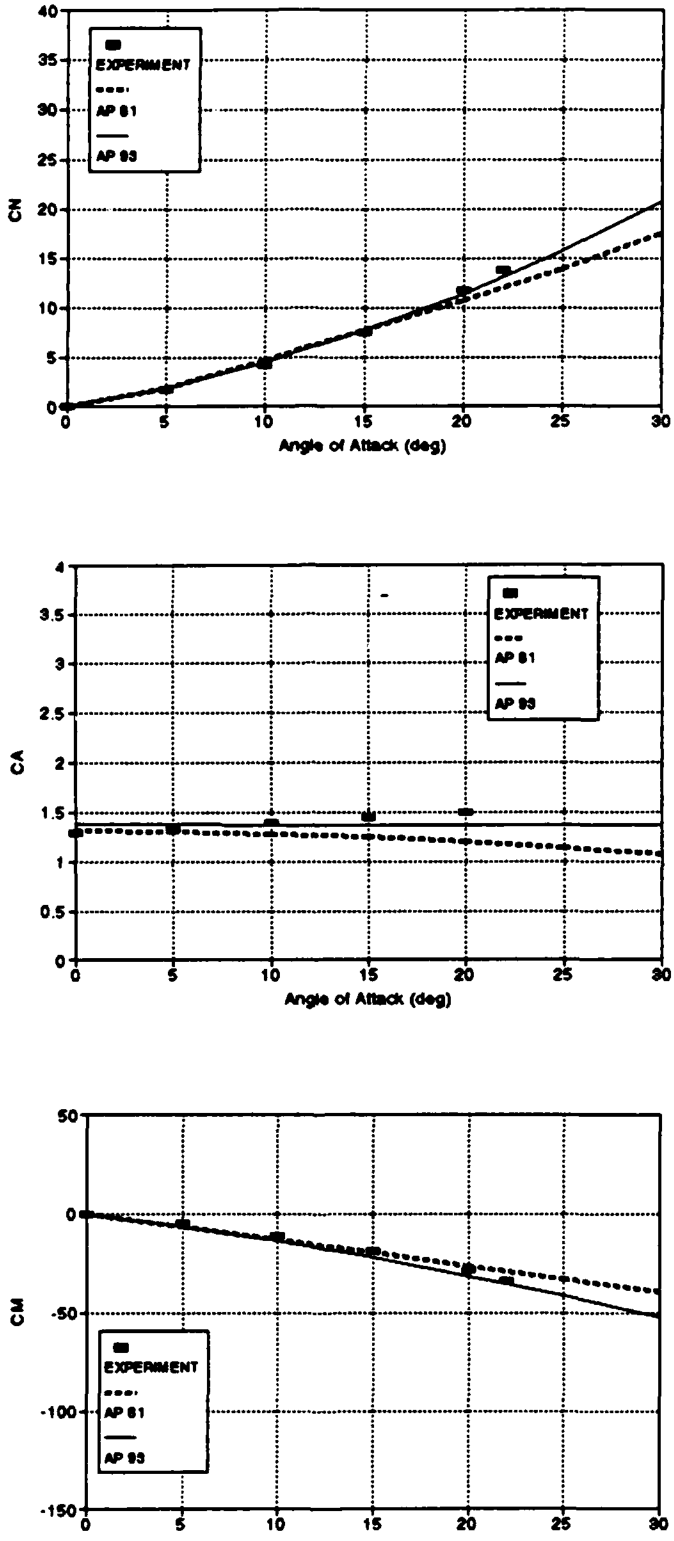

FIGURE 4-4C. NORMAL- AND AXIAL-FORCE AND PITCHING MOMENT COEFFICIENTS FOR CONFIGURATION OF FIGURE 4-4A ($M_\infty = 4.63$, $\delta = 0°$)

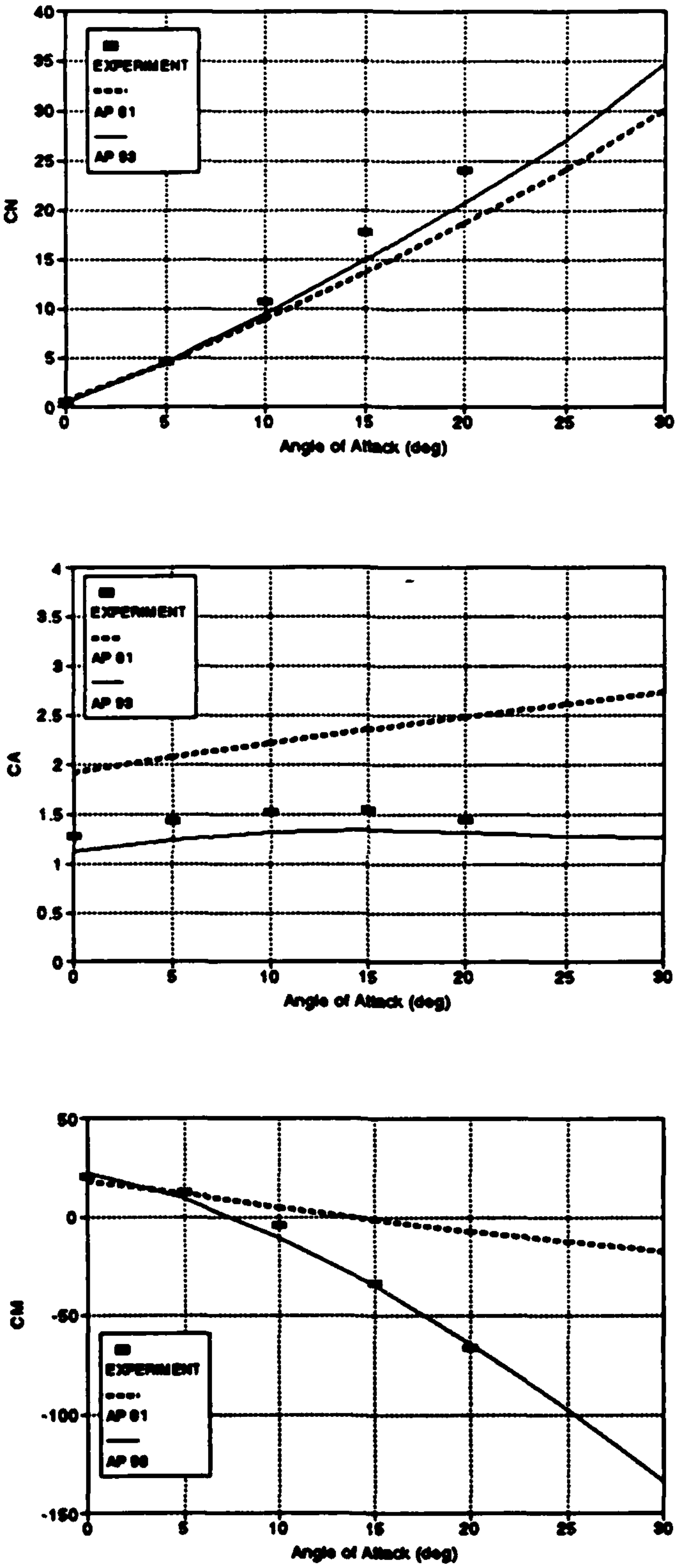

FIGURE 4-4D. NORMAL- AND AXIAL-FORCE AND PITCHING MOMENT COEFFICIENTS FOR CONFIGURATION OF FIGURE 4-4A ($M_\infty = 0.8$, $\delta = 10°$)

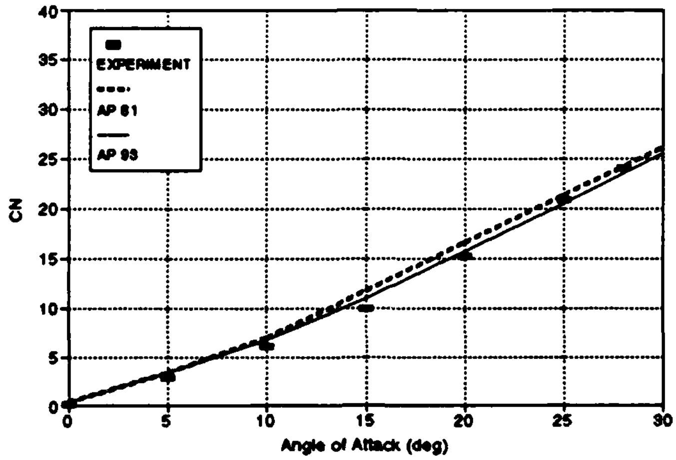

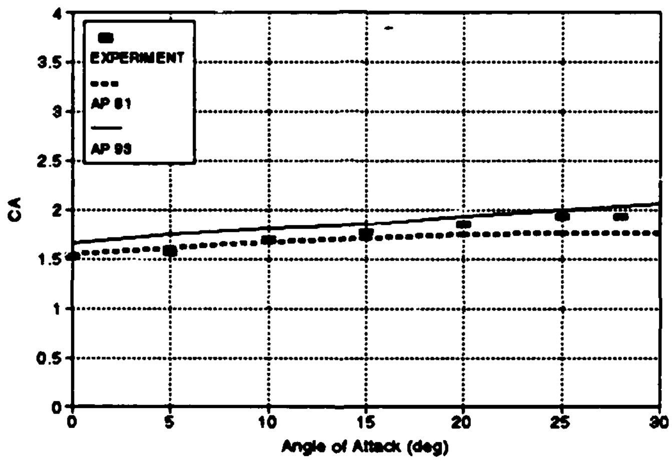

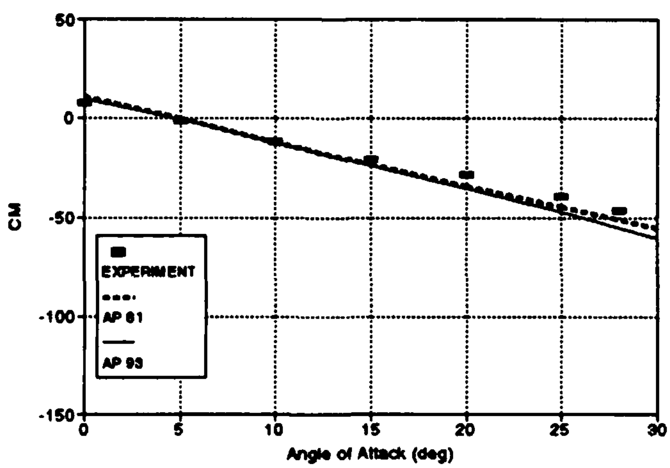

FIGURE 4-4E. NORMAL- AND AXIAL-FORCE AND PITCHING MOMENT COEFFICIENTS FOR CONFIGURATION OF FIGURE 4-4A ($M_\infty = 2.86$, $\delta = 10°$)

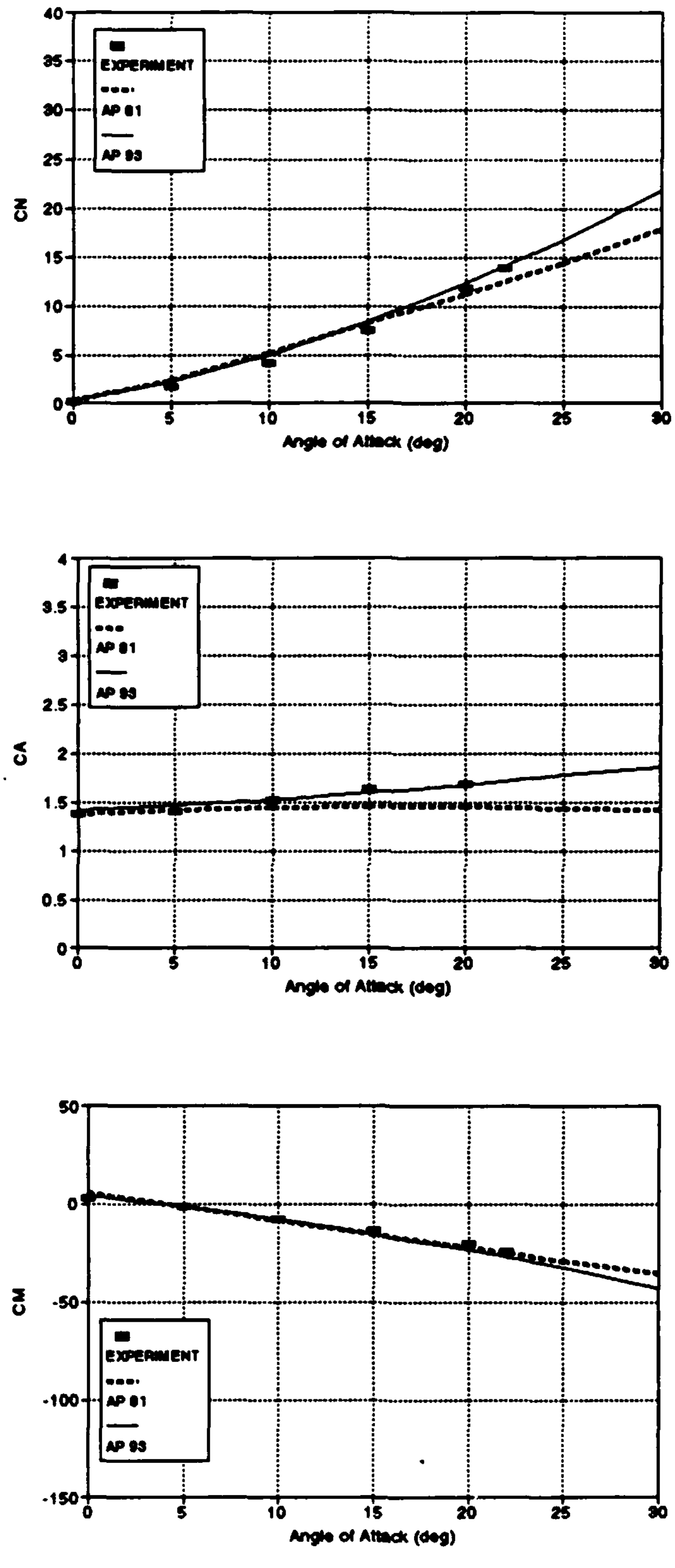

FIGURE 4-4F. NORMAL- AND AXIAL-FORCE AND PITCHING MOMENT COEFFICIENTS FOR CONFIGURATION OF FIGURE 4-4A ($M_\infty = 4.63$, $\delta = 10°$)

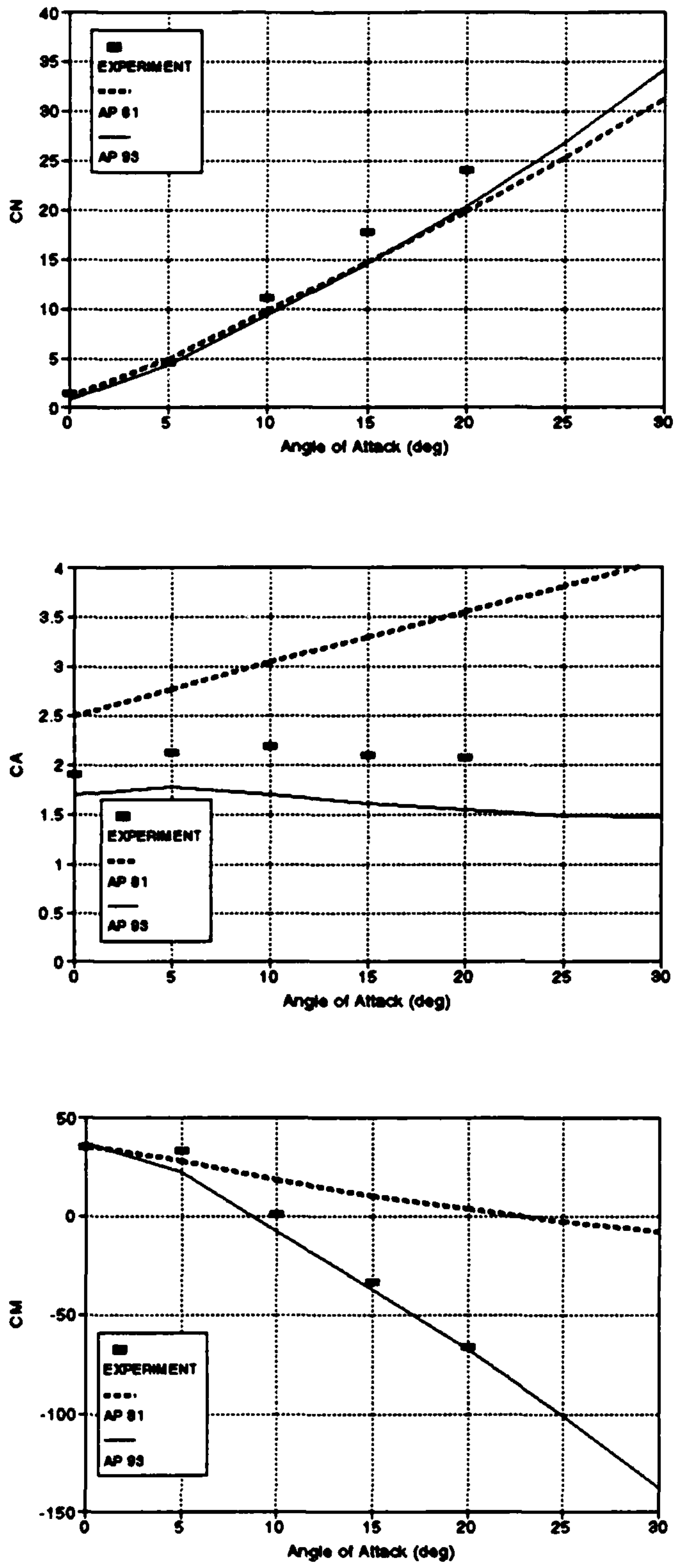

FIGURE 4-4G. NORMAL- AND AXIAL-FORCE AND PITCHING MOMENT COEFFICIENTS FOR CONFIGURATION OF FIGURE 4-4A ($M_\infty = 0.8$, $\delta = 20°$)

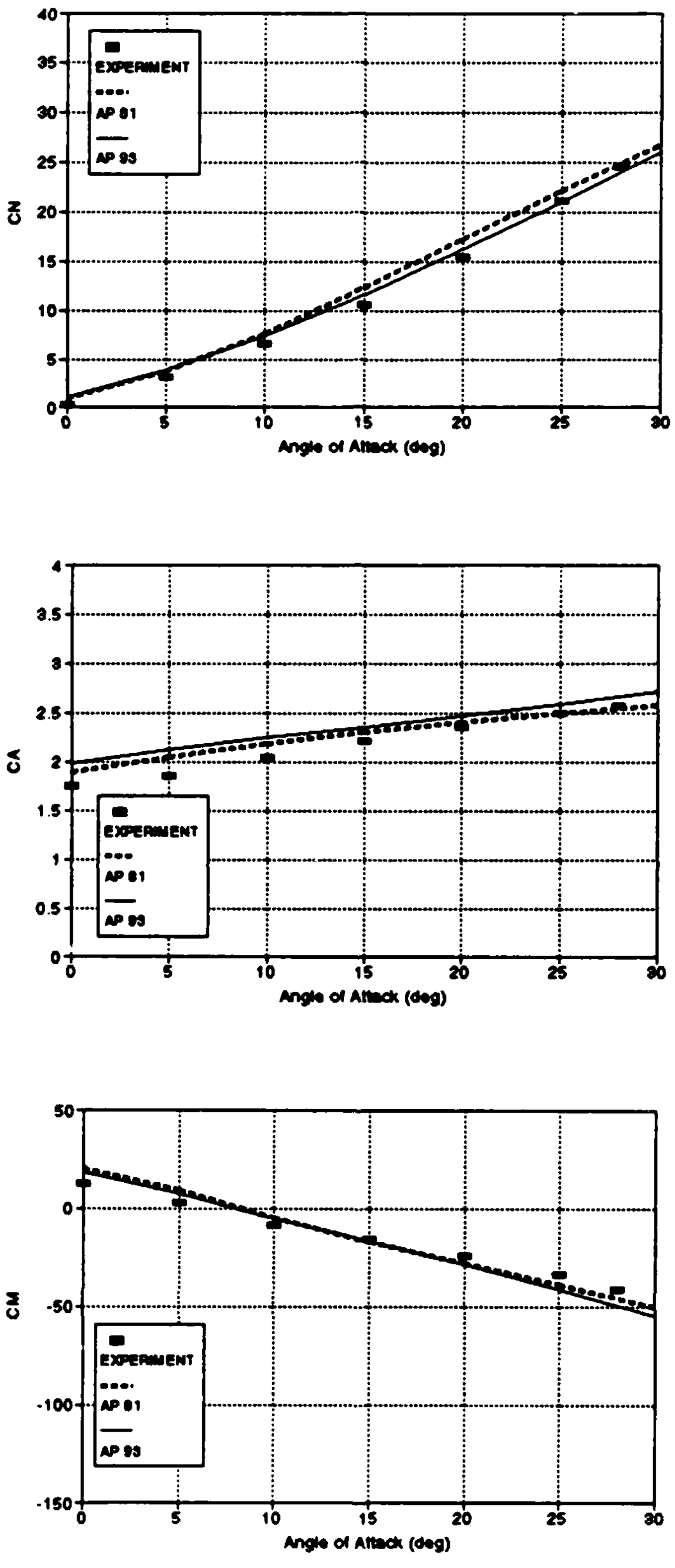

FIGURE 4-4H. NORMAL- AND AXIAL-FORCE AND PITCHING MOMENT COEFFICIENTS FOR CONFIGURATION OF FIGURE 4-4A ($M_\infty = 2.86$, $\delta = 20°$)

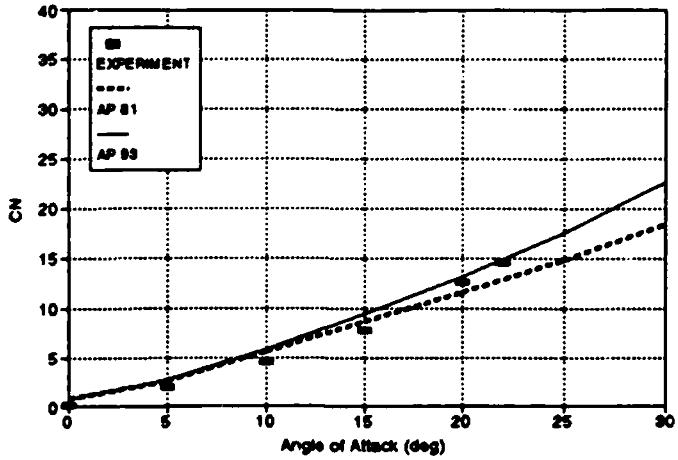

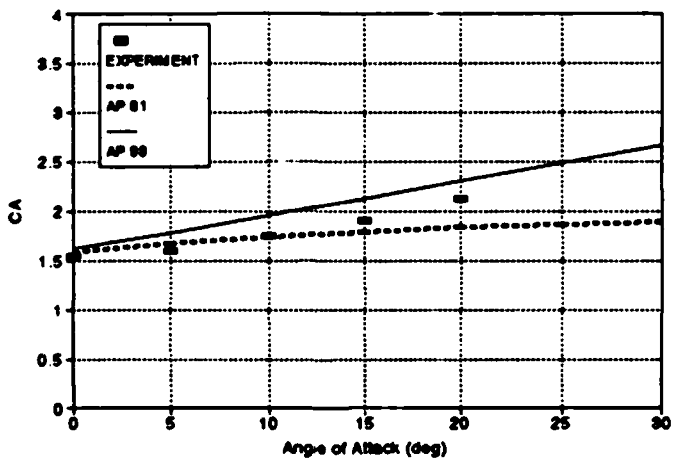

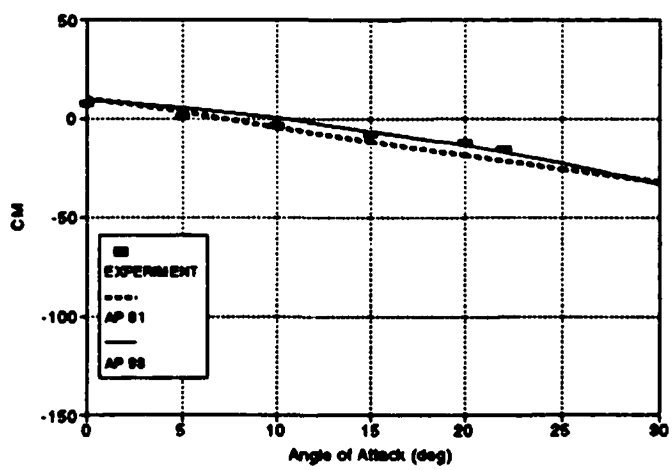

FIGURE 4-4I. NORMAL- AND AXIAL-FORCE AND PITCHING MOMENT COEFFICIENTS FOR CONFIGURATION OF FIGURE 4-4A ($M_\infty = 4.63$, $\delta = 20°$)

A fifth case considered in the validation of the AP93 code is a configuration representative of the SPARROW missile tested at NASA/LRC.[115, 116] The configuration tested and reported by Monta is shown in Figure 4-5A.[116] The configuration tested by McKinney is just like the one tested by Monta, except it had wiring tunnels and wave guides present.[115] These appendages add to the normal force and pitching moment, but were not accounted for in the analytical computations that are presented in Figure 4-5. The Monta configuration did not have these appendages present and was the main set of data used for the nonlinear empirical model validation. These results are distinguished in Figure 4-5 by the fact that the cases that had wave guides present are indicated.

Results of the AP81 and AP93, compared to the experiment for the configuration of Figure 4-5A, are shown in Figure 4-5B through 4-5G. Results are presented in terms of C_N and C_M versus angle of attack for various control deflections and Mach numbers. The nonlinear models with and without control deflection show the AP93 code agreeing much closer to the data at all Mach numbers than the linearized approaches of AP81. On the other hand, the fact that the body-alone normal force of AP81 had the nonlinearities included makes the comparisons to experimental data better than it would be otherwise.

In examing Figure 4-5B, it is seen that both C_N and C_M of AP93 agree with the experiment at $\delta = 0$ and $\delta = 10$ deg for $M_\infty = 1.5$ whereas, C_N and C_M of the AP81 are both considerably in error as angle of attack increases above 5 to 10 deg. For $M_\infty = 2.35$ (Figure 4-5C), both C_N and C_M of AP 93 at $\delta = 0$ and 20 deg agree with the data. Again, AP81 yields considerable error at $\alpha \geq 10$ deg, although the error is decreasing with increasing Mach number. For $M_\infty = 3.95$ (Figure 4-5C), AP81 gives acceptable results for C_N and C_M up to $\alpha = 15$ to 20 deg and at both $\delta = 0$ or 20 deg. The comparison with data gets worse above $\alpha = 20$ deg, whereas AP93 comparisons show good agreement at all values of α and δ. The same statements basically hold true for the $M_\infty = 4.6$ comparisons (Figure 4-5C).

Figures 4-5F and 4-5G show the comparisons of AP81 and AP93 to the McKinney data,[115] which is the same configuration as that of Figure 4-5A, except that wave guides and wiring tunnels were attached to the wind tunnel model. As already mentioned, no account was taken for these appendages in the analytical computations. Note that AP93 agrees much more with the data than AP81 for both $M_\infty = 2.3$ and 4.6 at all values of δ. In comparing the wind tunnel data for the cases with and without appendages, it can be seen that the appendages add only a few percent to the aerodynamics.

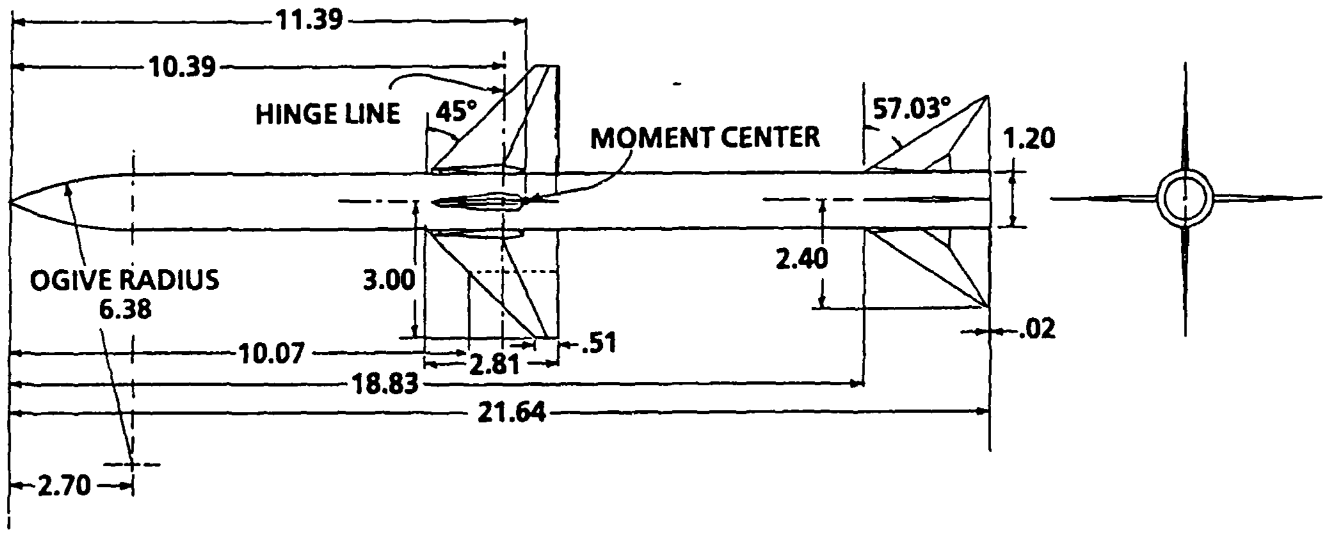

FIGURE 4-5A. AIR-TO-AIR MISSILE CONFIGURATION USED IN VALIDATION PROCESS[42, 43]

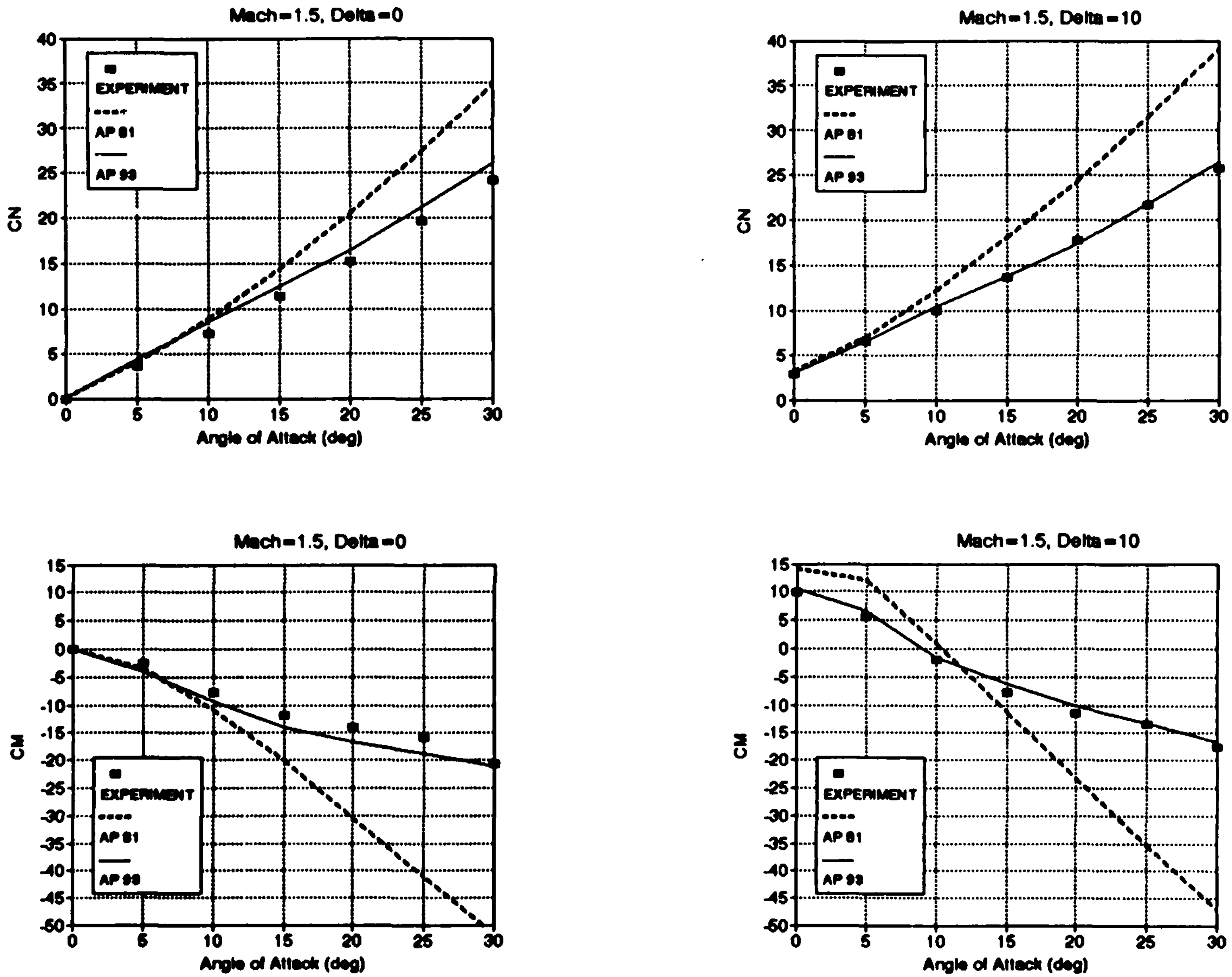

NO WAVE GUIDES

FIGURE 4-5B. NORMAL-FORCE AND PITCHING MOMENT COEFFICIENTS FOR CONFIGURATION OF FIGURE 4-5A FOR VARIOUS MACH NUMBERS AND CONTROL DEFLECTIONS

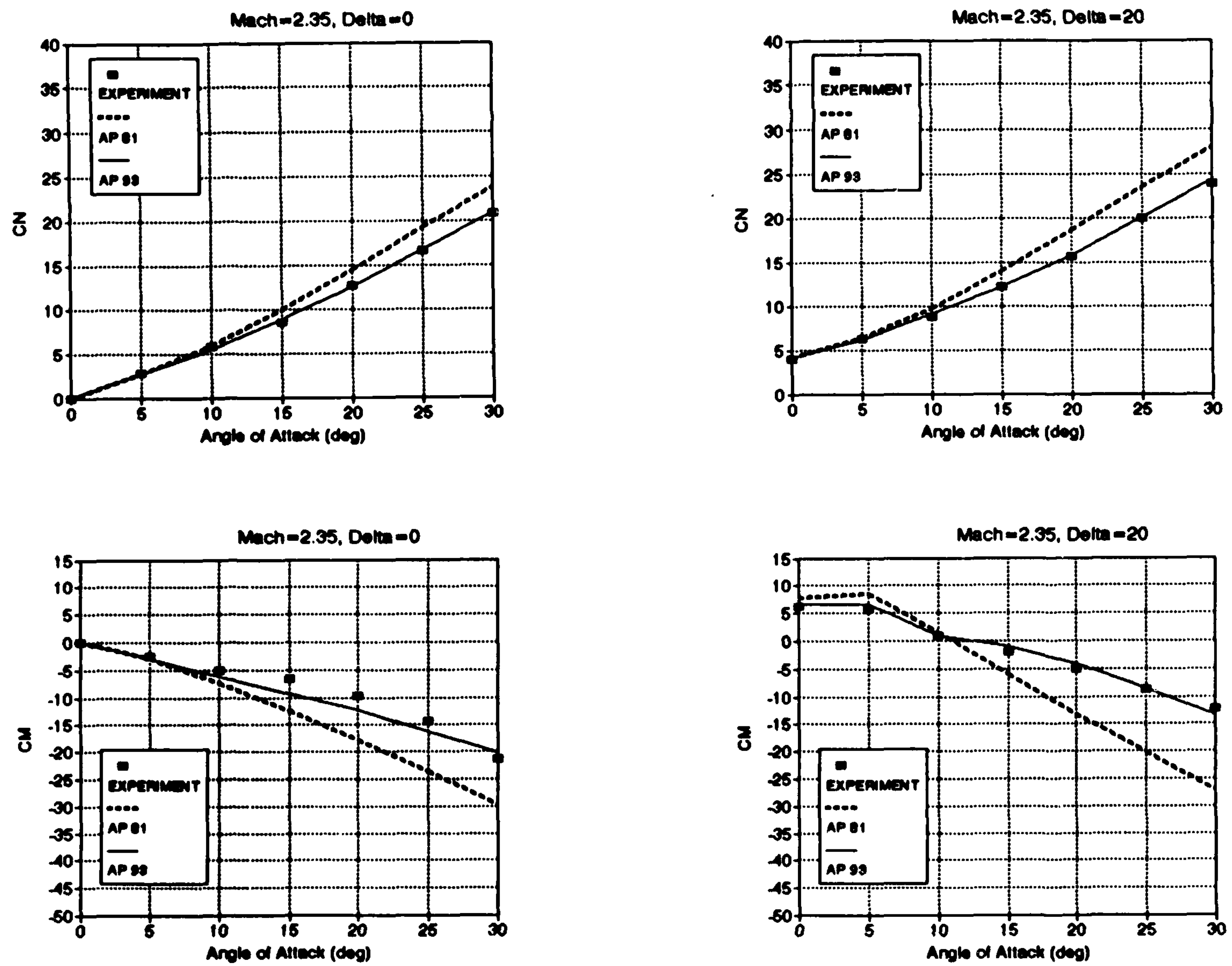

NO WAVE GUIDES

FIGURE 4-5C. NORMAL-FORCE AND PITCHING MOMENT COEFFICIENTS FOR CONFIGURATION OF FIGURE 4-5A FOR VARIOUS MACH NUMBERS AND CONTROL DEFLECTIONS (CONTINUED)

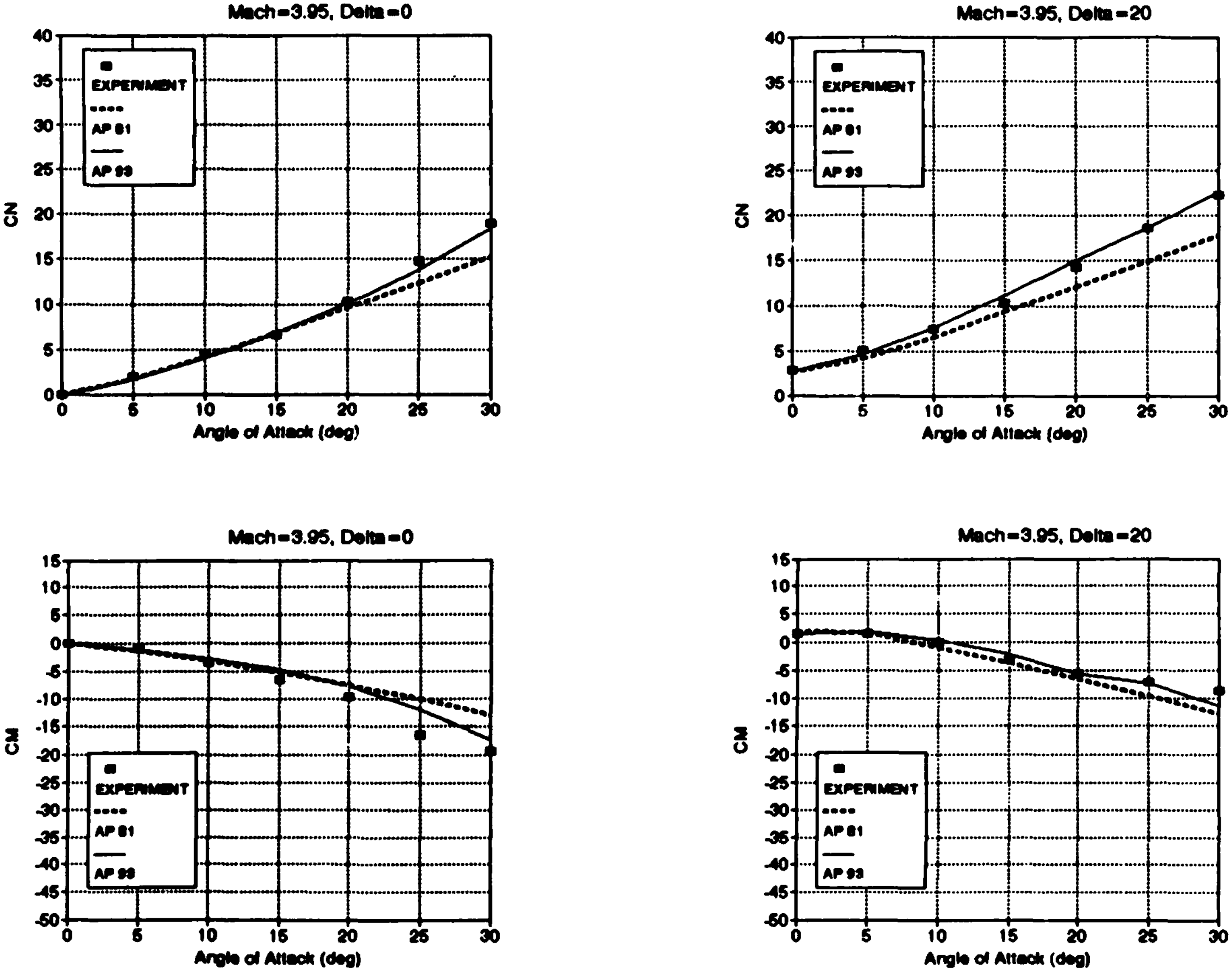

NO WAVE GUIDES

FIGURE 4-5D. NORMAL-FORCE AND PITCHING MOMENT COEFFICIENTS FOR CONFIGURATION OF FIGURE 4-5A FOR VARIOUS MACH NUMBERS AND CONTROL DEFLECTIONS (CONTINUED)

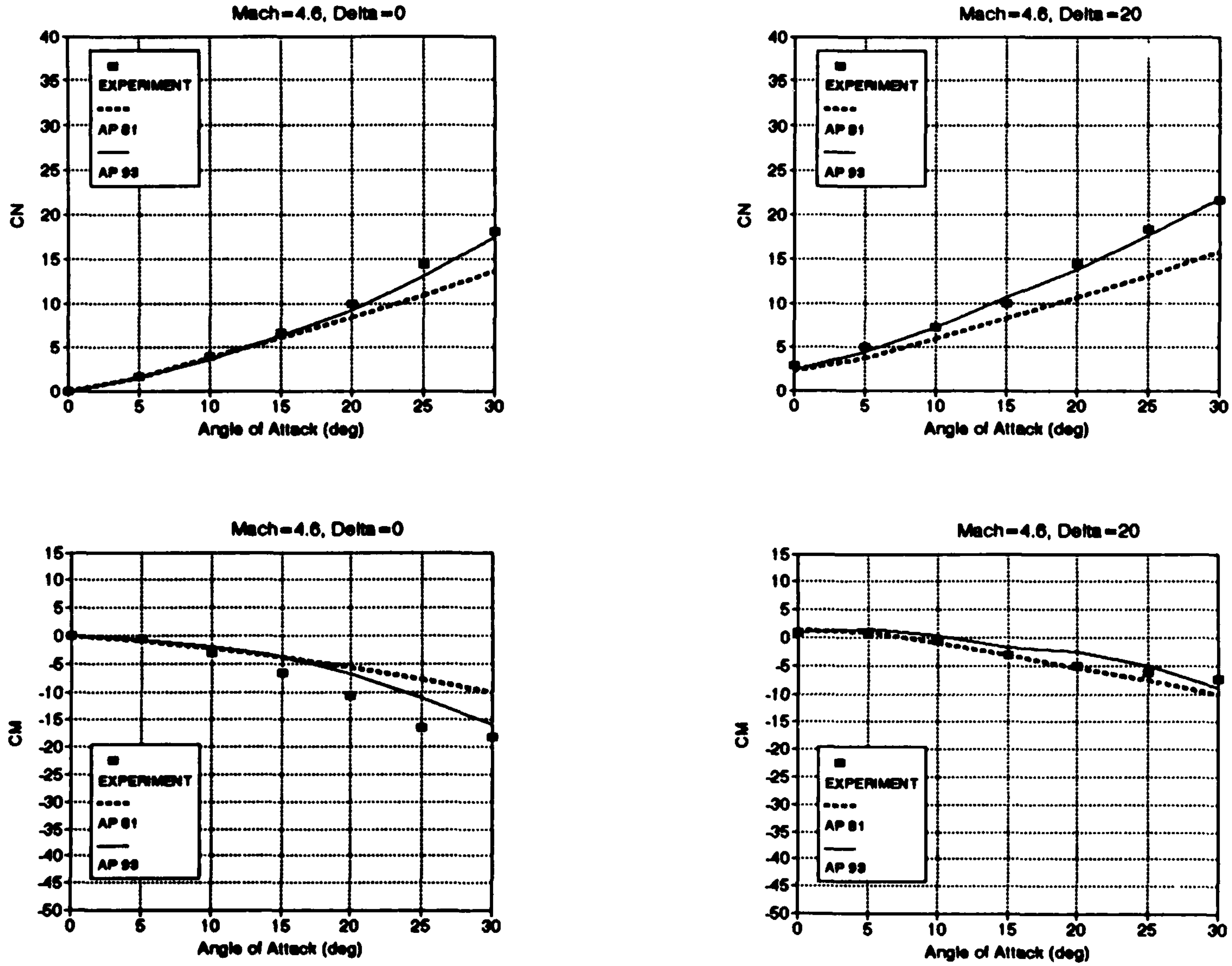

NO WAVE GUIDES

FIGURE 4-5E. NORMAL-FORCE AND PITCHING MOMENT COEFFICIENTS FOR CONFIGURATION OF FIGURE 4-5A FOR VARIOUSMACH NUMBERS AND CONTROL DEFLECTIONS (CONTINUED)

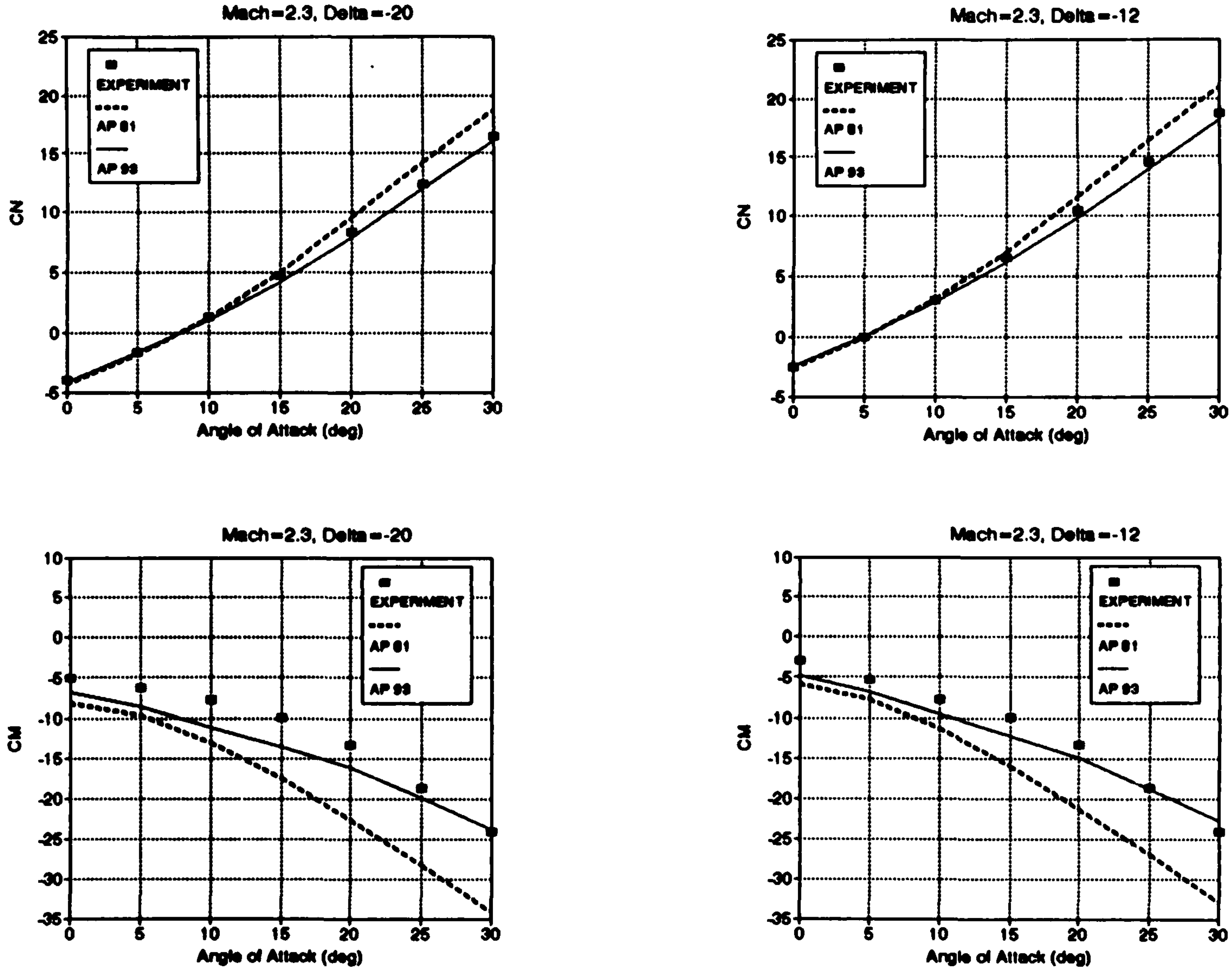

WITH WAVE GUIDES

FIGURE 4-5F. NORMAL-FORCE AND PITCHING MOMENT COEFFICIENTS FOR CONFIGURATION OF FIGURE 4-5A FOR VARIOUS MACH NUMBERS AND CONTROL DEFLECTIONS (CONTINUED)

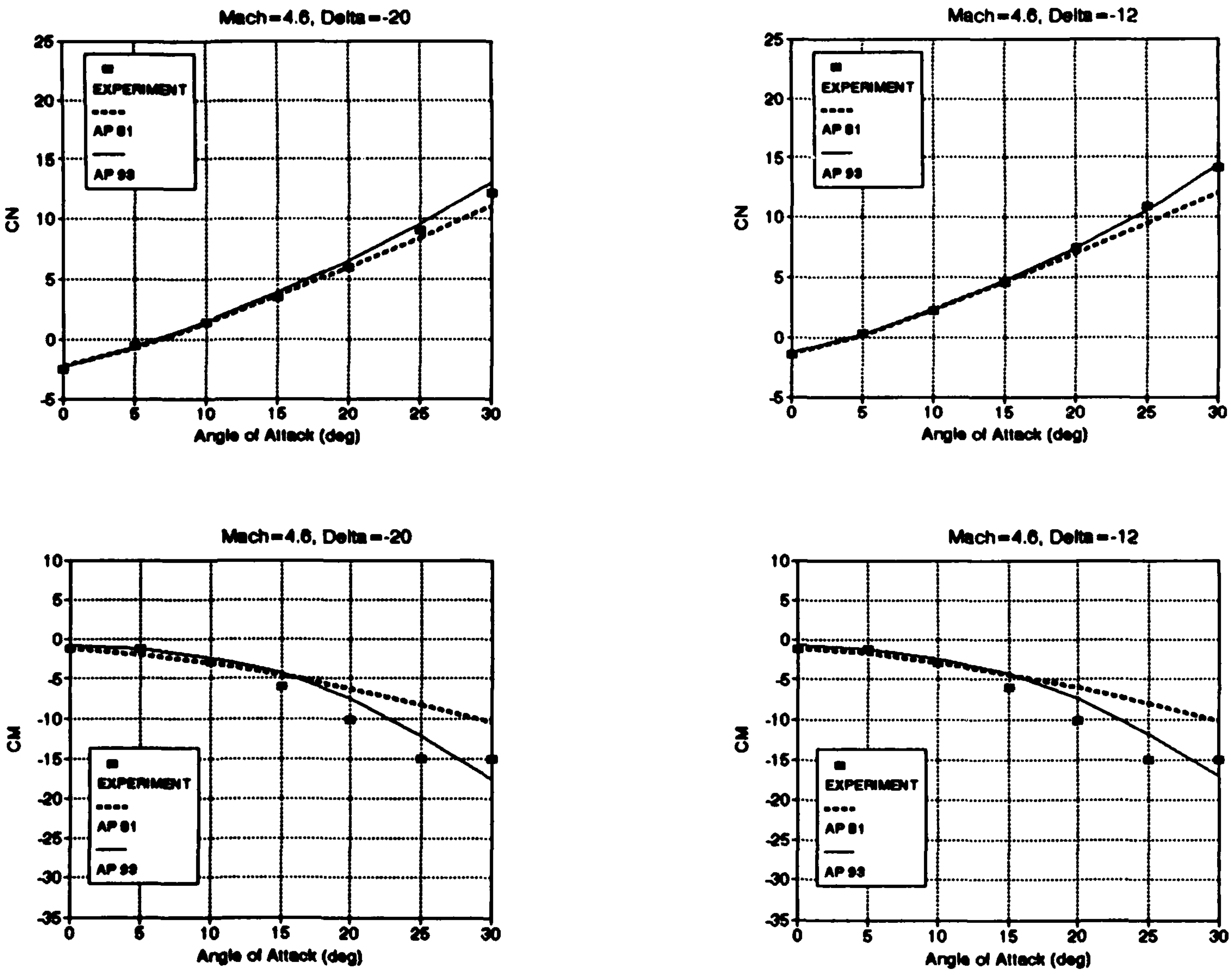

WITH WAVE GUIDES

FIGURE 4-5G. NORMAL-FORCE AND PITCHING MOMENT COEFFICIENTS FOR CONFIGURATION OF FIGURE 4-5A FOR VARIOUS MACH NUMBERS AND CONTROL DEFLECTIONS (CONTINUED)

A sixth and final case used in the validation and development of the nonlinear aerodynamics model is shown in Figure 4-6A. Note that in Figure 4-6A, two configurations were actually tested, one that had a full-tail surface and a second that had a partial cutout removed.[117] The AP93 will not handle the partial-wing configuration as it stands, so an engineering model of this wing must be created. Experience has shown that the lifting surface area, aspect ratio, span, leading edge sweep angle, and centroid of the presented area, must be held constant. The chord is varied so as to meet these constraints. Hence, the configuration that represents the partial-wing results is the body canard of Figure 4-6A, plus the AP93 representation of the partial tail shown in the lower right of Figure 4-6A.

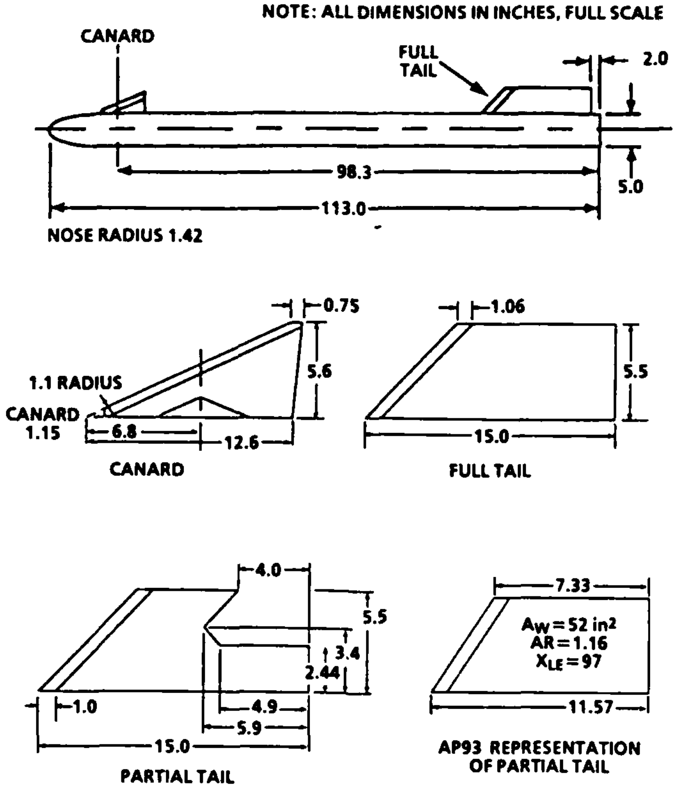

FIGURE 4-6A. CANARD-CONTROLLED MISSILE CONFIGURATION WITH FULL-TAIL, PARTIAL-TAIL, AND AP93 REPRESENTATION OF PARTIAL TAIL FOR USE IN VALIDATION PROCESS[117]

Figures 4-6B through 4-6D present the comparison of the AP93 with wind tunnel test data. Data were only available at $M_\infty = 0.2$; however, this complements the previous data set for the SPARROW missile in the sense that no subsonic data were available for that case. The full-tail and partial-tail results are denoted on the figure. Some results were available from reference 117 for the Missile Datcom.[17] These results are also shown where available.

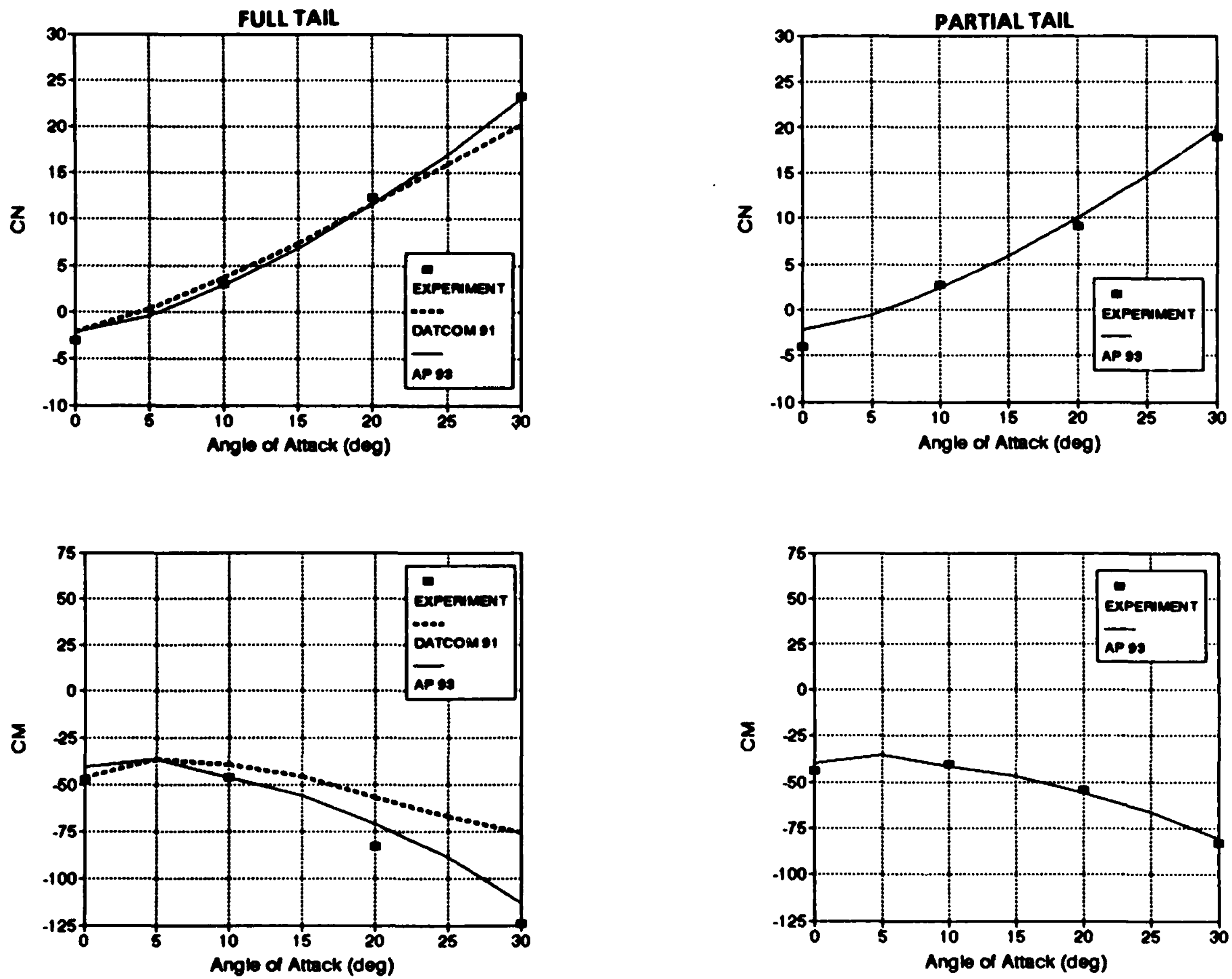

FIGURE 4-6B. COMPARISON OF AP93 TO WIND TUNNEL DATA AND MISSILE DATCOM FOR NORMAL-FORCE AND PITCHING MOMEN COEFFICIENTS OF FIGURE 4-6A CONFIGURATION (M_∞ = 0.2, δ_C = -20°)

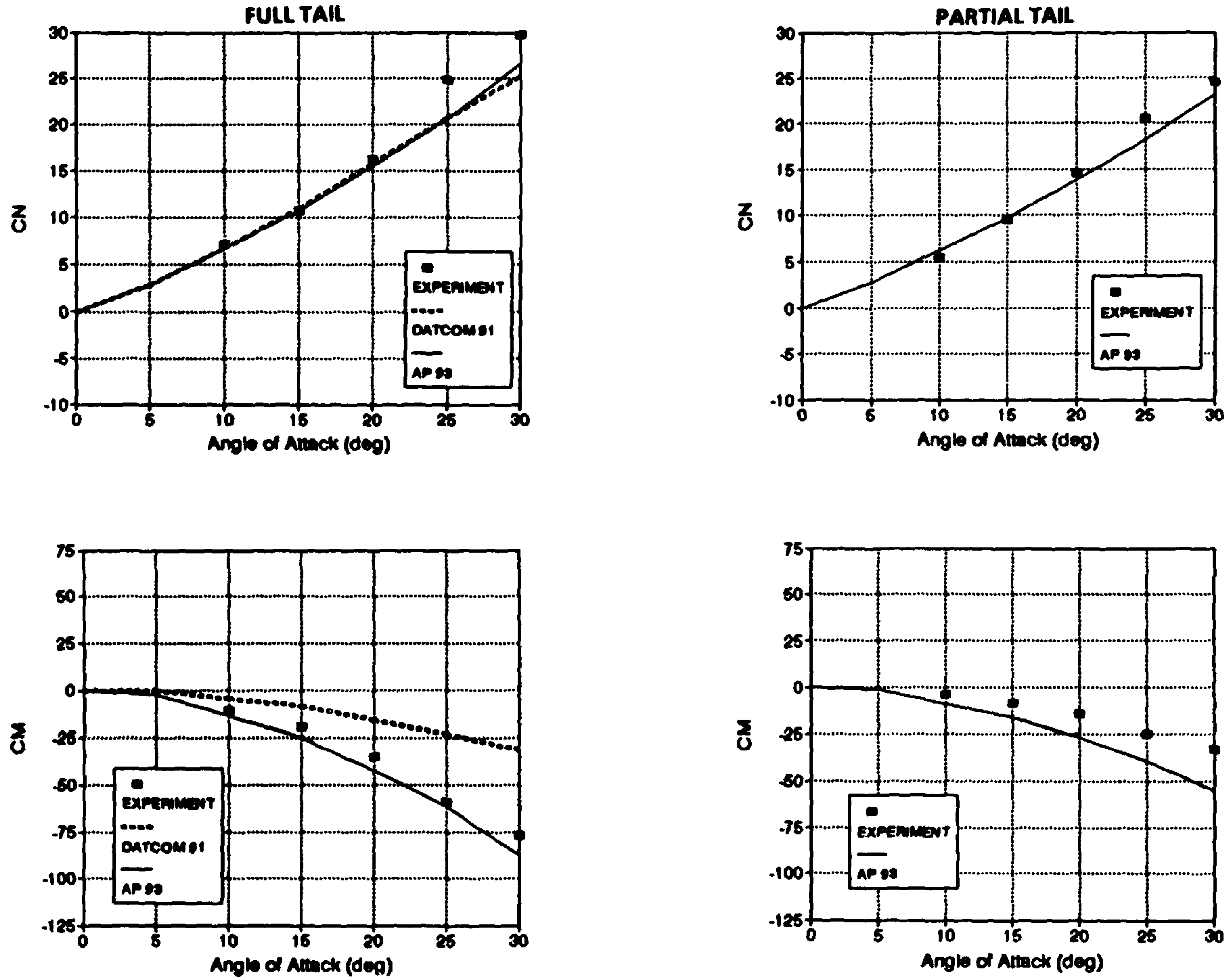

FIGURE 4-6C. COMPARISON OF AP93 TO WIND TUNNEL DATA AND MISSILE DATCOM FOR NORMAL-FORCE AND PITCHING MOMENT COEFFICIENTS OF FIGURE 4-6A CONFIGURATION ($M_\infty = 0.2$, $\delta = 0°$)

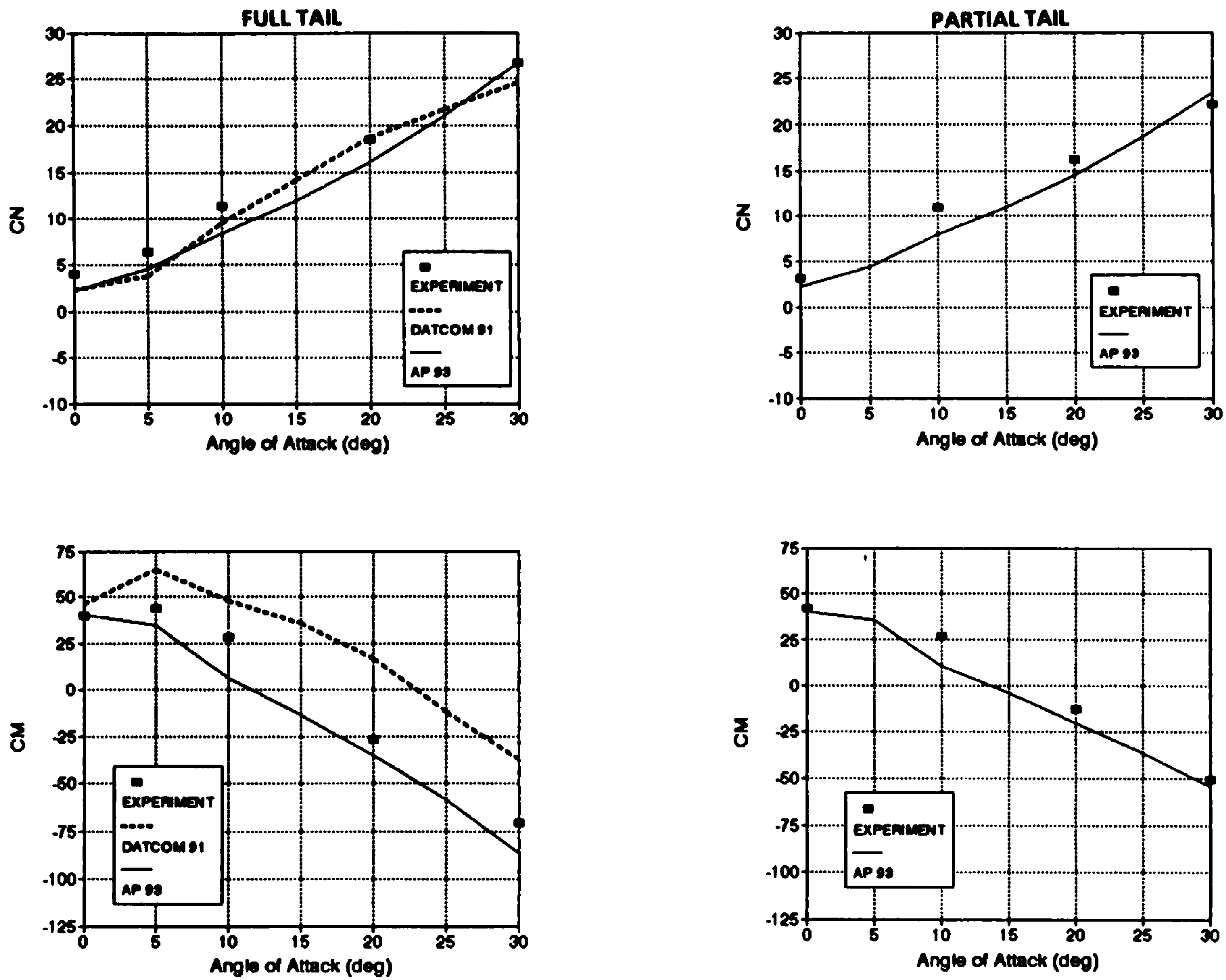

FIGURE 4-6D. COMPARISON OF AP93 TO WIND TUNNEL DATA AND MISSILE DATCOM FOR NORMAL-FORCE AND PITCHING MOMENT COEFFICIENTS OF FIGURE 4-6A CONFIGURATION ($M_\infty = 0.2$, $\delta = 20°$)

As seen in the figure, the AP93 gives improved results for pitching moment and normal force for most conditions, compared to the Missile Datacom. While center of pressure is not shown, the AP93 computations are generally within the goal of $\pm$ 4 percent of the body length. For example, at α = 30 deg, δ = -20 deg, x_{cp} for the data, AP93 and Missile Datacom are 5.39, 4.91, and 3.75 calibers, respectively, with respect to the moment reference point. This represents errors of 2.1 and 7.3 percent of the body length, respectively, for the AP93 and Missile Datacom codes.

Many other cases have also been considered in the validation of the new AP93 code.[8,109] In general, it has been found that, on average, the AP93 code has reduced the normal force and center of pressure errors of the AP81 code by half, and reduced the axial force errors by about twenty-five percent. There are cases where AP81 actually does better than AP93. However, these are quite rare, and in averaging several hundred data points for various configurations, at various Mach numbers and, at 5° increments in angle of attack from 0 to 30°, the reduction in errors of AP93 over AP81 is significant. While no equivalent systematic comparison with other SOTA codes has been made, the AP93 was superior to other engineering codes at most conditions where comparisons were made.

5.0 SUMMARY

In summary, various types of aeroprediction codes have been reviewed. Some of the more important conventional approximate aerodynamic techniques have been summarized. Recent new methods applicable to the semiempirical class of aeroprediction codes have been given in slightly more detail. Six complete missile configurations have been used for comparing the NSWCDD AP93 code to experiment and other approximate codes. It was seen that this new nonlinear theory gives significant improvement in aerodynamic estimation compared to the AP81.

Some areas where new technology is still needed for semiempirical codes is in skin friction drag treatment with angle of attack, transonic aerodynamics, base drag at $\alpha > 15$ deg., and a simple, accurate method for estimating roll-dependent aerodynamics.

6.0 ACKNOWLEDGEMENTS

Numerous investigators have assisted the author in the aeroprediction work at NSWCDD over the past 23 years. Many of them are listed in the references. These individuals include W. McKerley,Gil Graff, R. Swanson, L. Devan, L. Mason, J. Sun, M. Armistead, S. Rowles, T. Hymer, and R. McInville at NSWCDD. Also, contributions have been made by F. De Jarnette at N.C. State, Frank Baltakis of Advanced Technology Associates, Nielsen Engineering and Research, and Lockheed Missiles and Spacecraft. Appreciation is expressed to each of these individuals or organizations for their roles.

Those who had the foresight to sponsor the work are not referenced and are also acknowledged. W. Pasiuk of the Naval Sea Systems Command was the first individual to sponsor the work. He was joined by the Naval Air Systems Command, B. Volz and D. Hutchins in 1977. A small amount of support was also given by the U.S. Army Missile Command, R. Deep; and the Air Force Armament Lab, D. Daniel. Currently, the work is being supported by the Office of Naval Research, D. Siegel, through the Surface Launched Weapons Technology Program at NSWCDD (R. Staton) and the Air Launched Weapons Technology Program at the Naval Weapons Center, (T. Loftus). Other funding has also been obtained from the NSWCDD Independent Research Program.

7.0 REFERENCES

1. Moore, F. G., *Body Alone Aerodynamics of Guided and Unguided Projectiles at Subsonic, Transonic, and Supersonic Mach Numbers*, NWL TR-2796, Nov 1972, NWL, Dahlgren, VA.

2. Moore, F. G., *Aerodynamics of Guided and Unguided Weapons: Part I-Theory and Application,* NWL TR-3018, Dec 1973, NWL, Dahlgren, VA.

3. Moore, F. G. and McKerley, W. C., *Aerodynamics of Guided and Unguided Weapons: Part II-Computer Program and User Guide,* NWL TR-3036, Jan 1974, NWL, Dahlgren.

4. Moore, F. G. and Swanson, R. C., *Aerodynamics of Tactical Weapons to Mach Number 3 and Angle of Attack 15 Degrees: Part I-Theory and Application,* NSWCDL TR-3584, Feb 1977, NSWCDL, Dahlgren VA.

5. Swanson, R. C. and Moore, F. G., *Aerodynamics of Tactical Weapons to Mach Number 3 and Angle of Attack 15 Degrees: Part II-Computer Program and Usage,* NSWCDL TR-3600, Mar 1977, NSWCDL, Dahlgren VA.

6. Devan, L., *Aerodynamics of Tactical Weapons to Mach Number 8 and Angle of Attack 180°: Part I, Theory and Application,* NSWC TR 80-346, Oct 1980, NSWC, Dahlgren, VA.

7. Devan, L. and Mason, L., *Aerodynamics of Tactical Weapons to Mach Number 8 and Angle of Attack 180°: Part II, Computer Program and Users Guide,* NSWC TR 81-358, Sep 1981, NSWC, Dahlgren, VA.

8. Moore, F. G.; Hymer, T. C.; and McInville, R. M.; *Improved Aeroprediction Code: Part I-Summary of New Methods and Comparison with Experiment*, NSWCDD/TR-93/91, May 1993, NSWCDD, Dahlgren, VA.

9. Moore, F. G.; McInville, R. M.; and Hymer, T. C.; *Improved Aeroprediction Code: Part II-Computer Program Users Guide and Listing,* NSWCDD, Dahlgren, VA, Aug 1993.

10. Lacau, R. G.; "A Survey of Missile Aerodynamics," *proceedings of NEAR Conference on Missle Aerodynamics*, NEAR, Inc., Mountain View, CA, Oct 1988, paper 1.

REFERENCES (CONTINUED)

11. Herring, P.G.C., *A Computer Program Which Evaluates the Longitudinal Aerodynamic Characteristics of Typical Weapon Configurations,* AGARD-CP-336, 1982.

12. Hasselot, A., *Berakning Aerodynamiska Koefficienter for Rammotorroboter,* FFA AU-166, 1980.

13. Gustafsson, A., *A Computer Program for The Prediction of Aerodynamic Characteristics of Wing-Body-Tail Combinations at Subsonic and Supersonic Speeds,* FFA AU-635, 1972.

14. Baker, W. B., *An Aerodynamic Coefficient Prediction Technique for Slender Bodies with Low Aspect Ratio Fins at Transonic Mach Numbers and Angles of Attack to 180°*, AEDC-TR-77.97, 1978, AEDC, Tullahoma, TN.

15. Eaton, P. T., *A Method for Predicting the Static Aerodynamic Characteristics of Low-Aspect-Ratio Configurations,* DTMB-2216, 1966, Cardecrock, MD.

16. Sun, J.; Hansen, S. G.; and Cumming, R. M., August H., *Missle Aerodynamics Prediction (MAP) Code,* AIAA paper no 84-0389, 1984.

17. Vukelich, S. R. and Jenkins, J. E., *Missle DATCOM: Aerodynamic Prediction on Conventional Missiles Using Component Build-Up Techniques,* AIAA paper no 84-0388, 1984.

18. Boizard, B., *Missle ONERA* in Activities ONERA 1985-Aerodynamique (11-10).

19. Smith, C. A. and Nielsen, J. N., *Prediction of Aerodynamic Characteristics of Cruciform Missiles to High Angles of Attack Utilizing a Distributed Vortex Wake,* NEAR-TR-208, 1979, NEAR, Inc., Mountain View, CA.

20. Hemsch, M. J. and Mullen, J., *Analytical Extension of the Missle 1 and Missile 2 Computer Programs,* NEAR-TR-272, 1982, NEAR, Inc., Mountain View, CA.

21. Dillenius. M. F.; Hemsch. M. J.; Sawyer. W. C.; Allen. J. M.; and Blair. A. B., *Comprehensive Missile Aerodynamics Programs for Preliminary Design,* Journal of Spacecraft, Volume 20, no 4, 1983.

22. Lesieutre. D. J.; Mendenhall. M. R.; and Nazario. S. M., *Prediction of the Aerodynamic Characteristics of Cruciform Missiles Including Effects of Roll Angle and Control Deflection,* NEAR-TR-360, 1986, NEAR, Inc., Mountain View, CA.

23. Lesieutre, D. J.; Mendenhall, M. R.; and Nazario, S. M., *Aerodynamic Characteristics of Cruciform Missiles at High Angles of Attack,* AIAA paper no 87-0212.

REFERENCES (CONTINUED)

24. Williams, J. E. and Vukelich, S. R., *USAF Stability and Control DATCOM*, AFFDL-TR-75-45, Wright Patterson Air Force Base, Dayton, OH.

25. Gentry, A. E.; Smyth, D. N.; and Olivier, W. R., *The MARK IV Supersonic-Hypersonic Arbitrary Body Program,* AFFDL TR-73-159, 1973 Wright Patterson Air Force Base, Dayton, OH.

26. Barrowman, *An Improved Theoretical Aerodynamic Derivatives Computer Program for Sounding Rockets,* AIAA paper no 79-0504.

27. Wolfe, W. P. and Oberkampf, W. L., *Drag Predictions for Projectiles and Finned Bodies in Incompressible Flow,* AIAA paper no 85-0104.

28. Wolfe, W. P. and Oberkampf, W. L., *SANDRAG - A Computer Code for Predicting Drag of Bodies of Revolution at Zero Angle of Attack in Incompressible Flow,* SAND 85-0515, 1985.

29. Shankar, V. J.; Szema, K. Y.; and Bonner, E., *Full-Potential Methods for Analysis-Design of Complex Aerospace Configurations,* NASA CR-3982, 1986.

30. Dillenius, M. F. E. and Allen, J. M., "Paneling Methods with Vorticity Effects and Corrections for Nonlinear Compressibility," in *Tactical Missile Aerodynamics, AIAA Progress in Astronautics and Aeronautics*, Volume 104, 1986.

31. Dillenius, M. F. E. and Keirstead, *Panel Methods Applied to Supersonic Inlets Alone and to Complete Supersonic Air Breathing Configurations,* NASA CR-3979, 1986.

32. Fornassier, L., *Linearized Potential Flow Analysis of Complex Aircraft Configurations by HISSS, a Higher-Order Panel Method,* AIAA paper no 85-0281.

33. FFA Report 138, 1983.

34. Devan, L., *Nonaxisymmetric Body, Supersonic, Aerodynamic Prediction,* NSWC TR-86-253, 1986, NSWC, Dahlgren, VA.

35. Nikolitsch, D., *Calculation of Pressure Distributions, Forces and Moments of Cruciform Wing-Body Combination up to High Angles of Attack,* AIAA paper no 81-0397.

36. Hoeijmakers, H. W. M., "A Panel Method for the Prediction of Aerodynamic Characteristics of Complex Configurations in Linearized Subsonic and Supersonic Flow," in *Missile Aerodynamics*, AGARD CP-336, 1982.

REFERENCES (CONTINUED)

37. Dillenius, M. F. E; Perkins, S. C.; and Lesieutre, D. J., *Modified NWCDM-NSTRN and Supersonic Store Separation Programs for Calculating NASTRAN Forces Acting on Missiles Attached to Supersonic Aircraft,* NEAR TR-369, 1986, NEAR, Inc., Mountain View, CA.

38. Sidwell, K. W.; Baruah, P. K.; and Bussoletti, J. E., *A Computer Program for Predicting Subsonic or Supersonic Linear Potential Flows about Arbitrary Configurations using a Higher Order Panel Method,* Volume II NASA CR 3252, 1980.

39. Lotstedt, P., *A Three Dimensional Higher Order Panel Method for Subsonic Flow Problems Description and Applications,* SAAB L-O-1R 100, 1984.

40. Henning, P. and Hartner, E., *Instationare Beiwerte Von Flugkorpern, Teil V; Derivative Der Langsstabilitat Von Flugel-Rumpf-Leitwerks-Anordnungen in Unter Und Uberschallstromung,* MBB-Bericht UA-830-84, 1985.

41. Dillenius, M. F. and Nielsen, J. N., *Computer Programs for Calculating Pressure Distributions Including Vortex Effects on Supersonic Monoplane or Cruciform Wing-Body-Tail Combinations with Round or Elliptical Bodies,* NASA CR-3122, 1979.

42. Nikolitsch, D., *Flugel-Rumpfkonfigurationen im Nichtlinearen Austellwinkel-Bereich, Teil III,* MBB-Bericht UA-676/82, 1982.

43. Whitfield, D. L. and Janus, J. M., *Three-Dimensional Unsteady Euler Equations Solution using Flux Vector Splitting,* AIAA paper no 84-1552.

44. Eberle, A., *Euler Solution for a Complete Fighter Aircraft at Sub and Supersonic Speed,* AGARD-CP-412, 1986.

45. Chattot, J. J.; Kock, C.; and Elsaesser, E., "Solution of the EULER Equations for Missile Configurations," *Proceedings of the Sixth GAMM-Conference on Numerical Methods in Fluid Mechanics,* Volume 13, 1986, Vieweg.

46. Borrel, M. and Montagne, J. L., *Numerical Study of a Non-Centered Scheme with Applications to Aerodynamics,* AIAA paper no 85-1497, 1985.

47. Lordon, J.; Guillen, P.; Mortel, P.; and Lacau, R. G. L., "Calcul D' Ecoulements Supersoniques Autour De Missiles Tactiques," *23eme Colloque d' Aerodynamique Appliquee,* 1986.

48. Belk, D. M. and Whitfield, D. L., *Three-Dimensional Euler Solutions on Blocked Grids using an Implicit Two-Pass Algorithm,* AIAA paper no 87-0450.

REFERENCES (CONTINUED)

49. Wardlaw, A. B.; Priolo, F. G.; and Solomon, J. M., *An Inviscid Multiple Zone Method for Supersonic Tactical Missiles,* NSWC-TR-85-484, 1985, NSWC, Dahlgren, VA.

50. Daywitt, J. E.; Brant, D.; and Bosworth, F., *Computional Technique for Three-Dimensional Inviscid Flow Fields about Reentry Vehicles,* SAMSO TR-79-5, 1978.

51. Wardlaw, A. B.; Baltakis, F. P.; Solomon, J. M.; and Hackerman, L. B., *An Inviscid Computational Method for Tactical Missile Configurations,* NSWC-TR-81-457, 1981, NSWC, Dahlgren, VA.

52. Wardlaw, A. B.; Davis, S., *A Second-Order-Godmore Method for Supersonic Tactical Missiles,* NSWC TR-86-506, 1986, NSWC, Dahlgren, VA.

53. Thomas, J. L.; Taylor, S. L.; and Anderson, W. K., *Navier-Stokes Computations of Vortical Flows Over Low Aspect Ratio Wings,* AIAA paper no 87-0207, Jan 1987.

54. Walters, R. W.; Slack, D. C.; Cinnella, P., Applebaum, M. P.; and Frost, C., *A User's Guide to GASP,* Virginia Polytechnic Institute and State University, Dept. of Aerospace and Ocean Engineering, Nov 1990, Blacksburg, VA.

55. McGrory, W. D.; Slack, D. C.; Applebaum, M. P.; and Walters, R. B., *GASP Version 2, User's Manual*, AeroSoft, Inc., Blacksburg, VA, 1992.

56. Schiff, L. B. and Steger, J. L., *Numerical Simulation of Steady Supersonic Viscous Flow,* AIAA paper no 79-0130, 1979.

57. Kaul, U. K. and Chausee, D. *AFWAL Parabolized Navier-Stokes Code: 1983,* AFWAL/NASA Merged baseline version, AFWAL-TR-83-3118, 1984.

58. Van Dyke, M. D., *First and Second-Order Theory of Supersonic Flow Past Bodies of Revolution,* Journal of Aeronautical Sciences, Vol.18, No. 3, Mar 1951, pp.161-179.

59. Tsien, H. S., *Supersonic Flow Over an Inclined Body of Revolution, Journal of Aeronautical Sciences,* Vol. 5, No. 12, Oct 1938, pp. 480-483.

60. Syvertson, C. A. and Dennis, D. H., *A Second-Order Shock-Expansion Method Applicable to Bodies of Revolution Near Zero Lift,* NACA TR 1323, 1957.

61. Eggers, A. J.; Syvertson, C. A.; and Kraus, S.; *A Study of Inviscid Flow about Airfoils at High Supersonic Speeds,* NACA Report 1123, 1953.

REFERENCES (CONTINUED)

62. Eggers, A. J. and Savin, R. C., *A Unfied Two-Dimensional Approach to the Calculation of Three-Dimensional Hypersonic Flows, with Application to Bodies of Revolution,* NACA Report 1249, 1955.

63. Eggers, A. J. and Savin, R. C., *Approximate Methods for Calculating the Flow about Nonlifting Bodies of Revolution at High Supersonic Airspeeds,* NACA TN 2579, 1951.

64. Leis, L., "Hypersonic Flow," Inst. Aero. Science, preprint No. 554, 1955.

65. Jackson, C. M., Jr.; Sawyer, W. C.; Smith, R. S., *A Method for Determining Surface Pressures on Blunt Bodies of Revolution at Small Angles of Attack in Supersonic Flow,* NASA TN D-4865, Nov 1968.

66. De Jarnette, F. R. and Jones, K. M., *Development of a Computer Program to Calculate Aerodynamic Characteristics of Bodies and Wing-Body Combinations,* NSWC/DL TR-3829, Apr 1978, NSWC/DL, Dahlgren, VA.

67. De Jarnette, F. R. and Ford, C. P., "A New Method for Calculating Surface Pressures on Bodies at an Angle of Attack in Supersonic Flow," *Proceedings of the 11th Navy Symposium on Aeroballistics,* Vol.II, 22-24 Aug, 1978, pp. 199-231.

68. De Jarnette, F. R.; Ford, C. P.; and Young, D. E., *A New Method for Calculating Surface Pressures on Bodies at an Angle of Attack in Supersonic Flow,* AIAA Paper No. 79-1552, AIAA 12th Fluid and Plasma Dynamics Conference, Williamsburg, VA, Jul 1974.

69. Allen, J. H. and Purkins, E. W., *Characteristics of Flow over Inclined Bodies of Revolution,* NACA RM A 50L07, Mar, 1951.

70. Van Driest, E. R., "Turbulent Boundary Layers in Compressible Fluids," *Journal of Aeronautical Sciences,* Vol. 18, No. 3, 1951, pp. 145-160, 216.

71. Chadwick, W. R., "External Loads Using Nonplanar Lifting Surface Theory," *Journal of Aircraft,* Vol.11, No. 3, Mar, 1974, pp. 181-188.

72. Ashley, Holt, Landahl, Martin; *Aerodynamics of Wings and Bodies,* Addison-Wesley Publishing Company, Inc., Reading, Ms., 1965, Chapter 7.

73. Purvis, J. W., *Lifting Surface Theory Calculations of Aerodynamic Wing-Tail Load Distributions During Subsonic Maneuvers,* NWL TR-2787, Aug 1972 NSWCDD, Dahlgren, VA.

74. Bishop, R. A. and Cane, E. G., *Charts of the Theoretical Wave Drag of Wings at Zero Lift,* R. A. E. Tech. Note AERO 2421, 1956.

REFERENCES (CONTINUED)

75. Margolis, K.; *Supersonic Wave Drag of Sweptback Tapered Wings at Zero Lift,* NACA TN 1448, 1947.

76. Hannah, M. E. and Margolis, K.; *Span Load Distribution Resulting from Constant Angle-of-Attack, Steady Rolling Velocity, Steady Pitching Velocity, and Constant Vertical Acceleration for Tapered Sweptback Wings With Streamwise Tips,* NACA TN 2831, 1952.

77. Martin, J. C. and Jefferys, I.; *Span Load Distribution Resulting from Angle-of-Attack, Rolling and Pitching for Tapered Sweptback Wings With Streamwise Tips,* NACA TN 2643, 1952.

78. Malvestuto, Jr., F. S.; Margolis, K.; and Ribner, H., *Theoretical Lift and Dampening in Roll at Supersonic Speeds of Thin Sweptback Tapered Wings With Streamwise Tips, Subsonic Leading Edges, and Supersonic Trailing Edges,* NACA TR 970, 1950.

79. Lockwood, V. E. *Effects of Sweep on the Damping-in-Roll Characteristics of Three Sweptback Wings Having an Aspect Ratio of 4 at Transonic Speeds,* NACA RM L50J19, Dec 1950.

80. Edmondson, J. L., *Damping in Roll of Rectangular Wings of Several Aspect Ratios and NACA 65A Series Airfoil Sections of Several Thickness Ratios at Transonic and Supersonic Speeds as Determined With Rocket-Powered Models,* NACA RM L50E26, 1950.

81. Adams, G. J. and Dugan, D. W. *Theoretical Damping in Roll and Rolling Moment Due to Differential Wing Incidence for Slender Cruciform Wings and Wing-Body Combinations,* NACA TR 1088, 1952.

82. Tobak, M. and Lessing, H. C. *Estimation of Rotary Stability Derivatives at Subsonic and Transonic Speeds,* NATO Report 343, Apr 1961.

83. Cole, I. J. and Margolis, K. *Lift and Pitching Moment at Supersonic Speeds Due to Constant Vertical Acceleration for Thin Sweptback Tapered Wings With Streamwise Tips, Supersonic Leading and Trailing Edges,* NACA TN 3196, Jul 1954.

84. Martin, J. C.; Margolis, K.; and Jefferys, I., *Calculation of Lift and Pitching Moments Due to Angle of Attack and Steady Pitching Velocity at Supersonic Speeds for Thin Sweptback Tapered Wings With Streamwise Tips and Supersonic Leading and Trailing Edges,* NACA TN 2699, Jun 1952.

85. Malvestuto, F. S. and Hoover, D. M., *Lift and Pitching Derivatives of Thin Sweptback Tapered Wings With Streamwise Tips and Subsonic Leading Edges at Supersonic Speeds,* NACA TN 2294, Feb 1951.

REFERENCES (CONTINUED)

86. Tobak, M., *Damping in Pitch of Low-Aspect-Ratio Wings at Subsonic and Supersonic Speeds,* NACA RMA52L04a, Apr 1953.

87. Pitts, W. C.; Nielson, J. N.; and Kaatari, G. E.; *Lift and Center of Pressure of Wing-Body-Tail Combinations at Subsonic, Transonic, and Supersonic Speeds,* NACA TR 1307, 1957.

88. Park, C., and Leon, S., *Calculation of Real-Gas Effects on Blunt-Body Trim Angles,* AIAA paper no 89- 0685, Aerospace Sciences meeting, Reno, NV., Jan 1989.

89. Moore, F. G.; Armistead, M. A.; Rowles, S. H.; and De Jarnette, F. R.; *Second-Order Shock-Expansion Theory Extended to Include Real Gas Effects,* NAVSWC TR-90-683, Feb 1992, NSWCDD, Dahlgren, VA.

90. Moore, F. G.; Armistead, M. J.; Rowles, S. H.; and De Jarnette, F. R.; "New Approximate Method for Calculating Real Gas Effects on Missle Configurations," *Journal of Spacecraft and Rocketts,* Vol. 30, No.1, Jan-Feb, 1993.

91. Anderson, J. D., *Modern Compressible Flow*, McGraw-Hill Book Company, New York, NY, 1982.

92. Hudgins, Henry E., Jr., *Supersonic Flow About Right Circular Cones at Zero Yaw in Air at Chemical Equilibrium, Part I-Correlation of Flow Properties,* TM 1493, Picatinny Arsenal, PA, Aug 1965.

93. Wittliff, C. E. and Curtis, J. T., *Normal Shock Wave Parameters in Equilibrium Air,* Cornell Aero Lab Report, CAL-III, Nov 1961.

94. Tannehill, J. C. and Mugge, P. H., *Improved Curve Fits for the Thermodynamic Properties of Equilibrium Air Suitable for Numerical Computation using Time-Dependent Shock-Capturing Methods,* NASA CR-2470, 1974.

95. Srinivasan, S.; Tannehill, J.; and Wielmuenster, K., *Simplified Curve Fits for the Thermodynamic Properties of Equilibrium Air,* Report ISSU-ERI-AMES 86401, Jun 1986, Engineering Research Institute, Iowa State Univ., Ames, IA.

96. Morrison, A. M.; Solomon, J. M.; Ciment, M.; and Ferguson, R. E., *Handbook of Inviscid Sphere-Cone Flow Fields and Pressure Distributions: Volume I,* NSWC/WOL/TR 75-45, Dec 1975, White Oak, MD.

97. Jones, D. J., *Numerical Solutions of the Flow Field for Conical Bodies in a Supersonic Stream,* National Research Council of Canada, Report LR-507, Jul 1968, Otlawa, ON, Canada.

REFERENCES (CONTINUED)

98. McInville, R. and Moore, F. G., *Incorporation of Boundary Layer Heating Predictive Methodology into the NAVSWC Aeroprediction Code,* NSWCDD/TR-93/29, Apr 1993, NSWCDD, Dahlgren, VA.

99. Anderson, J. D., *Hypersonic and High Temperature Gasdynamics,* McGraw-Hill Book Co., New York, NY, 1989.

100. Beckwith, I. E. and Gallagher, J. J., *Local Heat Transfer and Recovery Temperatures on a Yawed Cylinder at Mach Numbers of 4.15 and High Reynolds Numbers,* NASA Technical Report R-104, 1961.

101. Hender, D. R., *A Miniature Version of the JA70 Aerodynamic Heating Computer Program, H800 (MINIVER),* McDonnell-Douglas Astronautics Co., Report MCD G0462, Jun 1970, St. Louis, MO.

102. Eckert, E. R. G., *Engineering Relations for Heat Transfer and Friction in High-Velocity Laminar and Turbulent Boundary Layer Flow over Surfaces with Constant Pressure and Temperature,* Transactions of the ASME, Vol. 78, No. 6, Aug 1956.

103. Eckert, E. R. G., *Survey of Boundary Layer Heat Transfer at High Velocities and High Temperatures,* WADC Technical Report 59-624, Apr 1960.

104. Riley, C. J. and De Jarnette, F. R., "Engineering Aerodynamic Heating Method for Hypersonic Flow," Journal of Spacecraft and Rockets, Vol. 29, No. 3, May-Jun 1992.

105. Cleary, J. W., *Effects of Angle of Attack and Bluntness on Laminar Heating Rate Distribution of a 15° Cone at a Mach Number of 10.6,* NASA TN D-5450, 1969.

106. Moore, F. G.; Wilcox, F.; and Hymer, T., *Improved Empirical Model for Base Drag Prediction on Missile Configurations Based on New Wind Tunnel Data,* NSWCDD/TR-92/509, Oct 1992, NSWCDD, Dahlgren, VA.

107. Moore, F. G.; Wilcox, F.; and Hymer, T., *Base Drag Prediction on Missile Configurations,* AIAA Paper, No. 93-3629, to be presented at Atmospheric Flight Mechanics Conference, Aug 1993, Monterey, CA.

108. Butler, C.; Sears, E.; and Pellas, S., *Aerodynamic Characteristics of 2-, 3-, and 4-caliber Tangent-Ogive Cylinders with Nose Bluntness Ratios of 0.00, 0.25, 0.50, and 0.75 at Mach Numbers from 0.6 to 4.0,* AFATL-TR-77-8, Jan 1977.

109. Moore, F. G.; Hymer, T.; and Devan, L., *New Methods for Predicting Nonlinear Lift, Center of Pressure, and Pitching Moment on Missile Configurations,* NSWCDD/TR-92/217, Jul 1992, NSWCDD, Dahlgren, VA.

REFERENCES (CONTINUED)

110. Moore, F. G.; Devan, L.; and Hymer, T., *A New Semiempirical Method for Computing Nonlinear Angle-of-Attack Aerodynamics on Wing-Body-Tail Configurations,* AIAA Paper, No. 93-0038, 31st Aerospace Sciences Meeting, Jan 1993.

111. Jorgensen, L. H., *Prediction of Static Aerodynamic Characteristics for Slender Bodies Alone and with Lifting Surfaces to Very High Angles of Attack,* NASA TR R-474, Sep 1977.

112. NASA Langley Research Center Tri-Service Missile Data Base, transmitted from NASA/LRC Jerry M. Allen to NAVSWC, 5 Nov 1991 (formal documentation in process).

113. Stallings, R. L., Jr. and Lamb, M., *Wing-Alone Aerodynamic Characteristics for High Angles of Attack at Supersonic Speeds,* NASA Technical Paper 1889, Jul 1981.

114. Nielsen, J. N.; Hemsch, M. J.; and Smith, C. A., *A Preliminary Method for Calculating the Aerodynamic Characteristics of Cruciform Missiles to High Angles of Attack Including Effects of Roll Angle and Control Deflections,* ONR Report CR 215-226-4F, Nov 1977, ONR, Arlington, VA.

115. McKinney, R. L., *Longitudinal Stability and Control Characteristics of an Air-to-Air Missile Configuration at Mach Numbers of 2.3 and 4.6 and Angles of Attack from -45° to 90°*, NASA TM X-846, 1972.

116. Monta, W. J., *Supersonic Aerodynamic Characteristics of a Sparrow III Type Missile Model with Wing Controls and Comparison with Existing Tail-Control Results,* NASA TP 1078, Nov 1977.

117. Smith, E. H.; Hebbar, S. K.; and Platzer, M., *Aerodynamic Characteristics of a Canard-Controlled Missile at High Angles of Attack,* AIAA Paper, No. 93-0763, Presented at 31st Aerospace Sciences Meeting, Reno, NV, 11-14 Jan 1993.

118. Howard, R. M. and Dunn, A., "Missile Loads at High Angles of Attack," *Journal of Spacecraft and Rockets,* Vol. 28, No. 1, Jan-Feb, 1991.

119. Bible, J. E. and Hardy, S. R., *Wind Tunnel Test Data of the High Performance Point Defense Missile HPPDM obtained in the NASA Langley Unitary Plan Wind Tunnel,* NAVSWC TR 90-475, in publication.

120. Graves, E. and Fournier, R., *Stability and Control Characteristics at Mach Numbers from 0.2 to 4.63 of a Cruciform Air-to-Air Missile with Triangular Canard Controls and a Trapezoidal Wing,* NASA-TM-X-3070, Nov 1974.

8.0 SYMBOLS AND DEFINITIONS

A_p	Planform area of the body or wing in the crossflow plane (ft^2)
A_{ref}	Reference area (maximum cross-sectional area of body if a body is present or planform area of wing if wing-alone) (ft^2)
A_W	Planform area of wing in crossflow plane (ft^2)
a	Speed of sound (ft/sec)
AR	Aspect ratio $= b^2/A_W$
b	Wing span (not including body) (ft)
C_A, C_{AB}, C_{AF}	Total, base, and skin friction axial force coefficients respectively
C_D	*Drag Coefficient* $= \dfrac{Drag}{\frac{1}{2}\rho_\infty V_\infty^2 A_{ref}}$
C_{dc}	Crossflow drag coefficient
$C_{f\infty}$	Mean skin friction coefficient based on freestream Reynolds number $(R_e)_\infty$
C_M	Pitching moment coefficient (based on reference area and body diameter if body present or mean aerodynamic chord if wing alone)
C_m	Spanwise pitching moment of wing airfoil section
$C_{Mq} + C_{M\dot{\alpha}}$	Pitch damping moment coefficient derivative
C_N	*Normal Force Coefficient* $\left(\dfrac{NormalForce}{\frac{1}{2}\rho_\infty V_\infty^2 A_{ref}}\right)$
C_n	Spanwise normal force of wing airfoil section
C_{N_B}	Body alone normal force coefficient
$C_{N_{B(V)}}$	Negative afterbody normal-force coefficient due to canard or wing shed vortices
$C_{N_{B(W)}}$	Additional normal-force coefficient on body due to presence of wing

$\Delta C_{N_{B(W)}}$	Additional normal-force coefficient on body due to a control deflection of the wing
C_{N_L}	Linear component of normal-force coefficient
$C_{N_{NL}}$	Nonlinear component of normal-force coefficient
$C_{N_{T(V)}}$	Negative normal-force coefficient component on tail due to wing or canard shed vortex
$C_{N_{W(B)}}$	Normal-force coefficient of wing in presence of body
$\Delta C_{N_{W(B)}}$	Additional normal-force coefficient of wing in presence of body due to a wing deflection
C_{N_α}	Normal-force coefficient derivative
C_p	Pressure Coefficient $\left(\frac{p-p_\infty}{\frac{1}{2}\rho_\infty V_\infty^2}\right)$
C_{P_B}	Base pressure coefficient
$(C_{PB})_{NF,\alpha}$	Base pressure coefficient with no fins present and at angle of attack
$(C_{PB})_{\alpha,\delta,t/c,x/c}$	Base pressure coefficient with fins present of some t/c, x/c, δ, and body at some α
C_{P_o}	Stagnation pressure coefficient
c_r	Root chord (ft)
c_t	Tip chord (ft)
d	Body diameter (ft)
d_{ref}	Reference body diameter (ft)
e	Internal energy (ft^2/sec^2)
F	Dimensionless empirical factor used in tail normal-force coefficient term due to canard or wing shed vortices to approximate nonlinear effects due to a control deflection
F_1, F_2, F_3	Symbols defining parameters used in base drag empirical model
f_w, f_t	Lateral location of wing or tail vortex (measured in feet from body center line)

H	Heat transfer coefficient based on wall local temperature (ft-lb)/(ft^2-sec-°R)
H_0	Total enthalpy (ft^2/sec^2)
H_1	Heat transfer coefficient based on wall local specific enthalpy [slug/(ft^2-sec)]
h	Specific enthalpy (ft^2/sec^2)
h_{aw}	Adiabatic wall specific enthalpy (ft^2/sec^2)
h_e	Specific enthalpy at outer edge of boundary layer (ft^2/sec^2)
h_T	Height of wing or canard shed vortex at tail center of pressure (ft)
h_w	Specific enthalpy at wall (ft^2/sec^2)
h^*	Reference value of specific enthalpy (ft^2/sec^2)
i	Tail interference factor
k_1	Empirical factor defined in wing-alone nonlinear normal-force coefficient term
$K_{B(W)}$	Ratio of additional body normal-force coefficient derivative due to presence of wing to wing-alone normal-force coefficient derivative at $\delta = 0$ deg
$K_{W(B)}$	Ratio of normal-force coefficient derivative of wing in presence of body to that of wing alone at $\delta = 0$ deg
$k_{B(W)}$	Ratio of additional body normal-force coefficient derivative due to presence of wing at a control deflection to that of the wing alone at $\alpha = 0$
$k_{W(B)}$	Ratio of wing normal-force coefficient derivative in presence of body due to a control deflection to that of wing alone at $\alpha \neq 0$ deg
$[k_{W(B)}]_{SB}$	Value of $k_{W(B)}$ calculated by slender-body theory at $\alpha = 0$
$\Delta K_{B(W)}$, $\Delta K_{W(B)}$	Nonlinear corrections to $K_{B(W)}$ and $K_{W(B)}$ due to angle of attack
l	Length (ft)
l_N	Nose length (can be in calibers or feet)
LT	Linear Theory
M	Mach number = V/a

M_N	Normal Mach number to body axis = M sin α
N_l, N_t	Transformation factors used in Eckert reference enthalpy to approximate three-dimensional effects for laminar and turbulent flow (= 3 and 2, respectively)
p	Pressure (lb/ft^2) or roll rate (rad/sec)
p_c	Pressure of a cone of given half angle (lb/ft^2)
P_r	Prandtl number
$\dot{q}$	Pitch Rate (rad/sec)
$\dot{q}_w$	Heat transfer rate (ft-lb)/(ft^2-sec) at wall
$\dot{q}_{w,l}$, $\dot{q}_{w,t}$	Heat transfer rate at wall for laminar or turbulent flow, respectively
R	Gas constant [for air R = 1716 ft-lb/(slug - °R)]
Re	Reynolds Number = $\frac{\rho V l}{\mu}$
$(Re)_c$	Critical Reynolds number where flow transitions from laminar to turbulent flow
Re_D	Reynolds number based on diameter of wing leading edge bluntness
r	Radius of body (ft)
r_n	Radius of nose tip (ft)
r_w r_t	Radius of body at wing or tail locations
r/s	Ratio of body radius to wing or tail semispan plus the body radius
S	Entropy (ft-lb)/(slug - °Rankine)
s	Distance along body surface in SOSET (also wing or tail semispan plus the body radius in wing-body lift methodology)
SB	Slender-body theory
T	Temperature (°R or °K)
T_{aw}, T_o, T_w	Adiabatic wall, total, and wall temperature, respectively

t/c_r	Tail thickness to its root chord
t/d	Tail thickness to body diameter
u,v,w	Perturbation velocity components, (ft/sec)
V	Velocity (ft/sec)
V_e	Velocity at edge of boundary layer (ft/sec)
V_p	Velocity parallel to leading edge of wing (ft/sec)
x	Distance along the axis of symmetry measured positive aft of nose tip (feet or calibers)
x/c	Parameter used in base drag methodology to represent the number of chord lengths from the base (measured positive upstream of base)
x_{cp}	Center of pressure (in feet or calibers from some reference point that can be specified)
x_L, x_T	Laminar and turbulent flow lengths on body (ft)
y_{cp}	Spanwise center of pressure of wing semispan
Z	Compressibility factor
α	Angle of attack (degrees)
$\dot{\alpha}$	Rate of change of angle of attack (deg/sec)
α_c	Angle of attack where wing-body interference factor starts decreasing from its slender-body theory value (degrees)
α_D	Angle of attack where the wing-body interference factor reaches a minimum (degrees)
α_w, α_T	Local angle of attack of wing or tail ($\alpha + \delta_w$ or $\alpha + \delta_T$, respectively, in degrees)

β	$\sqrt{M^2-1}$ or $\sqrt{1-M^2}$ depending on whether flow is supersonic or subsonic. Also, Mach angle, $\beta = \sin^{-1}(1/M)$.
δ	Control deflection (degrees)
δ_{eq}	Angle between a tangent to the body surface at a given point and the velocity vector (degrees)
δ_W, δ_T	Deflection of wing or tail surfaces (degrees), positive leading edge up
Φ	Velocity potential
ϕ	Circumferential position around body where $\phi = 0$ is leeward plane (degrees)
λ	Taper ratio of a lifting surface $= c_t/c_r$
Ψ_1, ζ_1	First order axial and crossflow solutions of velocity potential equation
Ψ_2	Second order particular solution to full potential equation
η	Parameter used in SOSET and also used in viscous crossflow theory for nonlinear body normal force (in this context, it is the normal force of a circular cylinder of given length-to-diameter ratio to that of a cylinder of infinite length)
η_o	Value of η in viscous crossflow theory for $M_N = 0$
μ_o, μ^*	Viscosity coefficient at stagnation or reference conditions, respectively (slug/ft-sec)
ρ, ρ_0, ρ^*	Density of air at local, stagnation, or reference conditions, respectively (slugs/ft^3)
γ	Specific heat ratio
θ	Local body slope at a given point (degrees)
θ_c	Cone half angle
Λ	Leading edge sweep angle of wing or tail (degrees)
∞	Free-stream conditions
2-D	Two dimensional
3-D	Three dimensional

3DTWT	3-D thin wing theory
AP81	Aeroprediction 1981
AP93	Aeroprediction 1993
APC	Aeroprediction code
BD	Base Drag
BL	Boundary Layer
FNS	Full Navier-Stokes
GSET	Generalized shock-expansion theory
IMNT	Improved modified Newtonian theory
MNT	Modified Newtonian theory
NASA/LRL	National Aeronautics and Space Administration/Langley Research Center
NS	Navier-Stokes
NSWCDD	Naval Surface Warfare Center, Dahlgren Division
PNS	Parabolized Navier-Stokes
SE	Shock expansion
SOSET	Second-order shock-expansion theory
SOTA	State-of-the-art
TAT	Turn-Around Time
TLNS	Thin Layer Navier-Stokes

DISTRIBUTION

	Copies
DOD ACTIVITIES (CONUS)	
ATTN CODE 04 (BISSON)	1
CODE 44 (ZIMET)	1
CODE 4425 (SIEGEL)	1
CODE 332FD (LEKOUDIS)	1
CODE 442 (WOOD)	1
CHIEF OF NAVAL RESEARCH	
BALLSTON TOWER 1	
800 N QUINCY ST BCT #1	
ARLINGTON VA 22217-5660	
ATTN CODE CL372 (LOFTUS)	1
CODE C2771 (SMITH)	1
CODE C2891 (PORTER)	1
CODE C2892 (STRUTZ)	1
CODE C2892 (HALTER)	1
CODE C2892 (GLEASON)	1
CODE C2894 (VAN DYKEN)	1
CODE C29B10	
TECHNICAL LIBRARY	1
COMMANDER	
NAVAL AIR WARFARE CENTER	
WEAPONS DIVISION	
CHINA LAKE CA 93555-6001	
ATTN TECHNICAL LIBRARY	1
COMMANDER	
NAVAL SEA SYSTEMS COMMAND	
WASHINGTON DC 20362-5160	
ATTN AIR 53012D (JOHNSON)	1
RM 904 JP 2	
TECHNICAL LIBRARY	1
COMMANDER	
NAVAL AIR SYSTEMS COMMAND	
WASHINGTON DC 20361-5120	
ATTN C KLEIN	1
TECHNICAL LIBRARY	1
COMMANDER	
NAVAL AIR WARFARE CENTER	
WEAPONS DIVISION	
POINT MUGU CA 93042-5000	

	Copies
ATTN T C TAI	1
M J MALIA	1
TECHNICAL LIBRARY	1
COMMANDER	
NAVAL SHIP RESEARCH AND DEVELOPMENT CENTER	
WASHINGTON DC 20034	
ATTN R M HOWARD	1
TECHNICAL LIBRARY	1
SUPERINTENDENT	
US NAVAL POSTGRADUATE SCHOOL	
MONTEREY CA 93943-5000	
ATTN S GREENHALGH	1
C REITZ	1
TECHNICAL LIBRARY	1
COMMANDING OFFICER	
NAVAL AIR WARFARE CENTER	
AIRCRAFT DIVISION WARMINSTER	
WARMINSTER PA 18974-5000	
ATTN HEAD WEAPONS DEPT	1
HEAD SCIENCE DEPT	1
SUPERINTENDENT	
US NAVAL ACADEMY	
ANNAPOLIS MD 21402	
ATTN M KRUMINS	1
TECHNICAL LIBRARY	1
OFFICER IN CHARGE	
NAVAL INTELLIGENCE SUPPORT CENTER	
4301 SUITLAND ROAD	
WASHINGTON DC 20390RM 810 CP5	
ALEXANDRIA VA 22217	
ATTN CODE 30	1
CHIEF OF NAVAL RESEARCH	
NAVY SDI	
2211 JEFFERSON DAVIS HWY	
ARLINGTON VA	

DISTRIBUTION (CONT.)

	Copies
ATTN DIAG DT 4T (PAUL MURAD)	2
DEFENSE INTELLIGENCE AGENCY	
WASHINGTON DC 20546	
ATTN CODE 50255 (WAGGONER)	1
COMMANDER	
NAVAL SURFACE WARFARE CENTER	
CRANE DIVISION	
CRANE IN 47522-5000	
ATTN CODE 5252P (KRAUSE)	1
TECHNICAL LIBRARY	1
COMMANDER	
NAVAL SURFACE WARFARE CENTER	
INDIAN HEAD DIVISION	
INDIAN HEAD MD 20640-5000	
ATTN TECHNICAL LIBRARY	1
COMMANDING GENERAL	
MARINE CORPS COMBAT	
DEVELOPMENT COMMAND	
QUANTICO VA 22134-5000	
ATTN TECHNICAL LIBRARY	1
AFATL (ADLRA) (DLGC)	
EGLIN AFB FL 32542-5000	
ATTN E SEARS	1
L E LIJEWSKI	1
C COTTRELL	1
TECHNICAL LIBRARY	1
EGLIN AFB FL 32542	
ATTN TECHNICAL LIBRARY	1
USAF ACADEMY	
COLORADO SPRINGS CO 80912	
ATTN TECHNICAL LIBRARY	1
ADVANCED RESEARCH PROJECTS AGENCY	
DEPARTMENT OF DEFENSE	
WASHINGTON DC 20305	

	Copies
ATTN B BLAKE (BLD 146)	1
D SHEREDA (BLD 450)	1
J JENKINS (BLD 146)	1
R SAMUELS (BLD 856)	1
TECHNICAL LIBRARY	1
COMMANDING OFFICER	
AFSC	
2210 8TH STREET	
WRIGHT PATTERSON AFB OH 45433	
ATTN J USSELTON	1
W B BAKER JR	1
TECHNICAL LIBRARY	1
ARNOLD ENGINEERING DEVELOPMENT CENTER USAF	
TULLAHOMA TN 37389	
ATTN H HUDGINS	1
G FRIEDMAN	1
TECHNICAL LIBRARY	1
COMMANDING GENERAL	
ARRADCOM PICATINNY ARSENAL	
DOVER NJ 07801	
ATTN C H MURPHY	1
R M MCCOY	1
W STUREK	1
C NIETUBICZ	1
A MIKHAIL	1
P PLOSTINS	1
TECHNICAL LIBRARY	1
COMMANDING GENERAL	
BALLISTIC RESEARCH LABORATORY	
ABERDEEN PROVING GROUND	
ABERDEEN MD 21005-5066	
ATTN CODE TNC (BLACKLEDGE)	1
CDR A KOREJO	1
DIRECTOR	
INTERCEPTOR TECHNOLOGY	
STRATEGIC DEFENSE INITIATIVE	
THE PENTAGON	
WASHINGTON DC 20350	

DISTRIBUTION (CONT.)

	Copies
ATTN SFAE SD ASP	1
SFAE SD HED	1
DEPUTY COMMANDER	
US ARMY STRATEGIC DEFENSE COMMAND	
P O BOX 1500	
HUNTSVILLE AL 35807-3801	
ATTN W WALKER	1
D WASHINGTON	1
COMMANDING GENERAL	
AMSI RD SI AT	
REDSTONE ARENSAL AL 35898	
DEFENSE TECHNICAL INFORMATION CENTER	12
CAMERON STATION	
ALEXANDRIA VA 22304-6145	
DEFENSE PRINTING SERVICE	1
WASHINGTON NAVY YARD	
WASHINGTON DC 20374	
DOD ACTIVITIES (EX-CONUS)	
NONE	
NON-DOD ACTIVITIES	
CENTER FOR NAVAL ANALYSIS	1
4401 FORD AVENUE	
ALEXANDRIA VA 22302-0268	
ATTN GIFT AND EXCHANGE DIVISION	4
LIBRARY OF CONGRESS	
WASHINGTON DC 20540	
GIDEP OPERATIONS OFFICE	
CORONA CA 91720	
ATTN TECHNICAL LIBRARY	1
NASA AMES RESEARCH CENTER	
MOFFETT CA 94035-1099	
ATTN C SCOTT	1
D CURRY	1
NASA JOHNSON SPACE CENTER	
HOUSTON TX 77058	
ATTN TECHNICAL LIBRARY	1
NASA	
WASHINGTON DC 20546	
ATTN W C SAWYER	1
B HENDERSON	1
D MILLER	1
J ALLEN	1
F WILCOX	1
TECHNICAL LIBRARY	2
NASA LANGLEY RESEARCH CENTER	
HAMPTON VA 23365	
ATTN D G MILLER	1
TECHNICAL LIBRARY	1
LAWRENCE LIVERMORE NATIONAL LABORATORY	
EARTH SCIENCES DIVISION	
UNIVERSITY OF CALIFORNIA	
P O BOX 808	
LIVERMORE CA 94550	
ATTN W RUTLEDGE (1635)	1
R LAFARGE	1
R EISLER	1
TECHNICAL LIBRARY	1
SANDIA NATIONAL LABORATORY	
P O BOX 5800	
ALBUQUERQUE NM 87185-5800	
ATTN DENNIS BROWN	1
NATIONAL AERONAUTICAL ESTAB	
NATIONAL RESEARCH COUNCIL	
MONTREAL RD	
OTTAWA ON CANADA K1A0R6	
ATTN ASSISTANT DEFENSE COOPERATION ATTACHE	1
EMBASSY OF SPAIN	
WASHINGTON DC 20016	
ATTN CDR R TEMPEST	1
BRITISH NAVY STAFF	
WASHINGTON DC 20008	
ATTN ASO LO IS	1
ISRAEL AIR FORCE	
LIAISON OFFICER	
700 ROBBINS AVE	
PHILADELPHIA PA 19111	

DISTRIBUTION (CONT.)

	Copies
ATTN GERMAN MILITARY REP US OA	1
GMR TRAFFIC AND TRANSPORATION DIVISION	
10 SERVICES ROAD	
DULLES INTERNATIONAL AP	
WASHINGTON DC 20041	
ATTN F D DEJARNETTE	1
NORTH CAROLINA STATE UNIVERSITY	
DEPT OF MECHANICAL AND AEROSPACE ENGINEERING	
BOX 7921	
RALEIGH NC 27695	
ATTN PROF J A SCHETZ	1
VIRGINIA POLYTECHNIC AND STATE UNIVERSITY	
DEPT OF AEROSPACE ENGINEERING	
BLACKSBURG VA 24060	
ATTN J M WU	1
C BALASUBRAMAYAN	1
TECHNICAL LIBRARY	1
THE UNIVERISITY OF TENNESSEE	
SPACE INSTITUTE	
TULLAHOMA TN 37388	
ATTN R NELSON	1
TECHNICAL LIBRARY	1
UNIVERISITY OF NOTRE DAME	
DEPT OF AEROSPACE AND MECHNICAL ENGINEERING	
BOX 537	
NOTRE DAME IN 46556	
ATTN PROF F NELSON	1
DEPT OF MECH AND AERO ENG	
UNIVERSITY OF MISSOURI ROLLA	
ROLLA MO 65401	
ATTN DR DONALD SPRING	1
AEROSPACE ENGINEERING DEPT	
AUBURN UNIVERSITY AL 36849-5338	
ATTN ROBERT ENGLAR	1
GEORGIA TECH RESEARCH INSTITUTE	
AEROSPACE SCIENCE AND TECHNOLOGY LAB	
ATLANTA GA 30332	

	Copies
ATTN E LUCERO	1
L TISSERAND	1
D FROSTBUTTER	1
L PERINI	1
TECHNICAL LIBRARY	1
APPLIED PHYSICS LABORATORY	
JOHN HOPKINS UNIVERSITY	
JOHNS HOPKINS RD	
LAUREL MD 20723-6099	
ATTN F PRILLMAN	1
W B BROOKS	1
R STANCIL	1
VOUGHT CORPORATION	
P O BOX 5907	
DALLAS TX 75222	
ATTN TECHNICAL LIBRARY	1
MARTIN MARIETTA AEROSPACE	
P O BOX 5837	
ORLANDO FL 32805	
ATTN B OMILIAN	1
CALSPAN ADVANCED TECHNOLOGY CENTER	
P O BOX 400	
BUFFALO NY 14225	
ATTN R CAVAGE	1
ADVANCED SYSTEMS DESIGN	
DEPT 113 407 (GB14)	
ROCKWELL	
NORTH AMERICAN AIRCRAFT OPERATIONS	
P O BOX 92098	
LOS ANGELES CA 90009	
ATTN TECHNICAL LIBRARY	1
HUGHES AIRCRAFT COMPANY	
MISSILE SYSTEMS SECTOR	
P O BOX 7928	
CANOGA PARK CA 91304-7928	
ATTN M DILLENIUS	1
NIELSEN ENGINEERING AND RESEARCH INC	
510 CLYDE AVE	
MOUNTAIN VIEW CA 95043	

DISTRIBUTION (CONT.)

	Copies
ATTN J XERIKOS	1
N CAMPBELL	1
TECHNICAL LIBRARY	1
MCDONNELL DOUGLAS ASTRONAUTICS CO (WEST)	
5301 BOLSA AVE	
HUNTINGTON BEACH CA 92647	
ATTN J WILLIAMS	1
S VUKELICH	1
J FIVEL	1
R GERBSCH (CODE 1111041)	1
TECHNICAL LIBRARY	1
MCDONNELL DOUGLAS ASTRONAUTICS CO (EAST)	
BOX 516	
ST LOUIS MO 63166-0516	
ATTN TECHNICAL LIBRARY	1
UNITED TECHNOLOGIES	
NORDEN SYSTEMS	
NORWALK CT 06856	
ATTN T LUNDY	1
D ANDREWS	1
TECHNICAL LIBRARY	1
LOCKHEED MISSILES AND SPACE CO INC	
P O BOX 1103	
HUNTSVILLE AL 35807	
ATTN R WYRICK	1
BOEING COMPUTER SERVICES INC	
P O BOX 24346	
SEATTLE WA 98124	
ATTN W CHRISTENSON	1
D WARNER	1
MN 11 2920	
ALLIANT TECHSYSTEMS INC	
600 SECOND ST NE	
HOPKINS MN 55343	
ATTN TECHNICAL LIBRARY	1
B SALAMI	1
J BOUDREAU	1
RAYTHEON MISSILE SYSTEMS	
50 APPLE HILL DR	
STOP T3TBB	
TEWKSBURY MA 01876-0901	

	Copies
ATTN LLOYD PRATT	1
AEROJET TACTICAL SYSTEMS CO	
P O BOX 13400	
SACRAMENTO CA 95813	
ATTN JOWEPH ANDRZIJEWSKI	1
MEVATEC CORP	
1525 PERIMETER PARKWAY	
SUITE 500	
HUNTSVILLE AL 35806	
ATTN DR G S SCHMIDT	1
LORAL DEFENSE SYSTEMS	
1210 MASSILLAN ROAD	
AKRON OH 44315-0001	
ATTN W NORDGREN 721	1
GOULD INC OSD	
18901 EUCLID AVE	
CLEVELAND OH 44117	
ATTN TECH LIBRARY	1
AEROJET ELECTRONIC SYSTEMS	
P O BOX 296 III	
AZUSA CA 91702	
ATTN L E ERICSSON	1
P REDING	1
G CHRUSCIEL	1
TECHNICAL LIBRARY	1
LOCKHEED MISSILES AND SPACE CO INC	
P O BOX 504	
SUNNYVALE CA 94086	
ATTN K C LEE	1
ACCUREX CORP	
P O BOX 7040	
520 CLYDE AVE	
MOUNTAIN VIEW CA 94039	
ATTN TECH LIBRARY	1
FMC NAVAL SYSTEMS DIV	
4800 E RIVER ROAD	
MINNEAPOLIS MN 55421-1402	
ATTN L. FRENCH	1
TRACOR AEROSPACE AUSTIN INC	
6500 TRACOR LANE	
AUSTIN TX 87825	

DISTRIBUTION (CONT.)

	Copies
ATTN DORIA GLADSTONE BATTELLE MEMORIAL INSTITUTE COLUMBUS DIVISION 505 KING AVE COLUMBUS OH 43201-2693	1
ATTN JAMES SORENSON ORBITAL SCIENCES 3380 SOUTH PRICE ROAD CHANDLER ARIZONA 85248	1
ATTN J FORKOIS KAMAN SCIENCES CORP 1500 GARDEN OF THE GODS ROAD P O BOX 7463 COLORADO SPRINGS CO 80933	1
ATTN M R D ANGELO MIT LINCOLN LABORATORY LEXINGTON MA 02173-0073	1
ATTN D J GRIESE BOEING DEFENSE AND SPACE GROUP P O BOX 3999 MS 4C-61 SEATTLE WA 98124-2499	1
ATTN W J CLARK DYNA EAST CORPORATION 3132 MARKET ST PHILADELPHIA PA 19104	1
ATTN D SCHMITZ CHAMBERLAIN MANUFACTURING CORP R AND D DIVISION P O BOX 2545 WATERLOO IA 50704-2545	1
ATTN BRIAN WALKUP HERCULES AEROSPACE PRODUCT CO ALLEGHANY BALLISTIC LAB ROCKET CENTER WV 26726	1
ATTN B D PRATS MARTIN MARIETTA ASTROSPACE AEROTHERMOPHYSICS 230 E GODDARD BLVD KING OF PRUSSIA PA 19406	1

	Copies
ATTN DR T LIN TRW ELECTRONICS AND DEFENSE SECTOR BLDG 527/RM 706 P O BOX 1310 SAN BERNADINO CA 92402	1
ATTN G VINCENT SPARTA INC 4301 CORPORATE DR HUNTSVILLE AL 35805	1
ATTN D P FORSMO	1
TECHNICAL LIBRARY RAYTHEON COMPANY MISSILE SYSTEMS DIVISION HARTWELL RD BEDFORD MA 01730	1
ATTN M S MILLER DYNETICS INC P O DRAWER B HUNTSVILLE AL 35814-5050	1
ATTN H A MCELROY GENERAL DEFENSE CORP P O BOX 127 RED LION PA 17356	1
ATTN R SEPLAK BRUNSWICK CORP DEFENSE DIVISION 3333 HARBOR BLVD COSTA MESA CA 92628-2009	1
ATTN J W MCDONALD GENERAL RESEARCH CORP ADVANCED TECHNOLOGY INC 5383 HOLLISTER AVE P O BOX 6770 SANTA BARBARA CA 93160-6770	1
ATTN CAROL BUTLER OTI INTERNATIONAL 60 2ND ST SUITE 301 P O BOX 37 SHALIMAR FL 32579	1

DISTRIBUTION (CONT.)

	Copies
ATTN ENGINEERING LIBRARY ARMAMENT SYSTEMS DEPT GENERAL ELECTRIC CO BURLINGTON VT 05401	1
ATTN TECHNICAL LIBRARY OAYNE AERONAUTICAL 2701 HARBOR DRIVE SAN DIEGO CA 92138	1
ATTN WILLIAM FACINELLI ALLIED SIGNAL P O BOX 22200 MS 1230 21E TEMPE AZ 85285	1
ATTN T LIBRARY RAYTHEON COMPANY SPENCER LABORATORY BOX SL 7162 BURLINGTON MA 01803	1
ATTN NEILL S SMITH ARAP 1950 OLD GALLOWS ROAD SUITE 302 VIENNA VA 22180	1
ATTN DR T P SHIVANANDA TRW BMD P O BOX 1310 SAN BERNADINO CA 92402-1313	1
ATTN T R PEPITONE AEROSPACE TECHNOLOGY INC P O BOX 1809 DAHLGREN VA 22448	1
ATTN ERIC MOORE LOCKHEED SANDERS MAILSTOP MER 24-1281 P O BOX 868 NASHUA NH 03061	1
ATTN J EVANS DREV P O BOX 8800 COURCELETTE PQ CANADA GOA 1RO	1
ATTN H G KNOCHE	1
DR GREGORIOU MESSERSCHMIDT BOLKOW BLOHM GMBH UNTERNEHMENSBEREICH APPARATE MUNCHEN 80 POSTFACH 801149 BAYERN FED REP OF GERMANY (DRF)	1
ATTN BOB WHYTE ARROW TECH ASSOCIATES INC 1233 SHELBURNE ROAD D8 SO BURLINGTON VT 05403	1
ATTN JUAN AMENABAR SAIC 1700 N MOORE ST STE 1820 ARLINGTON VA 22209	1
ATTN TECHNICAL LIBRARY TELEDYNE RYAN AERONAUTICAL 2701 HARBOR DRIVE SAN DIEGO CA 92138	1

INTERNAL

		Copies
C		1
D		1
D4		1
A		1
B05	(STATON)	1
B51	(ARMISTEAD)	1
E231		3
E232		2
E282	(WAITS)	1
F		1
G		1
G02		1
G04		10
G06		1
G20		1
G205		1
G23		1
G23	(CHADWICK)	1
G23	(DEVAN)	1
G23	(GRAFF)	1
G23	(HARDY)	1
G23	(HYMER)	1
G23	(McINVILLE)	1
G23	(ROWLES)	1

DISTRIBUTION (CONT.)

		Copies			Copies
G23	(WEISEL)	1	K20		1
G30		1	K204		1
G40		1	N		1
G50		1	N74	(GIDEP)	1
G60		1	R		1
GHO		1	R44		1
GH3		1	R44	(PRIOLO)	1
K		1	R44	(HSIEH)	1
K10		1	R44	(WARDLAW)	1

REPORT DOCUMENTATION PAGE

Form Approved OMB No 0704-0188

1. AGENCY USE ONLY *(Leave blank)*	2. REPORT DATE	3. REPORT TYPE AND DATES COVERED
	November 1993	FINAL

4. TITLE AND SUBTITLE H STATE-OF-THE-ART ENGINEERING AEROPREDICTION METHODS WITH EMPHASIS ON NEW SEMIEMPIRICAL TECHNIQUES FOR PREDICTING NONLINEAR AERODYNAMICS ON COMPLETE MISSILE CONFIGURATIONS

5. FUNDING NUMBERS

6. AUTHOR(S)

Frank G. Moore

7. PERFORMING ORGANIZATION NAME(S) AND ADDRESS(ES)

Naval Surface Warfare Center
Dahlgren Division (Code G04)
Dahlgren Virginia 22448-5000

8. PERFORMING ORGANIZATION REPORT NUMBER

NSWCDD/ TR-93/551

9. SPONSORING/MONITORING AGENCY NAME(S) AND

10. SPONSORING/MONITORING AGENCY REPORT NUMBER

11. SUPPLEMENTARY NOTES

12a. DISTRIBUTION/AVAILABILITY

Approved for public release; distribution is unlimited.

12b. DISTRIBUTION CODE

13. ABSTRACT *(Maximum 200 words)*

This report discusses the pros and cons of numerical, semiempirical and empirical aeroprediction codes and lists many state-of-the-art codes in use today. It then summarizes many of the more popular approximate analytical methods used in State-of-the-Art (SOTA) semiempirical aeroprediction codes. It also summarizes some recent new nonlinear semiempirical methods that allow more accurate calculation of static aerodynamics on complete missile configurations to higher angles of attack. Results of static aerodynamic calculations on complete missile configurations compared to wind tunnel data are shown for several configurations at various flight conditions. Calculations show the new nonlinear methods being far superior to some of the former linear technology when used at angles of attack greater than about 15 degrees.

14. SUBJECT TERMS

aeroprediction codes
nonlinear semiempirical methods
State-of-the-Art (SOTA) semiempirical aeroprediction codes
static aerodynamic calculations

15. NUMBER OF PAGES

164

16. PRICE CODE

17. SECURITY CLASSIFICATION OF REPORT	18. SECURITY CLASSIFICATION OF THIS PAGE	19. SECURITY CLASSIFICATION OF ABSTRACT	20. LIMITATION OF ABSTRACT
UNCLASSIFIED	UNCLASSIFIED	UNCLASSIFIED	SAR

GENERAL INSTRUCTIONS FOR COMPLETING SF 298

The Report Documentation Page (RDP) is used in announcing and cataloging reports. It is important that this information be consistent with the rest of the report, particularly the cover and its title page. Instructions for filling in each block of the form follow. It is important to ***stay within the lines*** to meet ***optical scanning requirements***.

Block 1. Agency Use Only *(Leave blank)*.

Block 2. Report Date. Full publication date including day, month, and year, if available (e.g. 1 Jan 88). Must cite at least the year.

Block 3. Type of Report and Dates Covered. State whether report is interim, final, etc. If applicable, enter inclusive report dates (e.g. 10 Jun 87 - 30 Jun 88).

Block 4. Title and Subtitle. A title is taken from the part of the report that provides the most meaningful and complete information. When a report is prepared in more than one volume, repeat the primary title, add volume number, and include subtitle for the specific volume. On classified documents enter the title classification in parentheses.

Block 5. Funding Numbers. To include contract and grant numbers; may include program element number(s), project number(s), task number(s), and work unit number(s). Use the following labels:

C	- Contract	**PR**	- Project
G	- Grant	**TA**	- Task
PE	- Program Element	**WU**	- Work Unit Accession No.

BLOCK 6. Author(s). Name(s) of person(s) responsible for writing the report, performing the research, or credited with the content of the report. If editor or compiler, this should follow the name(s)

Block 7. Performing Organization Name(s) and Address(es). Self-explanatory.

Block 8. Performing Organization Report Number. Enter the unique alphanumeric report number(s) assigned by the organization performing the report.

Block 9. Sponsoring/Monitoring Agency Name(s) and Address(es). Self-explanatory.

Block 10. Sponsoring/Monitoring Agency Report Number. *(If Known)*

Block 11. Supplementary Notes. Enter information not included elsewhere such as: Prepared in cooperation with...; Trans. of...; To be published in.... When a report is revised, include a statement whether the new report supersedes or supplements the older report.

Block 12a. Distribution/Availability Statement. Denotes public availability or limitations. Cite any availability to the public. Enter additional limitations or special markings in all capitals (e.g. NOFORN, REL, ITAR).

- **DOD** - See DoDD 5230.24, "Distribution Statements on Technical Documents."
- **DOE** - See authorities.
- **NASA** - See Handbook NHB 2200.2
- **NTIS** - Leave blank.

Block 12b. Distribution Code.

- **DOD** - Leave blank
- **DOE** - Enter DOE distribution categories from the Standard Distribution for Unclassified Scientific and Technical Reports.
- **NASA** - Leave blank
- **NTIS** - Leave blank.

Block 13. Abstract. Include a brief ***(Maximum 200 words)*** factual summary of the most significant information contained in the report.

Block 14. Subject Terms. Keywords or phrases identifying major subjects in the report.

Block 15. Number of Pages. Enter the total number of pages.

Block 16. Price Code. Enter appropriate price code ***(NTIS only)***

Blocks 17.-19. Security Classifications. Self-explanatory. Enter U.S. Security Classification in accordance with U.S. Security Regulations (i.e., UNCLASSIFIED). If form contains classified information, stamp classification on the top and bottom of the page.

Block 20. Limitation of Abstract. This block must be completed to assign a limitation to the abstract. Enter either UL (unlimited) or SAR (same as report). An entry in this block is necessary if the abstract is to be limited. If blank, the abstract is assumed to be unlimited.